Swift Heavy Ion Induced Modification of Aliphatic Polymers

Schnelle Schwerionen – induzierte Modifikation von aliphatischen Polymeren

Vom Fachbereich Material – und Geowissenschaften
der Technischen Universität Darmstadt

zur Erlangung des akademischen Grades
eines Doktor rerum naturalium (Dr. rer. nat.)
genehmigte Dissertation von

Dipl.-Chem. Umme Habiba Hossain
aus Munshiganj (Bangladesh)

Januar 2015-Darmstadt-D17

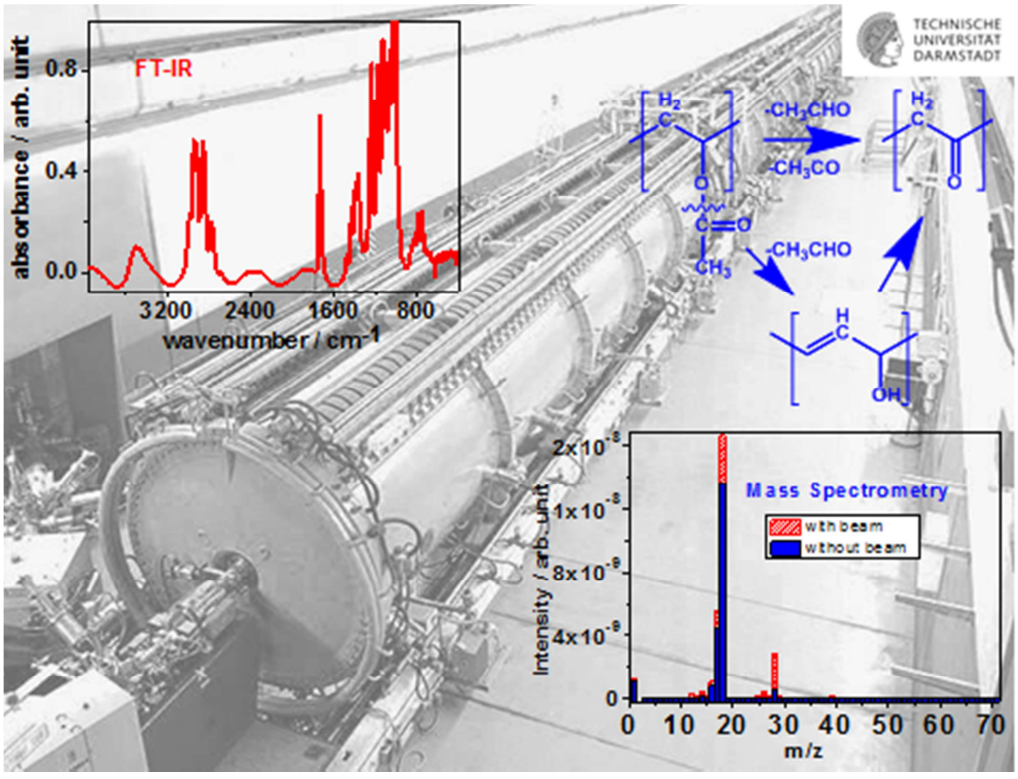

Swift Heavy Ion Induced Modification of Aliphatic Polymers

Schnelle Schwerionen – induzierte Modifikation von aliphatischen Polymeren

Vom Fachbereich Material – und Geowissenschaften der Technischen Universität Darmstadt zur Erlangung des akademischen Grades eines Doktor rerum naturalium (Dr. rer. nat.) genehmigte Dissertation von Dipl.-Chem. Umme Habiba Hossain aus Munshiganj (Bangladesh)

1. Gutachten: Prof. Dr. rer. nat. Wolfgang Ensinger
2. Gutachten: Prof. Dr. rer. nat. Matthias Rehahn

Tag der Einreichung : 14.11.2014

Tag der Prüfung : 16.12.2014

Darmstadt 2015, D 17

Erklärung zur Dissertation

Hiermit versichere ich, die vorliegende Dissertation ohne Hilfe Dritter nur mit den angegebenen Quellen und Hilfsmitteln angefertigt zu haben. Alle Stellen, die aus Quellen entnommen wurden, sind als solche kenntlich gemacht. Diese Arbeit hat in gleicher oder ähnlicher Form noch keiner Prüfungsbehörde vorgelegen.

Darmstadt, den 14. November 2014

(Umme Habiba Hossain)

Diese Arbeit wurde unter der Leitung von Prof. Dr. rer. nat. Wolfgang Ensinger im Fachgebiet Material Analytik des Fachbereichs Materialwissenschaft der Technischen Universität Darmstadt in enger Zusammenarbeit mit der Abteilung Materialforschung am GSI Helmholtz Zentrum für Schwerionenforschung GmbH in der Zeit von August 2009 bis Juli 2014 durchgeführt.

Teile der Dissertation wurden bereits veröffentlicht (siehe Publikationsliste)
Die Reproduktion der Abbildungen und Texte erfolgt mit Erlaubnis der Verlage.

Contents

Abstract VII
Zusammenfassung VIII

1. Introduction 1
1.1 General Introduction 1
1.2 Aims and Motivation 1
1.3 Materials and Methods 3

2. Theory 5
2.1 Energy Loss of Ions 5
Nuclear Energy Loss 5
Electronic Energy Loss 6
Bethe-Bloch Theory 6
Projected Range 7
2.2 Energy Transfer to Matter and Track Formation 8
Coulomb Explosion Model 9
Thermal Spike Model 9
2.3 Molecular Effects 10
2.4 Fluence and Flux 12

3. Experiments 13
3.1 Sample Preparation 13
3.2. Materials Description 14
3.2.1 Polyvinyl Polymers 14
Polyvinyl Formal (PVF) 14
Polyvinyl Acetate (PVAc) 14
Polyvinyl Alcohol (PVA) 15
Polymethyl-methacrylate (PMMA) 15
3.2.2. Fluoropolymers 16
Polyvinylidene Fluoride (PVDF) 16
Ethylene Tetrafluoroethylene (ETFE) 16

Tetrafluoroethylene-per-fluoromethoxyethelene(PFA)
and Tetrafluoroethylene-hexa-fluoropropylene (FEP).....17

4. GSI Accelerator Facilities 18

4.1 GSI Irradiation Facilities 18
4.2 Ion Irradiations at UNILAC 18
4.2.1 Ion Irradiation at X0-Beamline.....19
4.2.2 Ion Irradiation at M3-Beamline 21
4.3 Analysis Techniques.....26
4.3.1 Infrared Spectroscopy (IR) 26
Infrared Spectra of the Used Polyvinyl Polymers.....28
Infrared Spectra of the Used Fluoropolymers.....32
4.3.2 UV-Vis Spectroscopy 35
4.3.3 Residual Gas Analysis (RGA) 38
4.3.4 Thermo Gravimetric Analysis (TGA).....41
4.3.5 Mass Loss Analysis (ML).....43

5. Results and Discussion 45

5.1 Ion Induced Modification of Polyvinyl Polymers for FAIR–Project45
5.1.1 FT-IR Spectroscopy 45
5.1.1.1 Polyvinyl Formal (PVF) 45
5.1.1.2 Polyvinyl Acetate (PVAc).....48
5.1.1.3 Presence of CO_2 Absorption Band.....50
5.1.1.4 Polyvinyl Alcohol (PVA).....54
5.1.1.5 Polymethyl-methaycrylate (PMMA) 55
5.1.2 Residual Gas Analysis.....58
5.1.2.1 Polyvinyl Formal (PVF) 58
5.1.2.2 Outgassing During Heating Up.....62
5.1.2.3 Polyvinyl Acetate (PVAc).....63
5.1.2.4 Presence of CO_2.....64
5.1.2.5 Polyvinyl Alcohol (PVA).....67
5.1.2.6 Polymethyl-methacrylate (PMMA).....68

5.1.2.7 Discussion of Degradation Mechanism of Polyvinyl Polymers.70

5.1.3 UV-Vis Spectroscopy 78

5.1.3.1 *PVF, PVAc and PMMA.....78*

5.1.4 Thermo Gravimetric Analysis 82

5.1.4.1 Polyvinyl Formal (PVF) 82

5.1.4.2 Polyvinyl Acetate (PVAc).....83

5.1.5 Mass Loss Analysis 85

5.1.5.1 PVF, PVAc and PVA.....85

5.2 Ion Induced Modification of Fluoropolymers 86

5.2.1 FT-IR Spectroscopy and Residual Gas Analysis.....86

5.2.1.1 Polyvinylidene Fluoride (PVDF).....86

5.2.1.2 Ethylene Tetrafluoroethylene (ETFE).....90

5.2.1.3 Tetrafluoroethylene per-fluoromethoxyethelene (PFA).....92

5.2.1.4 Tetrafluoroethylene-hexa-fluoropropylene (FEP).....95

5.2.1.5 Comparison of the Four Fluoropolymers.....97

5.2.2 UV-Vis Spectroscopy 102

5.2.2.1 ETFE, PFA and FEP 102

6. Conclusion 106

7. Outlook 108

Bibliography 109

List of Figures..... 120

List of Tables 125

Abbreviations..... 127

Curriculum Vitae 128

Scientific Publications..... 129

Acknowledgements..... 131

Abstract

In this thesis, the high energy heavy ion induced modification of aliphatic polymers is studied. Two polymer groups, namely polyvinyl polymers (PVF, PVAc, PVA and PMMA) and fluoropolymers (PVDF, ETFE, PFA and FEP) were used in this work. Polyvinyl polymers were investigated since they will be used as insulating materials in the superconducting magnets of the new ion accelerators of the planned *International Facility for Antiproton and Ion Research* (FAIR) at the *GSI Helmholtz-Centre of Heavy Ion Research* (GSI) in Darmstadt. In order to study ion-beam induced degradation, all polymer foils were irradiated at the GSI linear accelerator UNILAC using several projectiles (U, Au, Sm, Xe) and experimentation sites (beam lines X0 and M3) over a large fluence regime (1×10^{10} – 5×10^{12} ions/cm^2). Five independent techniques, namely infrared (FT-IR) and ultraviolet-visible (UV-Vis) spectroscopy, residual gas analysis (RGA), thermal gravimetric analysis (TGA), and mass loss analysis (ML), were used to analyze the irradiated samples. FT-IR spectroscopy revealed that ion irradiation led to the decrease of characteristic band intensities showing the general degradation of the polymers, with scission of side groups and the main backbone. As a consequence of the structural modification, new bands appeared. UV-Vis transmission analysis showed an absorption edge shift from the ultraviolet region towards the visible region indicating double bond and conjugated double bond formation. On-line mass-spectrometric residual gas analysis showed the release of small gaseous fragment molecules. TGA analysis gave evidence of a changed thermal stability. With ML analysis, the considerable mass loss was quantified. The results of the five complementary analytical methods show how heavy ion irradiation changes the molecular structure of the polymers. Molecular degradation mechanisms are postulated. The amount of radiation damage is found to be sensitive to the used type of ionic species.

While the irradiation of polymers with high energy heavy ions represents a enforced simulation test of the radiation damage in accelerators, they correspond to real situation in space where devices are directly being hit by very high energy heavy ions.

Zusammenfassung

In dieser Arbeit wird die Veränderung aliphatischer Polymere durch hochenergetische Schwerionenbestrahlung untersucht. Zwei Polymergruppen, nämlich Polyvinyl-Polymere (PVF, PVAc, PVA und PMMA) und Fluor-Polymere (PVDF, ETFE, PFA und FEP) wurden betrachtet. Polyvinyl-Polymere werden als Isolationsmaterial in supraleitenden Magneten der geplanten internationalen Beschleuniger-Anlage *Forschung mit Antiprotonen und Ionen* (FAIR) an der GSI Helmholzzentrum für Scherionenforschung Verwendung finden. Um die ioneninduzierten Änderungen zu studieren, wurden alle Polymerfolien am Linearbeschleuniger UNILAC an der GSI bestrahlt. Um die Degradation untersuchen zu können, wurden verschiedene Ionensorten (U, Au, Sm, Xe), Experimentierstände (Strahlzweige X0 und M3) und ein weiter Ionen-Fluenz-Bereich ($1\times10^{10} – 5\times10^{12}$) Ionen/cm^2 genutzt. Fünf unabhängige Techniken, Infrarot (FTIR) – und (UV-Vis) Spektroskopie, Restgasanalyse (RGA), Thermogravimetrie (TGA) und Massenverlustanalyse (ML), dienten zur Untersuchung der Materialveränderungen. Durch die FT-IR-Spektroskopie konnte nachgewiesen werden, dass die Ionenbestrahlung zu einem Rückgang der charakteristischen Banden führt, die durch Abbau der Polymere hervorgerufen wird, mit Abspaltung der Seitenketten und Bruch des Polymerrückgrats. Als Konsequenz der strukturellen Änderung erschienen neue Banden. UV-Vis Absorptionsspektrometrie zeigt eine Verschiebung der Absorptionskante vom ultravioletten Spektralbereich ins Sichtbare, welcher auf die Entstehung von Doppelbindungen und konjugierten Doppelbindungen hinweist. On-line Restgasanalyse zeigt, dass als Fragmente kleine Gasmoleküle freigesetzt werden. TGA weist auf veränderte thermische Eigenschaften hin. Mit ML wurde der erhebliche Massenverlust quantifiziert. Die Ergebnisse der fünf unterschiedlichen analytischen Methoden zeigen, wie die Ionenstrahlung zu einer Veränderung der molekularen Struktur führt. Dazu werden molekulare Degradationsmechanismen postuliert. Die Höhe der Strahlungsschäden ist dabei abhängig von der Art der Ionensorte.

Während die Bestrahlung von Polymeren mit hochenergetischen schweren Ionen für Beschleunigeranlagen eine forcierte Testsituation darstellt, treten diese Bedingungen im Weltall an Geräten direkt auf, da diese dort von sehr hochenergetischen Schwerionen getroffen werden.

1. Introduction

1.1 General Introduction

In the last decades, radiation damage has been found to be an erudite tool to modify properties of materials making them available for various applications e.g. in nuclear reactors [1, 2] aerospace [3], medical technologies [4], automotive industry and numerous others [5-7]. When polymers are exposed to ionizing radiation, particularly energetic ions, they undergo several changes such as chemical structure degradation, and, as a consequence, deterioration in material performance [8-15]. Most intense material modification takes place when a polymeric material is exposed to heavy ion beams in the MeV-GeV energy region in which the ions lose their energy localized with the energy transfer from the ions into the material being in the order of keV/nm. This is far beyond any chemical bond strength, high enough to break all covalent bonds within a few nanometres around the ion track. The interaction is characterized by bond breaking, cross linking (formation of a new bond between two polymer chains), formation of free radicals and various other reactions, which are induced by the complex secondary chemical processes along the trajectory of the ion [9]. The fundamental events involved in ion irradiation of polymers are electronic excitation, ionization, and chain scission leading to outgassing of small volatile degradation products with the consequence of irreversible changes of material properties.

1.2 Aims and Motivation

The aim of the present work is to investigate material modifications generated by heavy ion irradiation in the MeV-GeV kinetic energy region. This in turn may provide a basis for the systematic investigation of polymer materials. In the present work, aliphatic polymers are chosen as the model material. Swift heavy ion irradiation modifications of polymers are further studies for various applications. The work presented here is motivated by two applications of the polymer.

The first one is the use of aliphatic polymers as insulating materials for superconducting accelerator magnets of the FAIR –project (Facility for Antiproton and Ion Research) at the GSI Helmholtz-Centre for Heavy Ion Research in Darmstadt, Germany [16, 17].

The second one is swift heavy ion induced modifications of polymers in space applications.

The international research project FAIR is one of the largest European projects. More than 13 countries are involved. The plan of this new facility is to provide an accelerator and experimental facility for high-energy physics experiments with research focus on nuclear structure, nuclear matter, atomic and plasma physics, antiprotons, as well as biological and material science [16, 17]. This new facility will provide higher intensity beams than the existing GSI facility and the energy of the heavy ion beam will increase by a factor of 10.

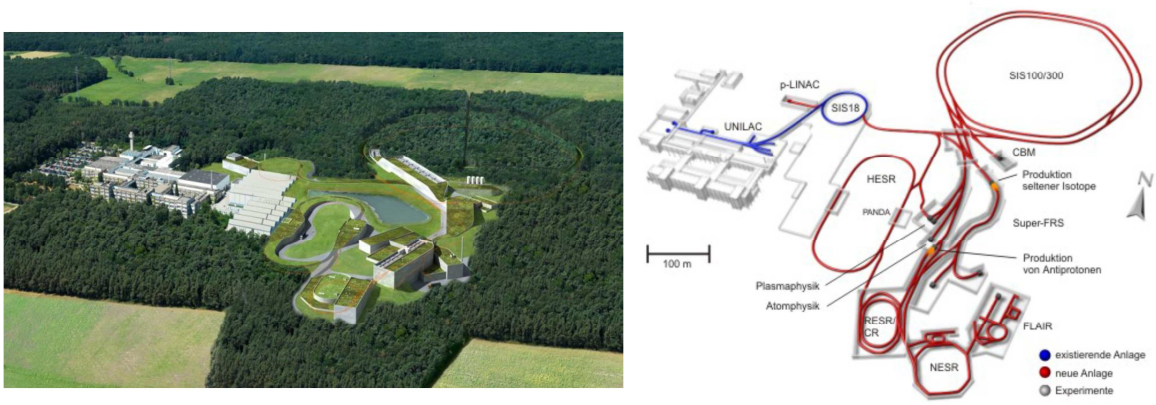

Figure 1.1: Pictures of the exsisting GSI Helmholtz-Centre of Heavy Ion Research (left) and the planned FAIR facility (right) [18].

An overview of scientific topics and their demands at FAIR can be found in the literature [19]. The secondary radiation (including heavy fragments of primary ions) of the highly intense and highly energetic ion beam may cause severe damage of materials close to the ion beamline, including polymers of magnet insulation. For safe long - term operation and lifetime estimations of the material under such extreme conditions, it is very important to better understand radiolytic degradation mechanisms. A simple insulation failure could cause severe damage, cost and facility shut-down times due to quenching of the superconducting magnets.

The same arguments hold **for space applications** where the components are being hit by cosmic rays, including heavy ions [20]. Here, the situation might be even more severe since the vehicle might be lost when the ions or their fragments pass the hull and hit e.g. electronic components.

1.3 Materials and Methods

For insulation in superconducting accelerator magnets of the FAIR–project polyvinyl formal (Formvar / PVF) will be used. This polymer has very favourable properties such as flexibility, abrasion resistance, high softening point as well as excellent electrical insulation characteristics, and is thus used as a principle element in enamels for electrical insulation on wires, particularly magnet wiring including coils of transformers, motors, inductors, and even for cryogenic applications in superconducting coils [21].The complex structure of this random ter-polymer bears three subunits: acetale with a 1,3-dioxane ring (a), alcohol (b), and acetate (c), giving the full name (Poly(vinyl acetale–*co*-vinyl alcohol-*co*-vinyl acetate). For a better understanding of ion induced degradation of this type of polymer we started a systematic investigation, considering reference polymers such as polyvinyl alcohol (PVA) and polyvinyl acetate (PVAc), which are subunits of PVF. Polymethyl-methacrylate (PMMA) has also been investigated to compare the results with those of the other polymers.

The fluoropolymers polyvinylidene fluoride (PVDF), ethylene tetrafluoroethylene (ETFE), tetrafluoroethylene-per-fluoromethoxyethylene (PFA) and tetrafluoroethylene-hexa-fluoropropylene (FEP) were investigated basically to understand swift heavy ion induced modification of fluorine-containing polymers. These high performance polymers have a carbon chain structure in which terminating hydrogen atoms are at least partly replaced by fluorine atoms. Usually they have a high resistance to solvents, acids and alkaline solutions. They exhibit a combination of interesting chemical and physical properties such as high mechanical and electrical resistance, thermal stability and low friction coefficient, which makes them usable in aerospace and other hi-tech applications [22, 23].

On-line analytical techniques have been combined with post irradiation analysis. The chemical modification of polymers induced by heavy ions was determined using different techniques, namely on-line Fourier Transform Infrared Spectroscopy (FT-IR), post irradiation FT-IR, post irradiation UV-Vis spectroscopy, on-line quadrupole mass spectrometry (QMS, outgassing of degradation products / residual gas analysis (RGA)), thermo graviometric analysis (TGA) and mass loss analysis (ML).

The complementary analytical methods FT-IR and QMS give a consistent picture of the degradation mechanism. Aspects of degradation, structural change and fragmentation are detected. Furthermore, experiments with UV-Vis spectroscopy indicate the carbon

unsaturation of the molecular structure. Hence this basic approach for the investigation of heavy ion induced modification of aliphatic polymers was followed.

The Investigation of the influence of irradiation temperature on the response of polymer materials is required for better understanding the ion-induced degradation process. Room temperature (RT) and cryogenic temperature (CT) are used for the irradiation experiments. Irradiation at RT shows the appearance of significant outgassing fragments of materials whereas at CT the radiation induced degradation products are less dominant. We know that temperature plays an important role to mobilize the radical or volatile fragments of the material. Therefore, the outgassing fragments are immobilized at low temperature (LT) which may causes accumulation inside the composite materials. Temperature dependence studies on ion induced degradation of material properties are rare in literature. Some groups show that the influence of irradiation temperature has inconsequential effect on the degradation behaviour [24, 25]. That is to say the effect of the temperature on the degradation behaviour is typically not large. Therefore the majority of the ion induced degradation experiments have been performed at RT. Some otherwise absent fragments were observed during irradiation of polyethylene (PE) and polyimide (PI) at low temperature [13, 26] which were assigned to a greater creation time of swift heavy ion (SHI) induced defects compared with the diffusion time of mobile species to escape on the bulk material [26]. Irradiation experiments at low temperature were performed in this study only on PVF with special focus on degradation processes of volatile polymer fragments during ion irradiation and heat-up cycles. The outgassing fragments are observed at low temperature for polymer materials so that the materials can be adjusted to the temperature necessary in the cryogenic application.

2 Theory

2.1 Energy Loss of Ions

The kinetic energy of a charged particle decreases when the particle hits a target. The energy loss of the particle is correlated with two processes, i.e. nuclear and electronic stopping. The following equation expresses the energy deposition dE in the materials along the particle trajectory dx, the so-called stopping power (S):

$$S = -\frac{dE}{dx} \tag{2.1}$$

$$S = S_{nuclear} + S_{electronic} \tag{2.2}$$

Nuclear Energy Loss

For low energy particles (E_{kin}< 100 keV / u) the energy loss process can be described by considering elastic collisions of the projectile and the target atoms. This regime is described as the nuclear energy loss regime. Here, nuclear energy loss (E_{kin}< 100 keV / u) is negligible, instead the electronic energy loss (E_{kin}> 100 keV/u) is essentially responsible for the induced material changes in the experiments considered in this study (Figure 2.1).

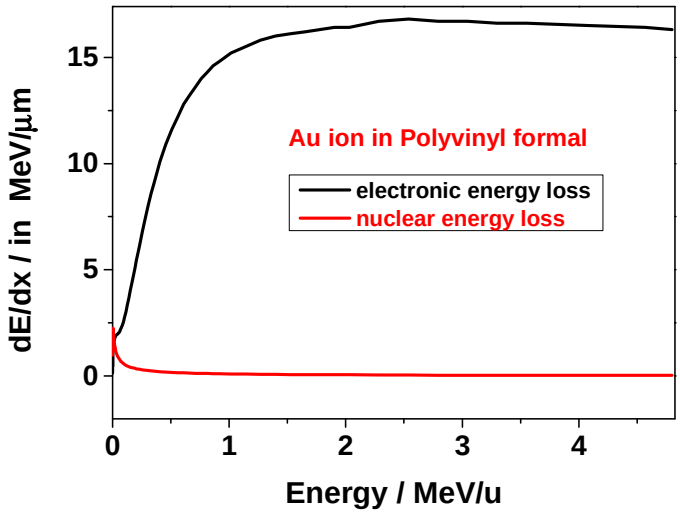

Figure 2.1: SRIM (Stopping and Range of Ions in Matter) calculations for Au ion in polyvinyl formal. Displayed is the stopping power per µm versus specific energy of the projectile.

Electronic Energy Loss

At high energies (above > 100 keV/u), the electronic stopping process becomes the dominating mechanism of energy exchange between the projectile ion and the target atoms. No interaction occurs between the target nuclei and the energetic ion because of its high speed. The energy loss process can be described by collisions between projectile and target electrons resulting in energy transfer to the electron shell and thus target excitation and ionization. As mentioned before, the nuclear energy loss is negligible for the higher energetic ions, the total energy loss is calculated at high energies only by the electronic energy loss and is described by the Bethe-Bloch formula [27-31].

Bethe-Bloch Theory

The Bethe-Bloch formula is well known. The energy transfer is described in terms of momentum transfer and impact parameters. Whereas the momentum transfer is a measurable quantity, the impact parameter is not. Eq. 2.3 is the Bethe-Bloch formula, which is commonly used for energy loss calculations.

$$-\frac{dE}{dx} = \frac{4\pi e^2 Z_{eff}^2 Z_t N_t}{m_e V_p^{\,2}} \left[\ln\left(\frac{2m_e c^2 \beta^2}{I} \right) - \beta^2 - \delta - U \right] \tag{2.3}$$

With

e : elementary charge

Z_{eff} : effective charge state of the projectile

Z_t : mean charge of the target material

N_t : density of target atom

m_e : electron mass

V_p : ion velocity

c : velocity of light

β : velocity in the unit of the speed of light

I : mean excitation potential of the target material

δ : density correction (due to the relativistic correction)

U : shell correction (due to the inner shell electron contribution)

This equation indicates that the electronic energy loss depends on ion velocity, the atomic number of the projectile ions and target atoms and the targets density.

Projected Range

The total penetration range (R) of a charged particle for a specific material can be calculated by the following equation [29].

$$R = \int_0^{E_0} \left(\frac{dE}{dx} \right)^{-1} dE \qquad (2.4)$$

Here the penetration range (projected range) R is connected to the specific energy loss $-dE/dx$ and the initial energy E_0 of the particle. The interaction between projectile ion and target atoms causes a damage track through the target material [32, 33]. The energy transfer to the target atom is different for different projectile ions. SRIM 2010 (Stopping and Range of Ions in Matter) is used to calculate the energy loss and range with an accuracy of about 15% [34]. Figure 2.2 shows the calculated ion trajectory in PVF concerning the electronic energy loss of two different projectiles with same energy, whereas Figure 2.3 indicates the calculated total penetration range (R) for one ion (Au) in different polymer materials. The differences in the latter are due to different densities and compositions, i.e. amount of H and F atoms, respectively.

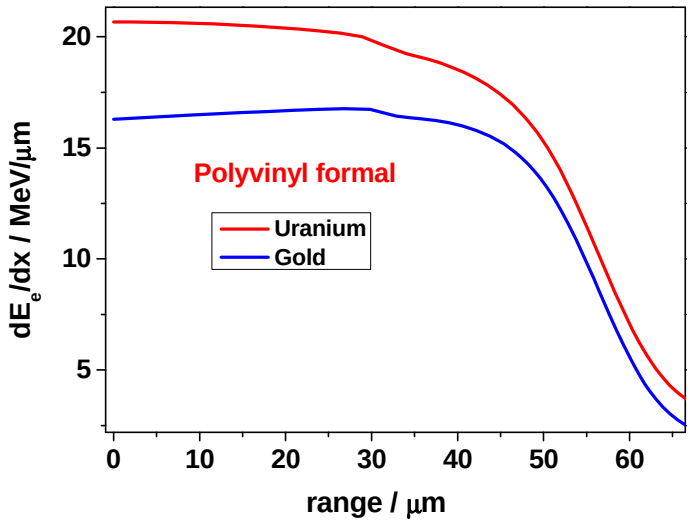

Figure 2.2: SRIM 2011 calculation for electronic energy loss (dE_e/dx) of two different ions in PVF versus the projected range (R).

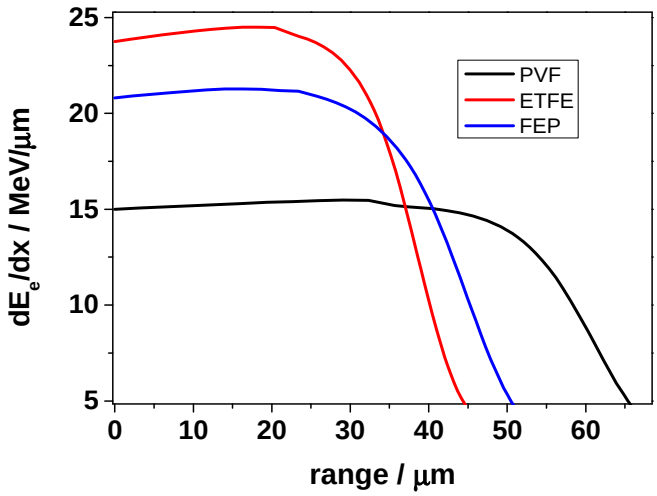

Figure 2.3: SRIM 2011 calculation for electronic energy loss (dE_e / dx) of Au ions in different aliphatic and fluoropolymers versus the projected range (R).

2.2 Energy Transfer to Matter and Track Formation

All energy deposited during the passage of the incident ions is spread and dissipated in solid matter. Besides the above mentioned ionization leading to electron cascades, other effects of energy loss of ions play an important role in the process of formation of damage tracks. Among them one can mention pressure pulses and radiation –enhanced diffusion of reactive species like free radicals. Electronic energy is converted into kinetic energy leading to atomic or molecular motion. The efficiency of energy conversion is governed by the lifetime of localized electronic excitations. One part of this conversion occurs by creating phonons in the network. Another part is used in chemical recombination (such as heat of reaction) or the rearrangement of molecular bonds. These rearrangements occur in time scales much larger than the typical duration of electronic excitations during the passage of the ion in the solid. Typically, the excitation and ionization of atoms occur in the first 10^{-14} s after the passage of the projectile, characterizing the physical stage of radiation action. In the range of 10^{-14} to 10^{-10} s, called physical-chemical stage; most of the energy is transformed into vibrational energy. Chemical reactions in the neighbourhood occur rapidly. For times greater than 10^{-12} s, bimolecular chemical reactions are dominant. After 10^{-10} s, thermal equilibrium is reached but not necessarily chemical balance. Diffusion processes and reactions of radicals occur. This alters the pattern of the initial structure of the latent track [35]. While the physical process is extremely fast, the same does not apply to the chemical process, and some excited states may

last for a long time like days or even months. Although ion track formation has been studied for many years, the primary mechanisms of track formation are still not completely understood. Two basic models are explaining these basic phenomena of track formation i) the Coulomb explosion model [36] and ii) Thermal-spike model.

Coulomb Explosion Model

This model assumes that a cloud of ionized atoms is created during the ion passage through the matter. This model is particularly suitable for insulators which have very high resistivity towards dissipating the inserted energy via the electronic subsystem [37]. A cylindrical ion track is formed along the ions path which is compactly filled with positively charged ions [38]. These positive lattice ions interact with each other which is the driving force for atomic collision cascades causing modified chemical bonds, melting, and vaporization, and may produce phase transitions or latent track formation [39-41].

Coulomb explosion can happen when the coulomb repulsive force is greater than the lattice bonding forces. The force between two ions in materials is proportional to average ionization, unit charge and inversely proportional to dielectric constant and average atomic space. When the average ionization is high, the electrostatic stress will be larger than the mechanical strength. Therefore the latent track can be found in materials of low mechanical strength, low dielectric constant and close atomic spacing. Another concept to Coulomb explosion relates to the repulsion of the ionized target ions which should be displaced from their original sites very fast in $\sim 10^{-13}$ s. That means low density of free conduction electrons is required to form latent track for insulator materials. In contrast, for a conduction material the density of free electrons is very high so that the ion cloud is neutralized immediately after the passage of the projectile ion [42].

Thermal Spike Model

The Thermal spike model [37] has been developed by several groups [43-47] in order to take the temperature effects into account where Coulomb explosion meets with pressure effects. Two different Thermal spike models [48-50] (i) inelastic thermal spike model (ITSM) and (ii) analytical thermal spike model (ASTM) with similar arguments to explain the radiation defect creation mechanism are used for swift heavy ion modification of materials. These can be described mathematically with the following two coupled differential equations [51].

$$C_e \frac{\partial T_e}{\partial t} = \frac{1}{r}\frac{\partial}{\partial r}(rK_e(T_e)\frac{\partial T_e}{\partial r}) - g(T_e - T_a) + A(r,t)$$

$$C_a \frac{\partial T_a}{\partial t} = \frac{1}{r}\frac{\partial}{\partial r}(rK_a(T_a)\frac{\partial T_a}{\partial r}) + g(T_e - T_a) \quad (2.5)$$

With $C_{(e,\,a)}$, $K_{(e,\,a)}$, $T_{(e,\,a)}$ are representing the specific heat, the thermal conductivity and the temperature of either the electrons (*e*) or the lattice atoms (*a*), r is the radius of a cylindrical ion track, *g* is the electron-phonon interaction [26] and *A(r, t)* is the energy density deposited by an incident ion in the target electrons at the time *t* and distance *r*. According to the equations, the deposited energy is transferred to the lattice via electron-phonon coupling and a local melting along the ion trajectory can occur when the melting point is low enough, under strong electron-phonon coupling conditions. This leads to the formation of strongly localised ion tracks followed by a fast cooling and the possibility of creation of an amorphous phase transformation. This model has been used for different materials, mostly inorganic insulators. The experimental data of ion track radii have been well matched for polymer materials with this mechanism [52-54].

The common basic idea of these models is that an expansion of the material will occur along the path of the ion leading to molecular motion and to sputtering at the vacuum surface interface. The mechanisms of energy transfer in polymers into heat or atomic movement is not thoroughly understood. Atomic / molecular motion and radical formation occur during the passage of the ion, followed by recombination chemistry.

2.3 Molecular Effects

Three main processes may occur under low radiation fluences leading to new chemical structures:

- chain scission - breaking the chains of the irradiated material
- cross-linking - formation of new connections between the broken chains.
- unsaturation - the formation of double and triple bonds and aromatization.

When the density of deposited energy is high enough, molecular bonds are broken. The main effect of chain scission, accompanied by fragmentation, is the reduction of the molecular

weight and the overall mass. Volatile compounds diffuse out of the irradiated area and leave the material in gaseous form.

By cross linking, the open bonds begin to react with each other in a process of recombination or the formation of new connections. With irradiation at high fluences, ion tracks start to overlap, which leads to formation of a large quantity of volatile products and occurrence of cross-linking. The process of unsaturation occurs due to the loss of bonding partners, particularly hydrogen with creation of allene and alkyne groups.

The intensity of these processes depend on the electronic energy loss of the projectile. Molecular dynamics calculations can be used to quantify the ion induced modification of materials. Most of such studies have been done for gamma and electron beams; there is still a lack of calculations of heavy ion induced effects in polymers [35].

Another issue also remaining to be investigated in detail is the influence of temperature. Some studies have shown that diffusion and mobility of radicals are decreasing when polymers are irradiated at low temperatures. By comparisons between room temperature and cryogenic temperature, FT-IR measurements gave different results, showing direct products of primary ion effects, fast recombination products, but also hints that temperature does not much affect the formation of the products obtained after equilibration of the region damaged by the passage of ions [26, 55]. In the present work, a small study on temperature effects is included.

2.4 Fluence and Flux

Some units are of great importance to explain ion beam modification or damage generated materials and will be mentioned several times over this work.

The fluence ϕ defines the number of projectiles incident on the material per unit area:

$$\phi = \frac{N}{A} \tag{2.6}$$

where N is the total number of incident ions and A is the total radiated area in cm^2. The unit of fluence is $1/cm^2$. Here we will give the fluence in $ions/cm^2$.

The flux $d\phi/dt$ sets the number of projectiles incident on the material per unit area and unit time. As an irradiation flux, the derivative can be replaced by the division and the flux of ions can be calculated from:

$$\frac{d\phi}{dt} = \frac{N}{A \cdot t} \tag{2.7}$$

where t is the total irradiation time measured in seconds and the unit of the flux is $1/s\ cm^2$. When the current of the beam is known as i (in Ampere), the flux can be calculated from:

$$\frac{d\phi}{dt} = \frac{i}{q \cdot e \cdot A} \tag{2.8}$$

where q is the charge state of the ion beam and e is the elementary charge (1.602×10^{-19} C).

3 Experiments

3.1 Sample Preparation

For transmission FT-IR spectroscopy a polymer film in an expedient thickness, typically in the order of (1-40) µm, is obligatory. There are various kinds of methods to prepare a foil as sample. In this study **"The Solution Grown Technique"** was used to prepare polymer foils.

Films of polyvinyl formal (PVF, Agar scientific, R1201), polyvinyl alcohol (PVA, Aldrich, Mw: 89000-98000) and polyvinyl acetate (PVAc, Aldrich, Mw: 100000) and polymethyl-methacrylate (PMMA, Agar Scientific, Mw: 350000) were prepared by the solution grown technique (Figure 3.1).

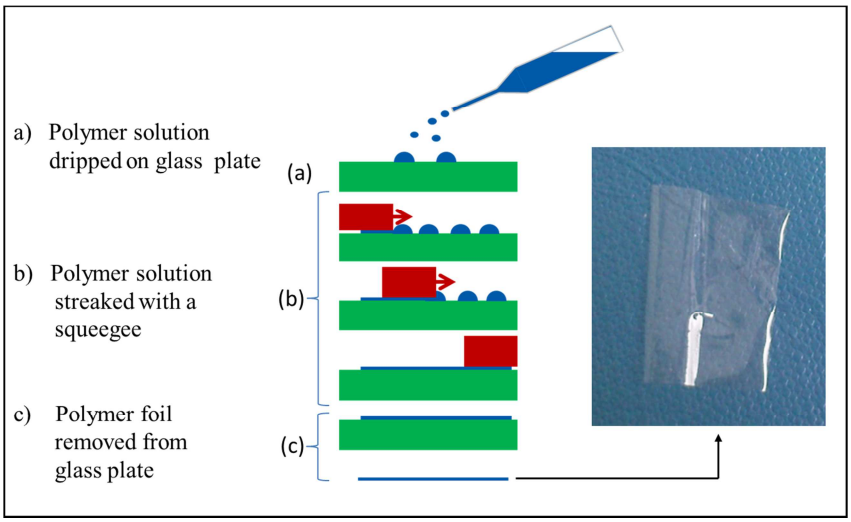

Figure 3.1: Sample preparation by solution grown technique. Left: preparation process, right: example of a transparent 20 µm PVF film.

All polymers were weighed in solution concentrations of (4-8) % and dissolved in distilled dichloromethane (CH_2Cl_2). Only for preparing PVA foil water was used as solvent. The mixtures were continuously stirred for 24 h at room temperature to create a homogeneous solution. A certain amount of the viscous solution was dripped on a cleaned glass plate and the drop was streaked slowly with a squeegee to an area of about 10 cm^2. After solvent evaporation in air for 24 h the polymer samples were carefully removed from the glass substrate. Homogeneous, transparent films were obtained without any gas bubbles having a thickness of (20-30) ± 2 µm as measured with a thickness gauge.

3.2 Materials Description

3.2.1 Polyvinyl Polymers

Polyvinyl Formal (Formvar™ / PVF)

Polyvinyl formal (PVF) is a polymer having functional groups linking together acetale with a 1,3-dioxane ring (a), alcohol (b), and acetate (c), giving the full name (Poly(vinyl acetale–*co*-vinyl alcohol-*co*-vinyl acetate). Formvar™ is a registered trade name for PVF. The chemical structure is depicted in Figure 3.2(i).

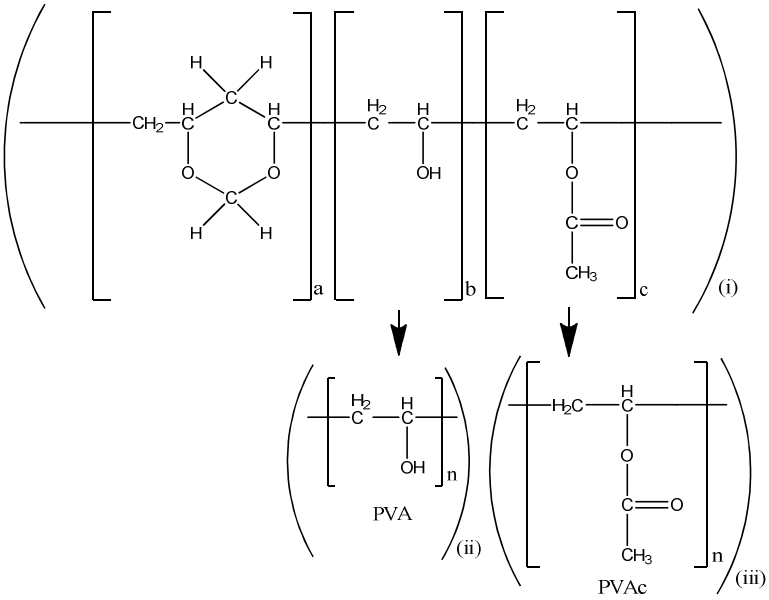

Figure 3.2: Scheme representing the structure of (i) polyvinyl formal (PVF), (ii) polyvinyl alcohol (PVA) and (iii) polyvinyl acetate (PVAc).

PVF (in the form of a foil) was prepared by the solution grown technique. The used polymer powder was supplied from Agar Scientific, Ltd with average molecular weight
Mw = 39600. The density of PVF is 1.3 g/cm^3.

Polyvinyl Acetate (PVAc)

PVAc is a thermoplastic polymer [56]. It is normally manufactured by the free radical polymerization of vinyl acetate. PVAc is primarily a synthetic resin polymer, which is insoluble in water, oils or fats. It is soluble in alcohols, ketones and esters. The chemical structure of PVAc is shown in Figure 3.2(iii).

Polyvinyl Alcohol (PVA)

Polyvinyl alcohol (PVA) is a thermoplastic polymer [56]. It is produced from PVAc, usually by a continuous process which is explained as follows. The acetate groups are hydrolyzed by ester interchange with methanol in the presence of anhydrous sodium methylate or aqueous sodium hydroxide. The physical characteristics and its specific functional use depend on the degree of polymerization and the degree of hydrolysis. The chemical structure is depicted in Figure 3.2(ii). PVA foils were prepared from 4% H_2O solution. The density of PVA is 1.2 g/cm^3.

Polymethyl-methacrylate (PMMA)

PMMA is the synthetic polymer of methylmethacrylate. PMMA is an aliphatic polar polymer. This thermoplastic and transparent plastic is commercially known as Plexiglas. For this study PMMA- foils were prepared by solution grown method, as described before. The polymer powder was supplied from Agar Scientific, Ltd with average molecular weight Mw= 350000. The density of PMMA is 1.2 g/cm^3. Its chemical structure is presented in Figure 3.3.

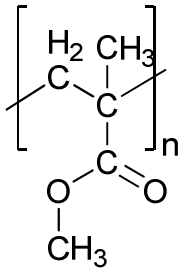

Figure 3.3: Molecular structure of polymethyl-methacrylate (PMMA).

The material properties of used vinyl polymers are presented in Table 3.1 according to the literature [57].

Table 3.1: Material properties of used polyvinyl polymers (PVF, PVAc, PVA and PMMA)

Polymers	Density (g/cm^3)	Melting Point (°C)	Glass transition Temperature(T_g) (°C)
PVF	1.3	-	-
PVAc	1.2	70-210	30
PVA	1.2	200-228	85
PMMA	1.2	160	105

3.2.2 Fluoropolymers

The following fluoropolymers (Figure 3.4) with a thickness of 25 µm as foils were commercially available polyvinylidene fluoride (PVDF), ethylene tetrafluoroethylene (ETFE), tetrafluoroethylene-per-fluoromethoxyethylene (PFA) and tetrafluoroethylene-hexa-fluoropropylene (FEP) supplied from DuPont as received.

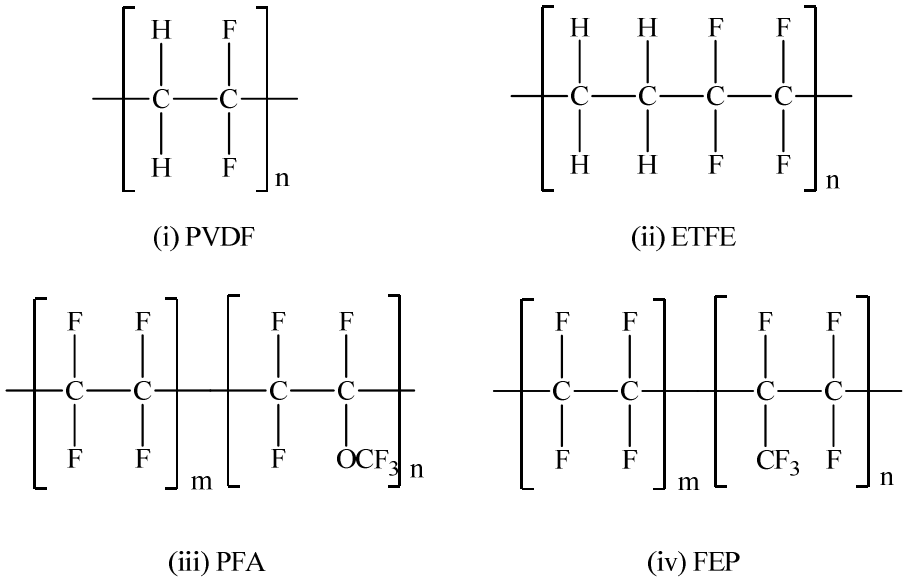

Figure 3.4: Structure of (i) polyvinylidene fluoride (PVDF), (ii) ethylene-tetrafluoroethylene (ETFE), (iii) tetrafluoroethylene-per-fluoromethoxyethylene (PFA) and (iv) tetrafluoroethylene-hexa-fluoropropylene (FEP).

Polyvinylidene Fluoride (PVDF)

PVDF with a low melting point is easy to structure and has a considerable degree of attention in many researches [10, 58-63] and for industrial use. Its molecular formula is $C_2H_2F_2$ composed with 2 fluorine and 2 hydrogen atoms, also it shows the lowest density of all fluoropolymers. ETFE and PVDF have a similar structure, with the difference being that ETFE contains vicinal C-F and C-H bonds in pairs of two, whereas PVDF is based on a backbone containing alternating C-F and C-H bonds, see Figure 3.4 (i, ii).

Ethylene Tetrafluoroethylene (ETFE)

ETFE is well known for its excellent thermal and chemical stability and mechanical properties [64]. Among these properties, it is used in many applications, e.g. in the coating industry, in manufacturing, food and pharmaceutical packing, medical supplies, as well as aerospace industries [65, 66]. Its molecular formula is $C_4H_4F_4$ composed with 4 fluorine and 4 hydrogen atoms. The ETFE polymer provides an interesting case for study, since its structure is closely

related to that of the polyethylene (PE) and polytetrafluoroethylene (PTFE) alternating copolymer.

Tetrafluoroethylene-per-fluoromethoxyethelene (PFA) and Tetrafluoroethylene-hexa-fluoropropylene (FEP)

PFA and FEP are very similar in composition to PTFE. Both of them have useful properties like low coefficient of friction and non-reactivity [64]. They are easily formable. Their molecular structures are composed of atoms of carbon, fluorine and oxygen. The structures of FEP and PFA differ in the presence of an O atom in the side-chain bearing monomer. While FEP has a trifluoromethyl group attached to the carbon chain by a C-C bond, PFA contains an ether bond.

Table 3.2 gives an overview of material properties of used four fluoropolymers.

Table 3.2: Material properties of used fluoropolymers (PVEF, ETFE, PFA and FEP)

Polymers	Density (g/cm^3)	Melting Point (°C)	Glass transition Temperature(T_g) (°C)	Thermal conductivity (W/mK)	Tensile strength (MPa)
PVDF	1.7	175	-35	0.12	20
ETFE	1.7	327	-100	0.24	44
PFA	2.1	310	100	0.19	30
FEP	2.1	270	80	0.19	30

4 GSI Accelerator Facilities

4.1 GSI Irradiation Facilities

All ion irradiation experiments were performed at the radiation facility of the GSI Helmholtz-Centre of Heavy Ion Research GmbH located in Darmstadt. Two different sample irradiation processes have been used in this thesis. For on-line investigations, irradiations were performed at the M3 branch [67] while post irradiation experiments were performed at the X0-beamline of the UNILAC of GSI. The setups involved are explained in detail in this section. A complete view of the GSI facility is shown in Figure 4.1.

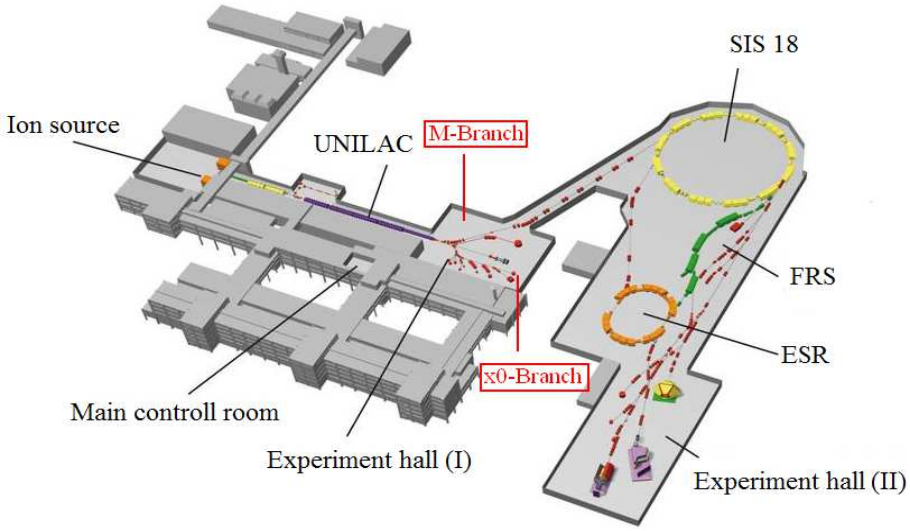

Figure 4.1: Schematic represents the GSI accelerator facilities for swift heavy ion irradiation research [68]. The used irradiation sites (M-Branch and X0-Branch) are marked in red colour.

The GSI accelerator facility provides a wide range of experimental activity mainly consisting of a 120 m long Universal linear accelerator (UNILAC) [69], heavy ion synchrotron (SIS) [70] and experimental storage ring (ESR) [71]. Ions were obtained from an Electron Cyclotron Resonance (ECR) ion source. In this work the ions were accelerated at the UNILAC to energies up to 11.4 MeV/u.

4.2 Ion Irradiation at UNILAC

The UNILAC operated by GSI can accelerate all stable elements from hydrogen to uranium in a suitable state of electric charge up to energies of 15% of the speed of light corresponding to about 11.4 MeV/u [72]. As mentioned before, the irradiation experiments were performed at

the X0-beamline for post irradiation analysis while at M3 analysis can be performed in-situ during irradiation.

4.2.1 Ion Irradiation at X0-Beamline

The polymer membranes were irradiated with swift heavy ions (U, Au, Sm, Xe) at RT and the applied fluences were between 1×10^{9} and 1×10^{13} ions/cm^{2}. The irradiation took place at the X0 site of the Materials Research Department of GSI which is located at the end of the UNILAC experimental hall. This beamline is equipped with a cryostat, automatic sample exchange system, multipurpose irradiation chamber and microprobe (Figure 4.2).

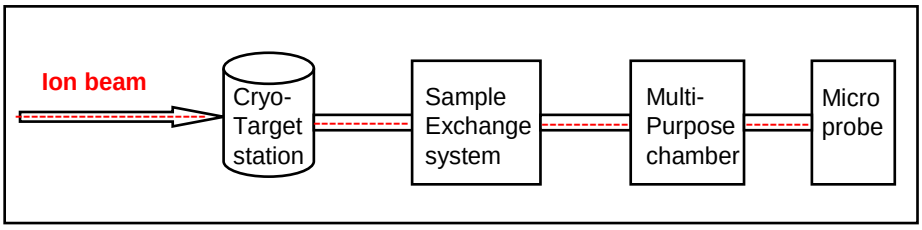

Figure 4.2: Schematic showing the components of X0-beamline of GSI accelerators facilities.

Samples are exchanged by an automatic system during the beam (Figure 4.3 left). A magazine contains 20 sample holders with a size of 5x5 cm^{2} (Figure 4.3 right). From the magazine each sample holder can be moved into the beamline with the automatic sample exchange system. After acquisition of the desired fluence the holder is moved back into the magazine. This allows for high-throughput irradiations.

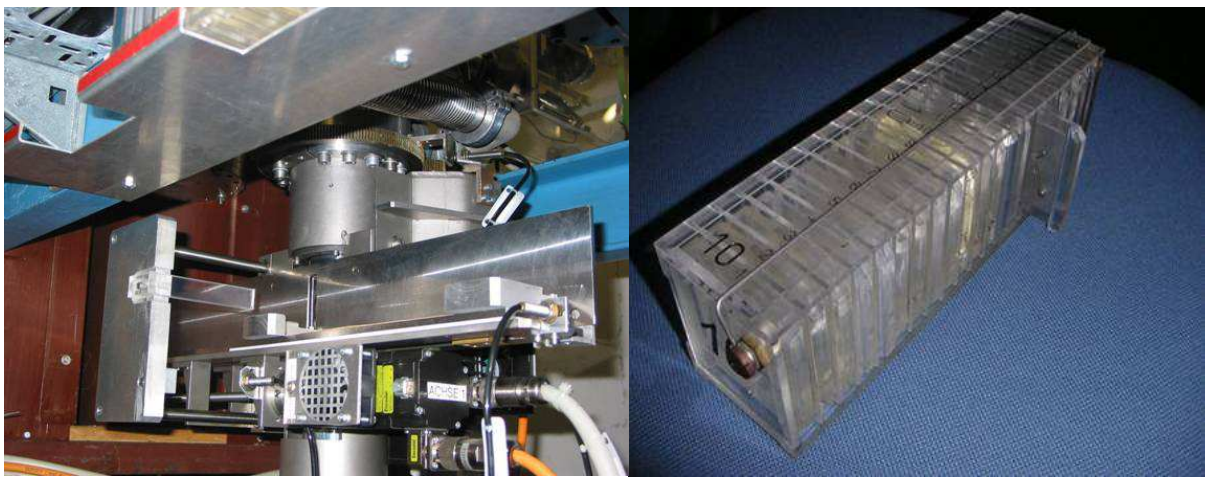

Figure 4.3: Photographs of the target station at X0-beamline showing the sample exchange system for remote control irradiation (left side) with the magazine (right side).

Measurement and control of fluence occurs with the help of a vertically arranged three foil detector (Figure 4.4) [73]. This three foil detector produces a signal proportional to flux on the sample. The first and the third foil are biased with +100V to catch the electrons knocked out by the passing ions. During irradiation, secondary electrons are produced und travel from the middle aluminium foil in the field of the outer two foils. Current is measured between centre foil and ground. With a Faraday cup this measured ionization current is calibrated. A Faraday cup collects the charged particles of the beam and directly measures the charge carried by the beam per time. Since the charge state of the incoming ions is well defined, this current can easily be translated into particle flux. To avoid macroscopic heating of the samples, the UNILAC was operated with an ion flux of 2×10^{8} ions/ $cm^{-2}s^{-1}$.

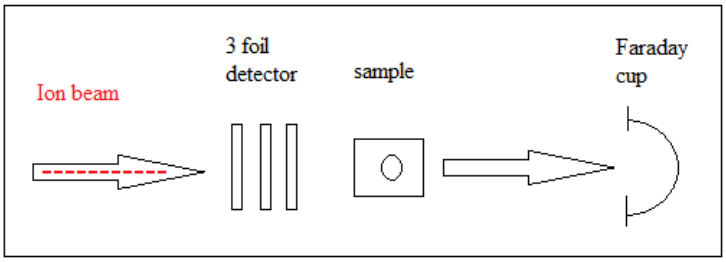

Figure 4.4: Schematics view of the ionization chamber.

Table 3.3 gives an overview of the irradiation experiments at X0 beamline for different polymer samples with different analysing methods. Details and results of these experiments are discussed in the results and discussion section.

Table 3.3: Used ion beam at X0 beamline for post irradiation analysis

Polymers	Ions	Energy MeV / u	Fluence Ions / cm^2	Analysing methods
PVF	Au Au U, Au	11.1	5×10^{10} - 1×10^{12} 1×10^{9} - 6×10^{11} 1×10^{10} - 5×10^{12}	UV-Vis TGA ML
PVAc	Au	11.1	5×10^{10} - 1×10^{12} 3×10^{10} - 5×10^{11} 1×10^{10} - 1×10^{12}	UV-Vis TGA, ML
PVA	Au	11.1	1×10^{10} - 5×10^{12}	ML
PMMA	U	8.3	3×10^{9} - 1×10^{11}	UV-Vis
PVDF	Au	4.5	1×10^{9} - 2×10^{12}	FT-IR
ETFE	Sm	11.1	1×10^{9} - 3×10^{12}	FT-IR, UV-Vis
PFA	Sm	11.1	1×10^{9} - 6×10^{12}	FT-IR, UV-Vis
FEP	Sm	11.1	1×10^{9} - 3×10^{12}	FT-IR, UV-Vis

4.2.2 Ion Irradiations at M3-Beamline

After acceleration in the UNILAC, the ions are redirected by a kicker magnet to the M-branch, with M standing for *Material* research. This target station provides on-line investigations of ion induced modification of materials with three single beamlines M1 to M3 with diverse experimental techniques, such as in-situ electron microscopy (SEM), X-ray diffraction (XRD), infrared spectroscopy (IR) and residual gas analyzing (RGA) [67]. For SEM analysis beamline M1 is equipped with a high resolution scanning electron microscope (HRSEM). Beamline M2 is used to determine the structural changes of materials during irradiation by means of X-ray diffraction.

For the present study, beamline M3 was used. A schematic is shown in Fig. 4.5. It consists of several chambers. A variable x-y-slit pair allows for ion beam shaping. A secondary electron transmission monitor (SEETRAM) is used for on-line ion flux monitoring during the irradiation, a Faraday cup serves for calibrating the flux and a luminescence screen with a CCD camera allows for beam diagnostics. After the beam-diagnostic chamber follows the pre-chamber which can be used for high temperature experiments up to 1100 K.

At the end of the M3 beamline the multipurpose diagnostic chamber, used for the present study, is mounted. Its sample holder can be moved up and down (about 90 mm) and can also be rotated (around +/- 180°). For low temperature experiments, a closed cycle He-refrigerator allows irradiations at temperatures down to 13K with a cooling finger attached to the sample holder.

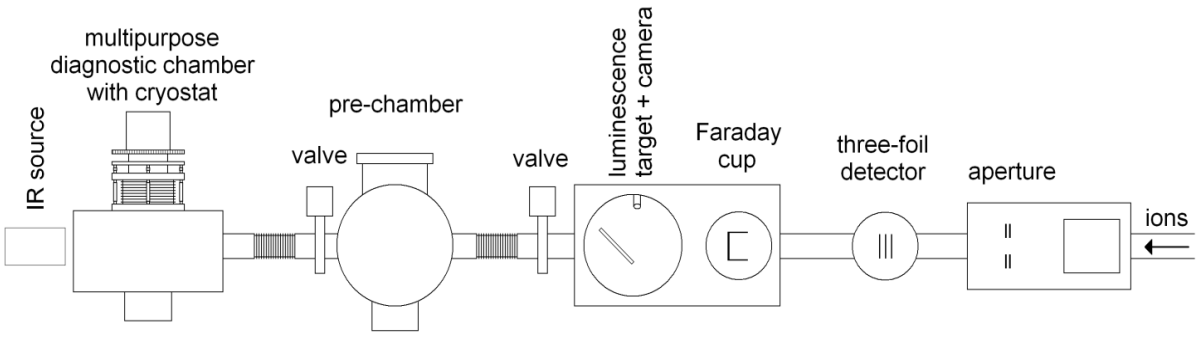

Figure 4.5: Schematics of target station M3. Ions have to pass the aperture for ion beam shaping, a beam diagnostic unit providing a SEETRAM (three foil detector), a Faraday cup, a luminescence screen, a chamber for high temperature experiments and the multipurpose diagnostic chamber. Reprinted with permission from [67].

This chamber provides two different analysis methods, FT-IR and RGA, which allow simultaneous experiments during the irradiation.

The FT-IR spectrometer with the IR source is installed outside the diagnostic chamber and placed at - 45° with respect to the ion beam (Figure 4.6). The IR detector is installed at the opposite side of the diagnostic chamber (135° with respect to the ion beam). Two flanges with 4 mm thick ZnSe windows are used to ensure infrared transparency. It is possible to mount a KRS-5 IR polarizer in front of the first IR window. The sample holder for transmission FT-IR spectroscopic measurements contains 6 apertures with a size of 10 mm in diameter (Figure 4.7 right).

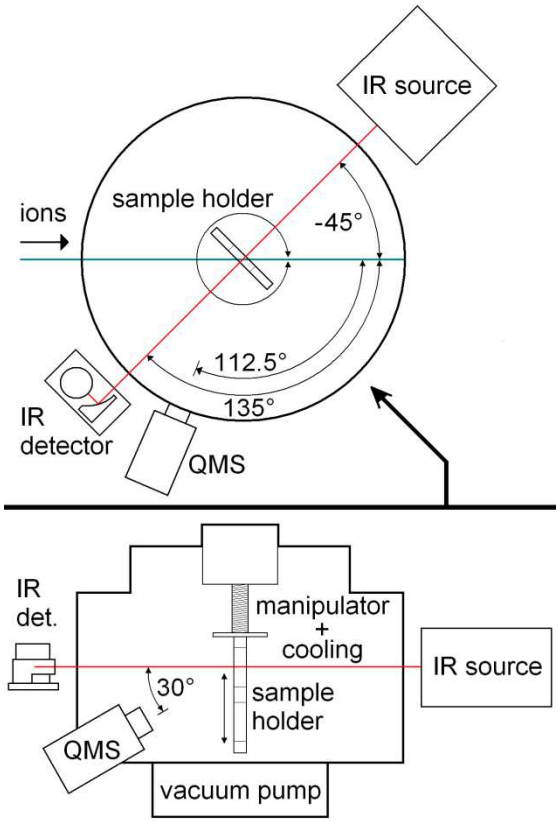

Figure 4.6: Schematics of the multipurpose chamber at target station M3. IR source and detection unit are placed outside the chamber. The angle between IR radiation and ion beam is -45°. The RGA is mounted near the IR detection unit and tilted downwards by 30°. The sample holder can be moved up and down and is rotatable. Reprinted with permission from [67].

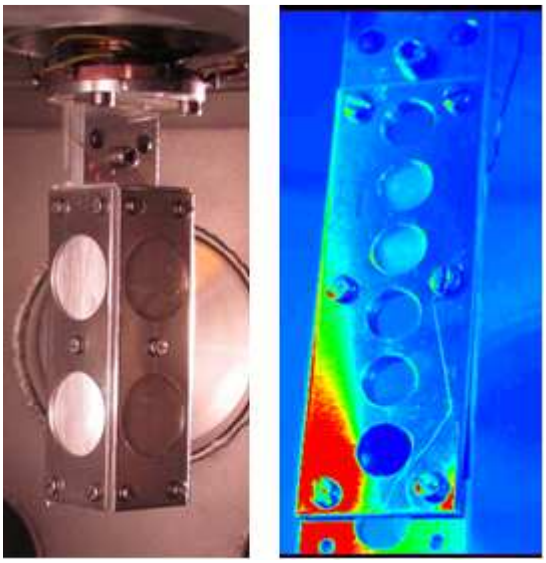

Figure 4.7: Photograph of the sample holder for on-line analysis. Sample holder for RGA analysis is shown in the left side and sample holder for the FT-IR measurement on the right side.

The RGA analyser is installed at 112.5° with respect to the ion beam and tilted 30° downward. Here, a sample holder with 4 polymer foils of 1 cm^2 area is used (Figure 4.7 left). Table 3.4 gives an overview of the irradiation experiments at M3 beamline for different polymer samples with different ion beams. Low temperature irradiation was performed for PVF polymer and compared with the result of the RT irradiation experiment.

Table 3.4: Used ion beam at M3 beamline for on-line analysis

Polymers	Ions	Energy MeV / u	Analysing methods	Temperature T
PVF	Au	4.5	FT-IR, RGA	RT, CT
PVA	Au	4.5	FT-IR, RGA	RT
PVAc	U Au Xe	8.6 4.8 11.4	FT-IR, RGA	RT
PMMA	Au	4.5	FT-IR, RGA	RT
PVDF	Sm	11.1	RGA	RT
ETFE	Sm	11.1	RGA	RT
PFA	Sm	11.1	RGA	RT
FEP	Sm	11.1	RGA	RT

RT = room temperature, CT = cryogenic temperature

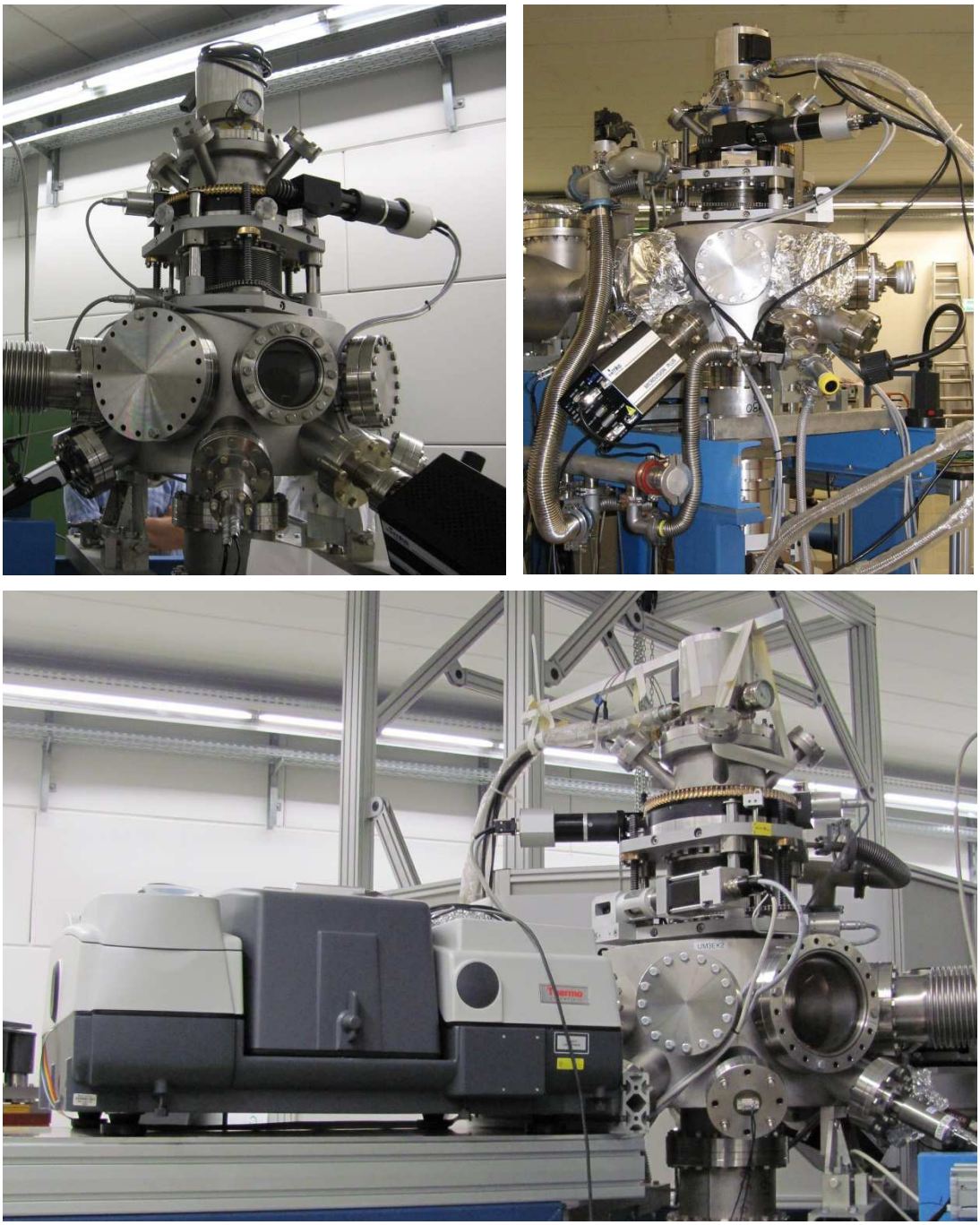

Figure 4.8: Photograph of the experimental setup at M3 beamline. Left side of the picture is the multipurpose chamber; right sight: Residual Gas Analyser by means of quadrupole mass spectrometry (QMS); bottom of the picture: FT-IR spectroscopy placed outside of the diagnostic chamber.

4.3 Analysis Techniques

4.3.1 Infrared Spectroscopy (IR)

Infrared spectroscopy (IR) is a physical analysis method, which is used for identification of substances by comparing the spectrum to a known reference spectrum or structure elucidation of unknown substances.

The method is based on the excitation of molecule vibrational modes by irradiation with electromagnetic waves in the IR range (Figure 4.9). Characteristic frequencies are absorbed by the molecules and can be subsequently identified in the spectrum. However, modes are only IR active when there is a change in the vibrational excitation of the dipole moment of the molecule. There are three different types of vibrations in different molecules: a) symmetric stretching vibrations are in the direction of the bond axis between two atoms or parts of the molecule through a stretch or compression of the bond, b) asymmetric stretching vibrations of the molecule are directed asymmetric from the centre, c) bending modes (bending vibrations) are oscillations in the deformation of the bond angle [74, 75].

The used wavenumber range of the radiation is between 400 and 4000 cm^{-1}. In the far infrared (3-400 cm^{-1}) the substances are absorbing because of molecule rotations, in the central or classical infrared (400-4000 cm^{-1}) because of molecular vibrations and in the near infrared (4000 - 12500 cm^{-1}) only overtones and combination vibrations of the mid-infrared are detectable.

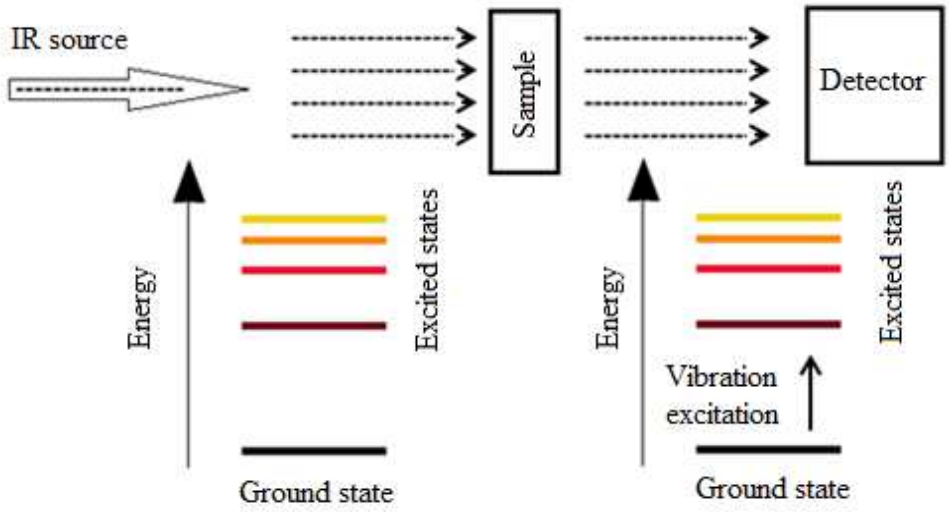

Figure 4.9: Schematics and principle of infrared spectroscopy (IR).

Polymer materials are composed of many repeated monomers. The characteristic absorption bands of these monomers can be detected according to the literature whereas the functional groups of organic molecules are classified in group vibration cause to identify the organic molecules having a structure similar to the repeating unit [75]. Table 4.1 describes some absorption bands of different functional groups in organic molecules [19].

Table 4.1: Characteristic absorption bands of some functional groups

Wavenumber region / cm^{-1}	**Functional group**
3600-2800	-OH
3400-3200	-CH
3050-3150	Unsaturated –CH
2960-2700	Saturated –CH
2280-2100	C≡C
1800-1700	-CO-
1700-1600	C=C
1500-400	Finger print region

Major advantages of this method over dispersive instruments are increased light throughput, short analysing time and high precision of the wavenumber of the spectrometer.

Infrared Spectra of the Used Polyvinyl Polymers

Figure 4.10 shows the FT-IR spectra of pristine PVF, PVAc, PVA and PMMA foils. They represent the starting situation of the ion irradiation experiments. According to the literature [76, 77], the major absorption bands of these polymers are described below.

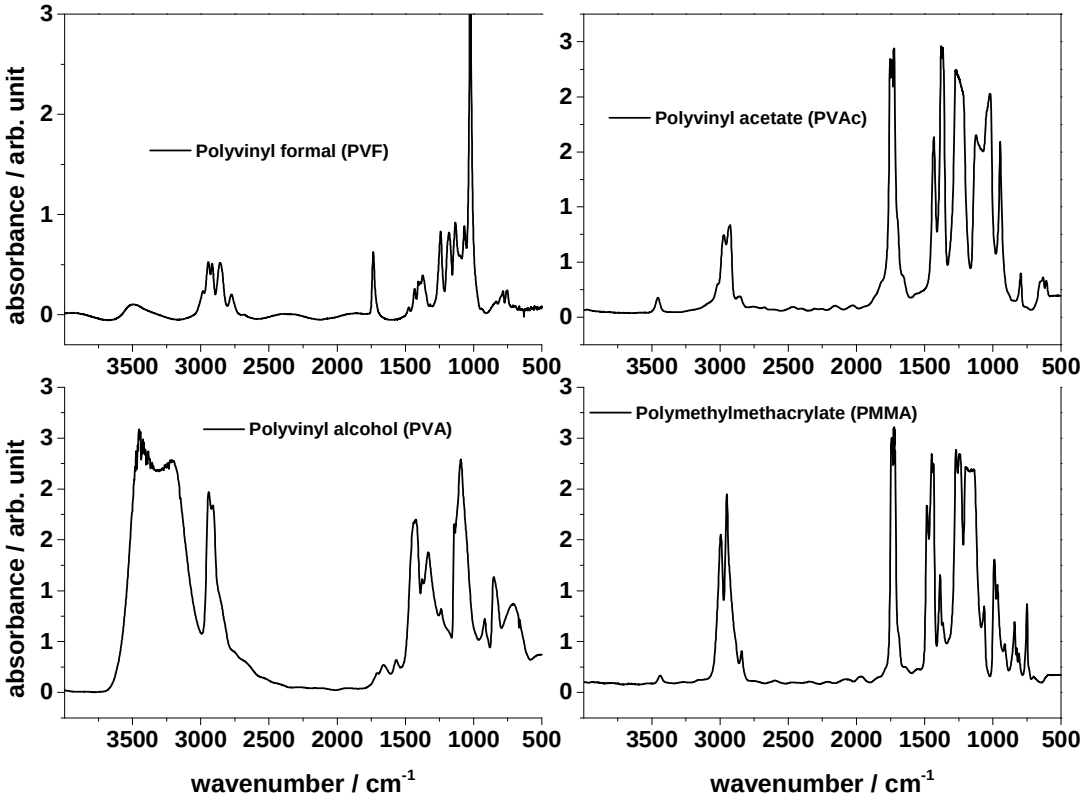

Figure 4.10: Infrared spectra of pristine PVF, PVAc, PVA and PMMA.

PVF: A very broad characteristic absorption peak centred at about 3490 cm^{-1} originates from the stretching vibration of the –OH groups. This broad band results from a combination of the -OH stretching vibration of the vinyl alcohol unit (at 3650–2800 cm^{-1}) and of the carboxylic acid (impurity from the hydrolysis of the ester) around 3000 cm^{-1}, as well as the first harmonic (at 3470 cm^{-1}) of the –O-C=O ester carbonyl vibration of the acetate unit at 1735 cm^{-1}. The five intense absorption bands in the (3040-2700) cm^{-1} region are identified as symmetric and asymmetric modes of the aliphatic –CH, -CH_2 and -CH_3-groups of the polymer backbone of acetale, alcohol and acetate. The strong sharp band at 1735 cm^{-1} is attributed to the stretching vibration of the carbonyl group of the acetate side chain. The fingerprint region between 1500 and 500 cm^{-1} contains a complex series of absorption bands. These may be ascribed to 1) stretching C-O vibrations, 2) wagging, twisting and rocking vibration of the chain –CH_2 group, 3) out-of-plane bending vibrations of the polymer

backbone and formal groups. According to the literature the bands at 1018 cm^{-1} correspond to the out-of-plane bending vibration of the –CH bands [78] and have a very high absorbance compared to the other bands in this region. The vibration band at 1372 cm^{-1} is assigned as in-plane bending vibration of -CH. The band at 1432 cm^{-1} is described in literature as wagging -CH_2 vibrations, and 780 cm^{-1} originates from stretching and rocking C-O vibrations. According to literature data [74, 79-81], the band at 749 cm^{-1} is assigned to the O-C=O in-plane bending vibration.

PVAc: A broad band is found at 3456 $cm^{-1}$of polyvinyl acetate assigned as the first harmonic of the ester carbonyl vibration (2 × O-C=O) at 1736 cm^{-1}. The typical four vibration bands of aliphatic groups (3001, 2970, 2925 and 2851 cm^{-1}) assigned to symmetric and asymmetric vibration modes show weak absorbance. A band at 1736 cm^{-1} is identified as carbonyl stretching vibration. The region from 1700 to 500 cm^{-1} is composed of stretching -C-O vibrations, rocking, wagging and twisting vibration of –CH_2 groups, out of plane bending vibrations of –CH chain and one or more stretching vibrations of the polymer chain.

PVA: The characteristic vibration bands of PVA can be assigned to the vibration of C-OH, C-H, C=O and C-O bonds. Above 3000 cm^{-1}, the absorption of PVA gives indication of a broad and very strong absorption band, which derives from the stretching vibration of the hydroxyl group (at 3650-2800 cm^{-1}). In the wavenumber range (3000-2800) cm^{-1} PVA exhibits two absorbance bands at 2943 and 2912 cm^{-1}. They correspond to the symmetric and asymmetric stretching vibration of -CH_2 groups [74]. Three characteristic vibration bands of carbonyl function are found at 1707, 1657 and 1564 cm^{-1}, where the band at 1564 cm^{-1} can be identified as stretching vibrations of C=O groups attached to hydroxyl groups via hydrogen bonds. The bending vibrations of the C-H bands are located at 1427 and 1334 cm^{-1}. The two bands found at 1371 and 1085 cm^{-1} are assigned to the C-O-H bending and C-O stretching coupled with O-H bending vibrations. An absorption band at 1135 cm^{-1} is originating from the C-C and C-O-C stretching vibrations of PVA polymer. At the spectral region of low wavenumbers, the absorption bands at 916 and 848 cm^{-1} can be assigned to the presence of -CH_2 bonds.

PMMA: The main characteristic vibration bands of PMMA can be assigned to the vibration of C-O-C and C-H bonds. Above 3400 cm^{-1}, the absorption of PMMA gives indication of an absorption band of the first harmonic of the ester carbonyl vibration. In the wavenumber

range (3000-2800) cm^{-1} PMMA exhibits three absorbance bands at 2994, 2950 and 2842 cm^{-1}. They correspond to the symmetric and asymmetric stretching vibrations of $–CH_3$, $-CH_2$ and –CH groups of side chains and backbone. The vibration band of the ester function is to be found at 1740 cm^{-1}. The deformation vibrations of the C-H bands are located at 1448, 1437 and 1387 cm^{-1}. The vibration bands at 1273, 1241, 1196, 1143 and 1065 cm^{-1} (stretching) and at 987, 967, 910 and 840 cm^{-1} (deformation) are assigned to the vibration of the C-O-C groups.

Table 4.2: IR bands of the used polyvinyl polymers (PVF, PVAc, PVA and PMMA) [77, 82-84]

Wavenumber / cm^{-1}				**Vibrational mode**
PVF	**PVAc**	**PVA**	**PMMA**	
3490	3456	3500-3000	3400	υ(OH)
2982	3001	-	2994	υ(CH)
2945	2970	2943	2950	υas(CH_2)
2917	2925	2912	-	υs(CH_2)
2858	2851	-	2842	υas(CH_2)
2775	-	-	-	υs(CH_2)
1735	1736	1707-1564	1740	υ(C=O)
-	-	-	1448	δas(CH_3)
1432	1433	1427	1437 - 1387	δ(CH_2)
1372	1367	1371	-	δg(CH_3)
-	-	1334	-	δ(C-CH_3)
-	1274	-	1273	υ(C-O-C)
1241	1217	-	1241	υ(C-O)
1180	-	-	1196	υ(C-O-C)
1133	1128	1135	1143	υ(C-C-C) υ(C-C-O)
1068 - 1019	1017	-	1065	υ(C-C)
-	946	916-848	987-827	r(CH_3)
-	796	-	810 - 750	r(CH_2)
780 - 749	633	-	-	δ(CH3CO)
-	607	-	-	δ(CH3COO)

Infrared Spectra of the Used Fluoropolymers

Figure 4.11 shows the IR spectra of pristine PVDF, ETFE, PFA and FEP foils. The characteristic absorption bands are discussed according to the literature as follows:

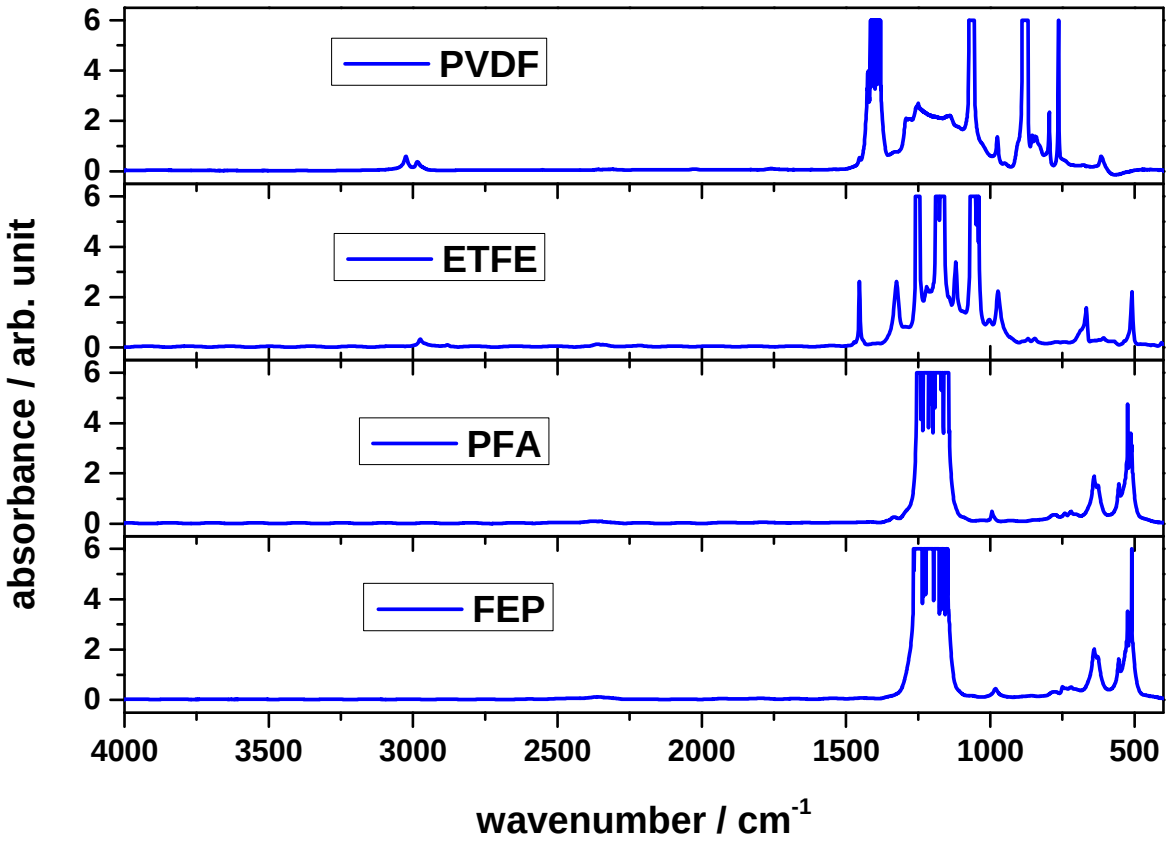

Figure 4.11: Infrared spectra of pristine PVDF, ETFE, PFA and FEP foils.

PVDF

The two absorption bands in the 3040-3000 cm^{-1} region are identified at 3024 and 2985 cm^{-1} as symmetric and asymmetric modes of the aliphatic $–CH_{2}-$ groups.

ETFE

Characteristic vibration bands of pristine ETFE foil can be found in the wavenumber range 3000-2800 cm^{-1} exhibiting two absorption bands at 2975 and 2881 cm^{-1}. They correspond to the symmetric and asymmetric stretching vibration of –CH and $-CH_2$ groups. At the low wavenumber region (1500-500 cm^{-1}), several absorption bands can be assigned to the presence of hydrocarbon and C-F bonds.

PFA

The major absorption bands of pristine PFA are found at low wavenumber region and are at 994 and 775 cm^{-1} as well as at 741 and 720 cm^{-1} assigned as the $–CF_3$ vibration bands. Other absorption bands above fingerprint region (550-500 cm^{-1}) indicate the presence of C-H and C-F bending vibration [74, 85].

FEP

Characteristic absorption bands of pristine FEP foil are found at low wavenumber regions e.g. 982, 779, 749, 642 and 704 cm^{-1}, which are assigned as the $–CF_3$ and –CH vibration bands [74, 85]. As the individual structure of PFA and FEP is very similar differing only by the presence of oxygen atoms in the PFA they show very similar IR absorption bands observed by FT-IR spectroscopy.

The spectral assignments of fluoropolymers are presented in Table 4.3 [86, 87]. It is important to note that the assignments of the fingerprint region are complex and can be misinterpreted due to overlapping of bands.

Table 4.3: IR bands of the used fluoropolymer materials (PVDF, ETFE, PFA and FEP)

Wavenumber / cm^{-1}				**Vibrational mode**
PVDF	**ETFE**	**PFA**	**FEP**	
3024	2975	-	-	$\upsilon as(CH_2)$
2985	2881	-	-	$\upsilon s(CH_2)$
1453	1454	-	-	$\delta(CH_2)$
1424- 1379	1325	-	-	$\delta(CH_2)$
1279	1258-1244	1247 - 1144	-	$\upsilon as(CF_2)$
1258-1140	1219-1210	-	-	$\upsilon s(CF_2)$
1075 - 1062	1069 – 1004	-	-	υas(C-C) υs(C-C)
976	974	994	982	τCH_2
883- 870	870	775	779	υs(C-C)
854 - 796	846	-	-	$\rho(CH_2)$
-	-	-	-	$\rho(CH_2)$
765	-	741-720	749	$\delta(CF_2)$
615	608	628	630	$\omega(CF_2)$
532	509	532 - 509	521 - 512	$\delta(CF_2)$
489	-	-	-	$\delta(CF_2)$
409	407	-	-	$\rho(CF_2)$

Experiment setup for post irradiation and on-line IR spectroscopy

The off-line FT-IR spectral measurements were performed with a NICOLET spectrometer of Magna-IR 550 with TGS detector.

On-line FT-IR measurements were performed using a NICOLET 6700 spectrometer of Thermo Fisher Scientific. A novel setup for on-line FT-IR spectroscopy at M3 beamline is discussed in chapter M3-beamline.

For both processes, four successive scans were recorded in the range of (4000-400) cm^{-1} and the average was taken for each spectrum. The resolution of the spectrum was 2 cm^{-1}. The software OMNIC 7.0 was used for data processing.

4.3.2 UV-Vis Spectroscopy

UV-Vis spectroscopy is used to analyse the intensity of electromagnetic radiation in the ultraviolet (wavelength range between 100 and 400 nm) and visible range (wavelength range between 400 and 900 nm) that is absorbed when UV-Vis radiation is passing through a material. The molecules with electromagnetic waves in the visible and ultraviolet light are stimulated by valence electrons of the outer shells. The characteristic absorption bands of organic molecules are presented in Table 4.4 [74].

Table 4.4: characteristic absorption of organic chromophores

Chromophor	Transitions	Examples	Absorption wavelength / nm
C-H	σ- σ^*	CH_4	122
C-C	σ- σ^*	C_2H_4	135
-O-	n- σ^*	H_2O	167
-O-	n- σ^*	H_3C-OH	183
C=C	π- π^*	C_2H_4	165
C=O	n- π^*	C_2H_4O	296
C=O	π- π^*	C_3H_6O	187
C=O	n- π^*	C_3H_6O	273

The electronic transitions resulting from the absorption of UV-Vis can occur between the energy levels of the molecules in the valence band (VB) and conduction band (CB). For the material with incident photons of energy values less than the separation between the two bands, no absorption is observed. On the other hand, the photons with energy greater than or equal to the separation between the bands are absorbed by electrons between the two schemes. For a solid with zero absolute temperature that edge should be sharp and located in the value of the energy separation between VB and CB, also known as optical gap *Eg*. Tauc plot [88] is used to determine the optical band gap defined by:

$$Ahf = C(hf - E_g)^m \qquad 4.1$$

where *h* is the Planck constant, *f* is the frequency of UV-Vis, A is an absorption coefficient, and C is a dimensional constant indicating the type of electronic transitions. The energy absorption of the investigated molecule gives information about the absorption edge and band gap E_g of a material [89]. Figure 4.12 depicts an example of a Tauc plot of pristine ETFE foil.

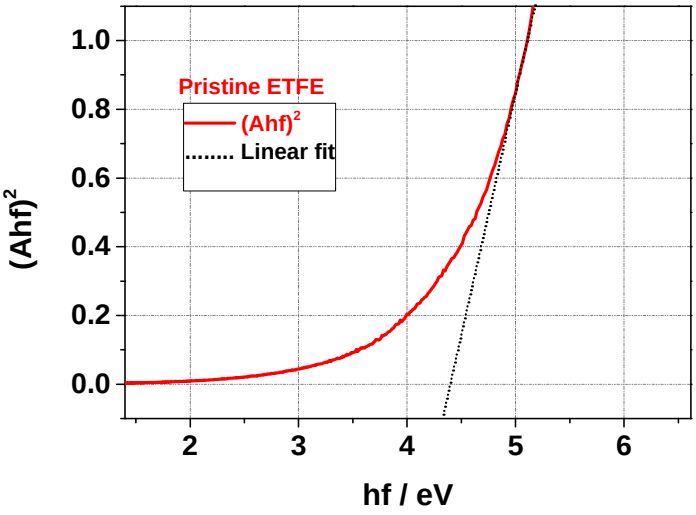

Figure 4.12: An example Tauc plot of a pristine ETFE.

An example UV-Vis spectrum of pristine ETFE foil is presented in figure 4.13. This simple spectrum shows the wavelength range from 200 to 900 nm. Ion irradiation causes the increase of the absorption edge. Polymer samples having low band gap E_g are considered as semiconductors. Ion induced material properties are analysed by determining the different energy gaps.

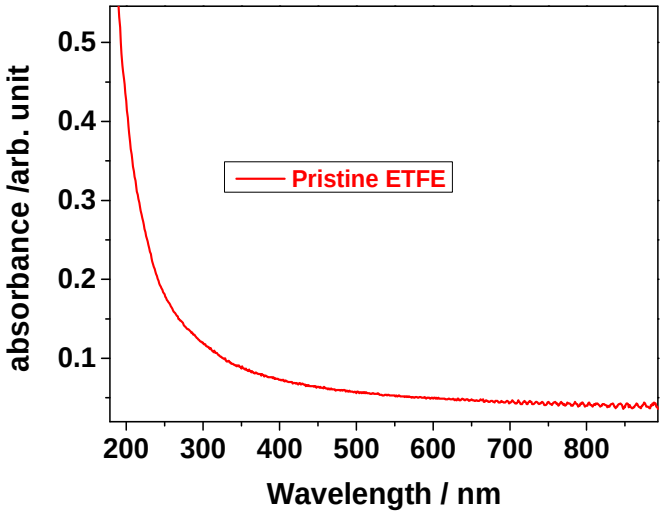

Figure 4.13: UV-Vis spectrum of pristine ETFE foil of 25 µm thickness.

Experimental set-up for UV-Vis spectroscopy

The UV–Vis spectroscopy was performed with a double beam spectrometer (UV4) of Unican, in the range of 190–900 nm with resolution of 2 nm. In this study the formation of new bonds caused by ion induced degradation was investigated.

4.3.3 Residual Gas Analysis (RGA)

In addition to the spectroscopic techniques, other techniques like Residual Gas Analysis (RGA) can provide important information about the radiation degradation of polymers [90]. This technique is applied to determine the composition of gases emitted during the irradiation of the polymer. The fragments generated within different polymers are detected considering their original structures. Moreover, the analysis of the gases emitted after irradiation can also provide information about the diffusion constants of gases in irradiated materials [91, 92].

The RGA is a mass spectrometric technique to detect leaks, and desorption in the high vacuum environment (Figure 4.14). The RGA system has three main parts: i) an ionizer; ii) a separator device; and iii) an ion mass detector.

The ionizer is responsible for producing an ion beam of the gases to be analysed.

While there are several ways to ionize molecules, the technique used in most systems is the RGA electron impact ionization. The process consists in producing an electron beam from a heated filament. An electric field is applied to deflect these electrons in the direction of the gas molecules. By collisions between electrons and gas molecules the molecules are ionized and separated from each other depending on their mass-to-charge ratio.

There are several ways to accomplish the separation of mass, with the quadrupole radio-frequency device being the most common systems. The RF quadrupole consists of four cylindrical rods which create adjustable DC and AC electric fields in the region between the rods. Only ions with a certain mass-to-charge ratio can pass through this region and reach the detector. A scan of mass to charge ratio of the ions allows acquiring the mass spectrum. In general this method is called Quadrupole Mass Spectrometry (QMS).

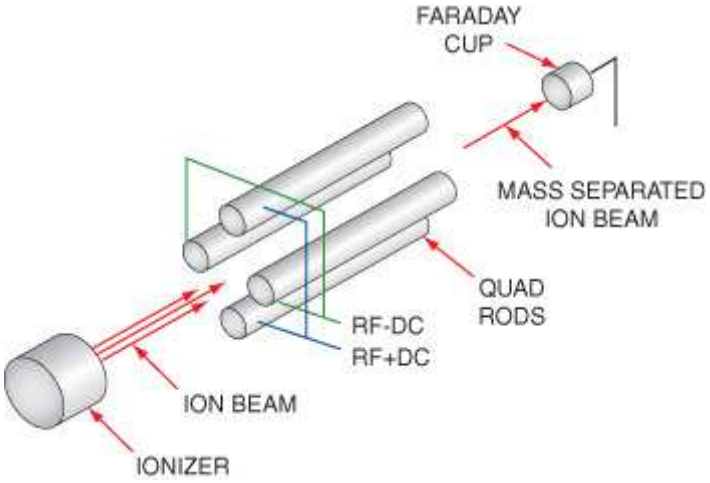

Figure 4.14: Schematics of the Residual Gas Analyser (RGA) containing an ionizer, a separator device and a detector [93].

Finally, the ions pass through the region of the electrical field leading into the detector which is used to measure the intensity. For detection, a Faraday cup or a SEM (secondary electron multiplier) can be used. In the case of higher resolution the electron multipliers are required. The measurement finally results in a mass spectrum containing the detected intensity as a function of the mass to charge ratio. The charge of each ion depends on the conditions of ionization. By tuning the energy of the electrons to a specific value, only single ionization occurs. In this case the spectrum can be analysed only on the basis of mass. Unfortunately this does not guarantee the analysis being easier because the impact with electrons generates typically fragmentation of the gas molecules during the ionization stage. In this case, it is necessary to analyse the masses of the detected fragments and the ratio of the intensities to determine the composition of the original gas. It is important to note that the identification of the fragment of the mass value is not unambigious, since different fragments may have the same amount of mass. Despite these difficulties, knowing the rules of fragmentation of molecules and having a system with good accuracy it is possible to obtain an absolute identification of analysed gases.

Background mass spectrum of the vacuum chamber

Figure 4.15 shows a typical background spectrum from a polymer (PVF) on a sample holder in the vacuum chamber. The spectrum arises from gas desorption from the chamber walls mainly H_2O (m/z=18), leakage, outgassing of the polymer, and to a small extent from the vacuum pump system such as oil from the foepumps. Details will be given later.

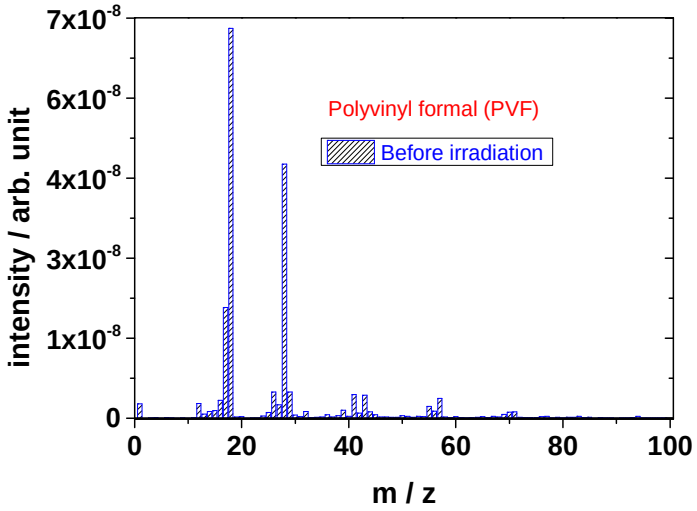

Figure 4.15: Typical mass spectrum of the polyvinyl formal (PVF) on the sample holder as background spectrum.

Experimental setup of RGA

The RGA analysis was performed with a Microvision Plus quadrupole mass spectrometer (QMS) of MKS which provides a detection range between 6.7×10^{-12} and 6.5×10^{-2} Pa. All molecular masses within the range of 0-100 m/z were analysed. All RGA measurements were performed in analogue mode with a resolution of 0.03. The acquisition time of each mass spectrum was approximately 35s and the spectra were acquired continuously throughout the irradiation experiment.

4.3.4 Thermo Gravimetric Analysis (TGA)

TGA is an analytical method in which the weight loss of a material is measured as a function of temperature (T) in a controlled atmosphere. This technique is a standard tool giving useful information about the chemical structure and the degradation behaviour of the analysed sample.

Schematics of TGA analysis are presented in Figure 4.16. The sample is placed in a crucible made of a refractory material and heated in a furnace. The sample holder is coupled to a microbalance, which determines the mass loss during the heating process. A thermocouple near to the crucible measures the temperature. Before the measurement, it is possible to set certain parameters such as final temperature and heating rate. During the analysis the sample chamber is flashed with Argon (Ar) gas [94].

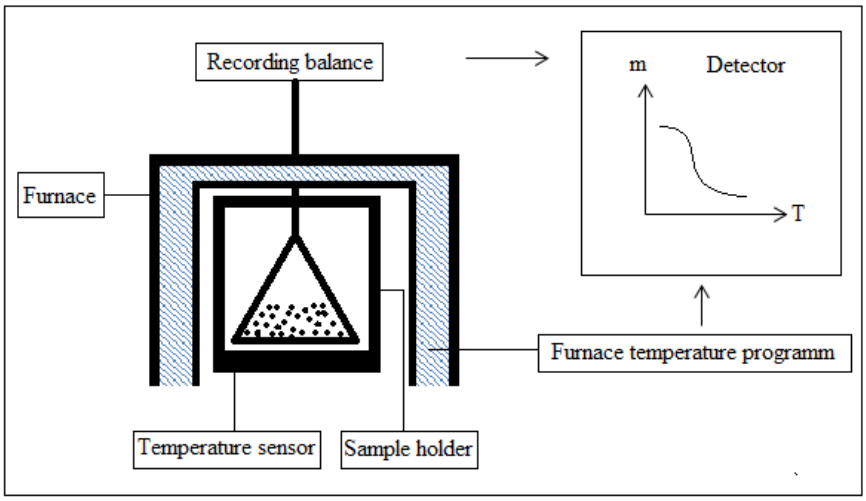

Figure 4.16: Schematics of a Thermo gravimetric analysis (TGA).

This method is used to get information about the thermal stability of polymer materials. The primary atomic bonds of polymer are broken by the thermal degradation process in dependence on the temperature.

The definitions of some important values extracted from TGA curves are introduced below:

Initial decomposition temperature ($T_{(d,0)}$): The weight loss starts to become measurable at this temperature. (The typical value of 5% and 10% was used in this study.)

Half decomposition temperature ($T_{(d,1/2)}$): The weight loss reaches 50 % of its final value.

Maximum decomposition temperature ($T_{(d,max)}$): These are taken from the derivative of the TG curve.

The average activation energy ($E_{(act,d)}$).

TGA analysis of polyvinyl formal (PVF)

Figure 4.17 illustrates the TGA curve of a pristine PVF sample.

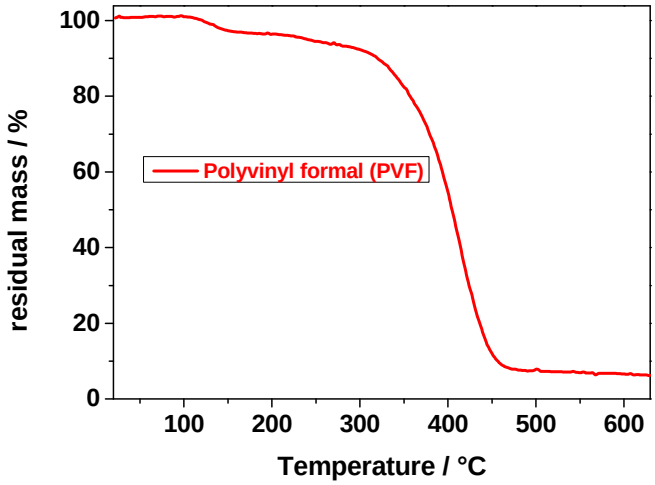

Figure 4.17: TGA analysis of a 20 µm thickness of pristine polyvinyl formal (PVF) foil.

The curve shows two steps: First a small initial weight loss occurs between 104 and 153ºC which is commonly attributed to the release of water absorbed in the polymer. Between ~300°C and 420°C a significant weight loss occurs with around 5% of char residue. The decomposition of nearly the entire polymer indicates that the thermal degradation follows a depolymerisation process and not a so-called random scission process, which would lead to a great amount of char.

Experimental setup of TGA analysis

The TGA measurements were performed with a Simultaneous Thermal Analysis STA 429 from Netzsch GmbH Instrumentation (Selb / Bayern). Crucible material of sample holder was Al_2O_3. The experiment was performed in an inert gas (Ar) atmosphere. The usual flow rate of argon was 75 ml / min. The temperature range was from room temperature up to 630 ° C at a heating rate of 8 K/min. Before each sample measurement, correction measurements were carried out under the same conditions and then subtracted from the sample measurement.

4.3.5 Mass Loss Analysis (ML)

Mass loss analysis [95] is a simple technique to estimate the mass loss induced by the irradiation. About 25 µm thick PVF, PVAc and PVA foils were weighed before (M_0) and after the irradiation (M_{irr}) with an analytical balance from Mettler Toledo (UMX2). The mass loss values of the analysed foils were listed in Table 4.5. Errors, occurring due to handling and due to the analytic balance, were estimated to ± 0.1 mg.

$$Mass\ \ loss\ \ in\ \ \% = \left(\frac{M_{irr}}{M_o} \right) \times 100 \qquad 4.2$$

Table 4.5: Mass loss values induced by ion irradiation for used polymer sample

Sample	Ion	Fluence / ions/cm^2	Before irradiation (M_0) /mg	After irradiation (M_{irr}) / mg
PVF	U	1×10^{10}	5.30	5.20
		3×10^{10}	5.39	5.13
		1×10^{11}	5.85	5.53
		3×10^{11}	5.93	5.17
		6×10^{11}	6.18	4.73
		1×10^{12}	6.65	4.6
		3×10^{12}	7.43	2.73
	Au	5×10^{10}	4.07	4.00
		1×10^{11}	4.97	4.69
		3×10^{11}	3.72	3.14
		1×10^{12}	4.97	4.11
		2×10^{12}	5.42	3.56
		5×10^{12}	7.55	3.50
PVAc	Au	5×10^{10}	4.55	4.40
		1×10^{11}	6.69	6.23
		3×10^{11}	5.21	4.48
		1×10^{12}	4.91	4.09
PVA	Au	5×10^{10}	4.93	4.78
		1×10^{11}	4.35	4.00
		3×10^{11}	5.38	4.86
		1×10^{12}	5.66	4.59
		2×10^{12}	5.69	3.78
		5×10^{12}	4.45	1.65

5. Results and Discussion

5.1 Ion Induced Modification of Polyvinyl Polymers for FAIR – Project [96, 97]

As mentionded before polyvinyl formal (PVF) has been taken as a polymeric model material to investigate radiation-sensitive polymers for the FAIR-project. The complex structure of this random ter-polymer bears three subunits: acetale with a 1,3-dioxane ring (a), alcohol (b), and acetate (c), giving the full name (Poly(vinyl acetale–*co*-vinyl alcohol-*co*-vinyl acetate). For a better understanding of ion induced degradation of this type of polymer a systematic investigation was started, considering reference polymers such as polyvinyl alcohol (PVA) and polyvinyl acetate (PVAc), which are subunits of polyvinyl formal. Polymethyl-methacrylate (PMMA) has been investigated to compare the results with those of the vinyl polymers. In the following experimental resuls of the described methods on PVF, PVA, PVAc and PMMA are discussed in detail.

5.1.1 FT-IR Spectroscopy

5.1.1.1 Polyvinyl Formal (PVF)

Figure 5.1 shows the infrared absorption spectra of 12 µm thick polyvinyl formal foil irradiated with Au ions of a kinetic energy of around 900 MeV at RT.

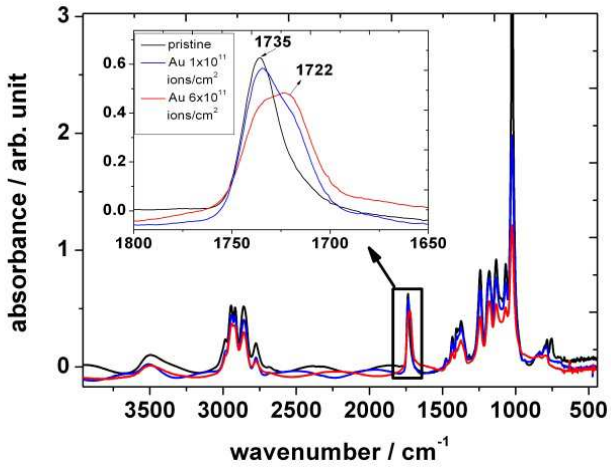

Fig 5.1: FT-IR spectra of polyvinyl formal before (black) and after (blue, red) irradiation with 4.5 MeV/u Au ions performed at RT.

During irradiation all band intensities in the fingerprint region are decreasing with increasing ion fluence. However, the absorption band at 749 cm^{-1}exhibits a considerably stronger decrease compared to all other bands and disappears at a fluence of around 6×11^{11} ions/cm^2. This may be attributed to the breaking of ester bonds when the acetate side chain is eliminated.

Ion irradiation within the explored fluence regime leads to a decrease in intensity of all characteristic absorption bands mirroring the molecular degradation of the polymer. As mentioned before, the strong sharp band at 1735 cm^{-1} is attributed to the stretching vibration of the carbonyl group of the acetate side chain. While during irradiation this band decreases, like the other bands, a new feature appears close to it, a shoulder at around 1722 cm^{-1} (Figure 5.1). Figure 5.2 shows the evolution of the bands at 1735 cm^{-1} (A) and at 1722 cm^{-1} (B) after background subtraction with increasing ion fluence. While the band intensity of A is decreasing due to elimination of the acetate side chain, the production of B, corresponding to a keto group, is increasing and finally saturates at about 3×10^{11} ions cm^{-2}.

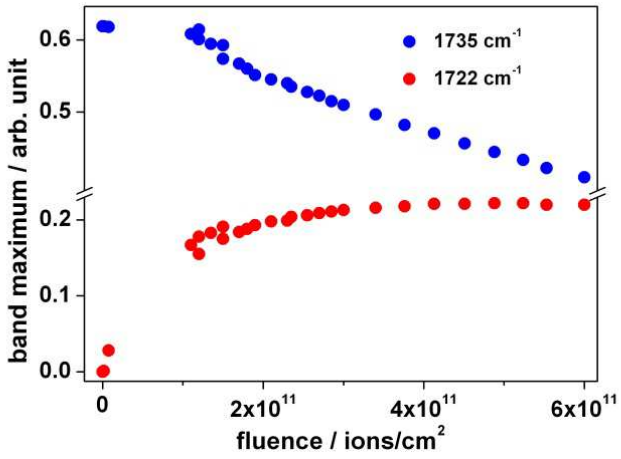

Figure 5.2: Maximum intensity of absorption bands at 1735 and 1722 cm^{-1} as a function of the fluence during irradiation with 4.5 MeV/u Au ions.

Deconvolution of the band at 1735 cm^{-1} of the data set of the irradiated sample (blue curve in zoom of Figure 5.1) using Lorentzian functions yields best results when fitting three bands namely at 1738, 1722, and 1682 cm^{-1} (Figure 5.3 blue, green and black curves). Since ester carbonyl groups typically absorb in the wavenumber region between 1750 and 1735 cm^{-1}, it is suggested that the two latter bands do not originate from the ester group but have rather to be

assigned to a ketone group (1725–1705 cm^{-1}) and a C=C double bond (1682 cm^{-1}) formed by the elimination of hydrogen or water from the vinyl alcohol unit.

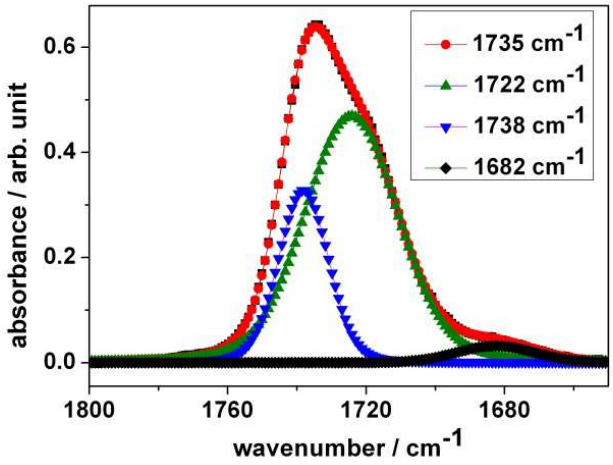

Figure 5.3: Band deconvolution of the irradiated data set using Lorentzian functions as a fit.

Temperature dependent changes in the peak intensity of several representative absorption bands of polyvinyl formal are shown in Figure 5.4. The spectrum of polyvinyl formal at around 40 K is similar to the corresponding spectrum of polyvinyl formal at 290 K and gives very similar results during irradiation, namely (a) an overall reduction in absorption intensity of the characteristic bands and (b) the appearance of a new absorption band around 1722 cm^{-1}.

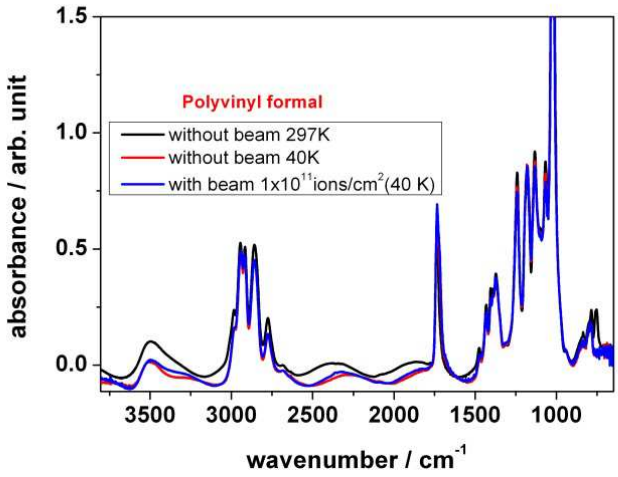

Figure 5.4: FT-IR spectra of polyvinyl formal during irradiation at 40 K and RT.

In summary, it can be stated that ion irradiation of polyvinyl formal leads to a general degradation of the subunits acetal, alcohol and acetate, with scission of the C-C backbone, the acetale ring, and elimination of the side chains of acetate and alcohol. Oxygen-bearing parts with hydroxyl and ester/acetate at the backbone are partially changed into keto groups. C-H bonds are reduced in number, the number of C=C bonds is slightly increased.

5.1.1.2 Polyvinyl Acetate (PVAc)

Figure 5.5 represents the FT-IR spectra of a 20-µm PVAc foil irradiated with Au ions in comparison with the non-irradiated foil (room temperature). The major absorption bands of PVAc has been presented in Table 4.2, according to the literature [76, 77].

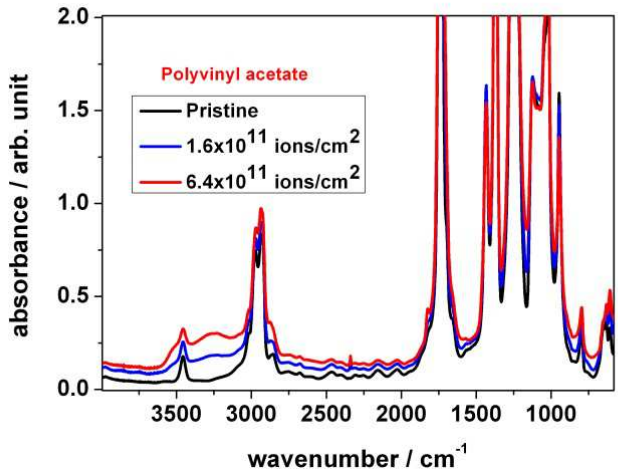

Figure 5.5: FT-IR spectra of polyvinyl acetate irradiated with different fluences.

As shown in Figure 5.5, the wavenumbers and peak intensities of the IR absorption bands changed significantly upon ion irradiation. Once the foil was irradiated with fluence beyond 1×10^{11} ions/cm^2, the background increased, while the intensities of characteristic absorption bands at 3001, 2970, 2925, 2851 and 1736 cm^{-1}, as well as the bands at the fingerprint region from 1700 to 500 cm^{-1} decreased.

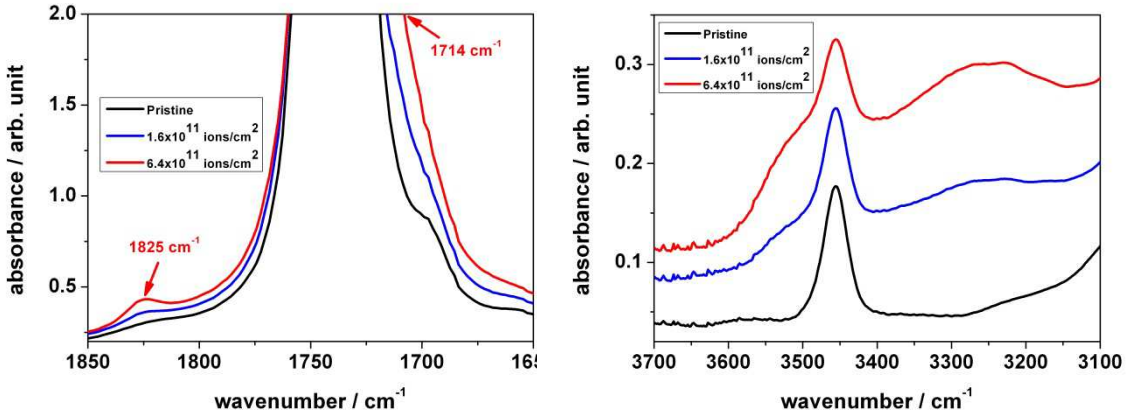

Figure 5.6: Expanded FT-IR spectra of polyvinyl acetate irradiated with different fluences; left: the region of 1850-1600 cm^{-1}, right: the region of 3700-3100 cm^{-1}.

During irradiation the carbonyl stretching vibration band at 1736 cm^{-1} shows a tendency to decrease, while the shoulder at around 1714 cm^{-1}increases (see Figure 5.6 left). This could be interpreted as an additional hydroxyl band. The figure also shows a new band appears at around 1825 cm^{-1}. According to literature [74], the region (1850-1745) cm^{-1} can be assigned to i) acid anhydride ii) peroxy acid or iii) lactone. Peroxy acids, commonly synthesized via reactions of peroxides with carboxylic acid, are unstable molecules and are unlikely to be formed under the given conditions. Acetic anhydride and lactones, the cyclic esters of hydrocarbon acids, such as γ-butyrolactone or δ-valerolactone, can be produced via thermal degradation and therefore could be an explanation for the band. Therefore, the acetate with a ring-forming reaction or the formation of acetic anhydride might be the source of the new band.

During irradiation the overtone peak of acetate band at 3456 cm^{-1} was observed (Figure 5.6 right) to increase in intensity because of a broad absorption band beneath, assigned to -OH. After subtraction of this band the peak area is found to decrease with ion fluence, which is correlated to the increase of the stretching mode of the -OH band. This result supports -OH formation as a consequence of the scission of the ester group of the acetate side chain.

The non-oxidative thermal decomposition of PVAc has been studied by several groups. Throughout the literature, one finds that PVAc in the first step degrades by elimination of acetic acid from the side chain, leading to carbon double bonds. Grassie had claimed that a polyene residue is developed [98], Troitskii et al. described the kinetics [99], and Ballistieri et al. [100] found a two-step process, including elimination of acetic acid as the first step,

followed by the formation of aromatic hydrocarbons. Holland and Hay [101] found new bands at 1600 and 3070 cm^{-1} in the IR spectrum which were assigned to C=C bonds and C-H bonds which are adjacent to C=C bonds. Additionally, they also found indications of the presence of ketones while acetate bands of the side chains at 1240 cm^{-1} decreased in their intensity. They describe a process with elimination of acetic acid and acetic anhydride by hydrolysis, leaving back a hydroxyl group which turns into a keto group by double bond migration. A similar mechanism is formation of ketene, also followed by double bond migration. Additionally they claimed four- and six-membered elimination reactions of acetate side groups, leading to polyenes. They conclude that formation of acetic acid increases as the degradation process proceeds, due to the increasing formation of C=C bonds. Costa et al. [102] investigated the degradation of PVAc in a nitrogen atmosphere. The degradation started at 300° C. The ester bands (-C=O stretching at 1749, -CH_3 bending at 1370 (1365) cm^{-1}, and C-O stretching at 1264 cm^{-1}) were decreased. Double bonds C=C were formed at 990-960 cm^{-1}. Elimination of ketene led to O-H stretching at 3460 cm^{-1}.

Hence, both thermal and ion induced degradation show a reduction of the number of aliphatic C-H groups, elimination of the acetate side groups, and an increase in hydroxyl groups due to the ester scission. Additionally, some formation of keto groups from reaction of the hydroxyl groups was found.

5.1.1.3 Presence of CO_2 Absorption Band

Here, swift heavy ion induced degradation of PVAc foils with different ions, namely U, Au and Xe is discussed. It turns out that, in general, a comparable degradation is found as is known from thermal degradation experiments [98-102] despite the fact that the polymer temperature was low (essentially room temperature). The observation includes not only the decrease in numerous IR absorption bands with increasing fluence but also the formation of new bands assigned to C-C double bonds [101]. Furthermore, ion irradiation even at low fluences gives an additional new feature. Figure 5.7 exhibits the FT-IR spectra of a pristine and an Au irradiated PVAc foil indicating a new absorption band at 2339 cm^{-1}. According to literature it corresponds to the asymmetric stretching vibrations of –CO_2 groups [74]. The appearance of this new absorption band was also found for U and Xe irradiated PVAc foils, as illustrated in Figure 5.8, however, with different intensities. The formation of this band is attributed to the degradation of the polymer, in particular to the bond breaking of the ester side chains which upon further degradation gives CO_2 group.

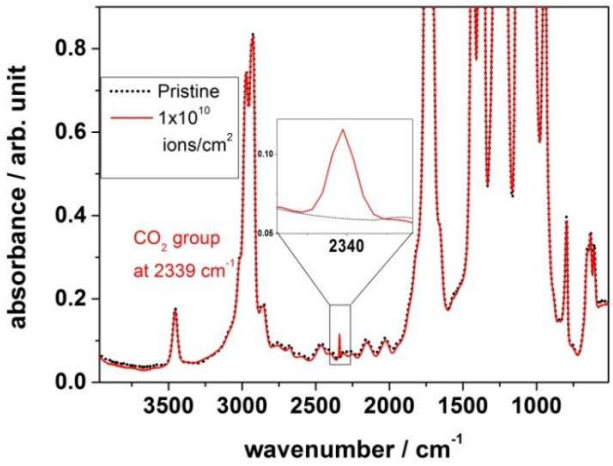

Figure 5.7: FT-IR spectra of 20 µm thick pristine and ion irradiated PVAc foils (Au ion with 4.8 MeV/u kinetic energy). The magnified inset indicates the appearance of the new CO_2 group at 2339 cm^{-1}.

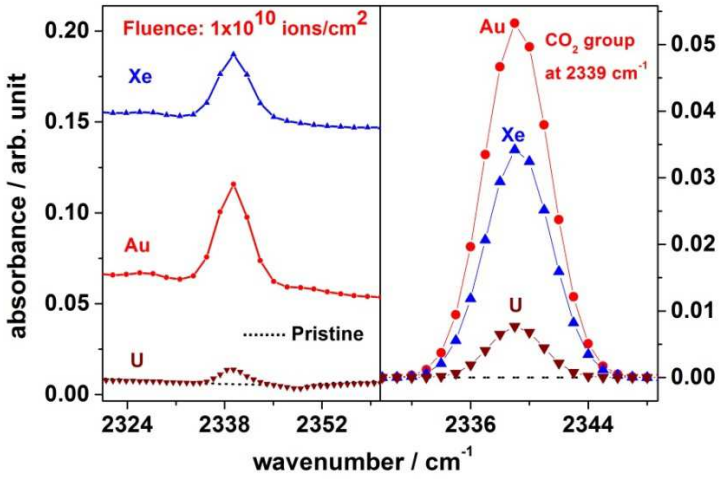

Figure 5.8: FT-IR spectra of the CO_2-region of PVAc, before and after irradiation with U (8.6 MeV/u), Au (4.8 MeV/u) and Xe (11.4 MeV/u) ions (left). For better understanding a zoom of the line was made and shifted them to the same base line (right).

The development of the CO_2 absorption band at 2339 cm^{-1} with ion fluence is shown in Figure 5.9 for the three different ionic species (U, Au and Xe) where the band maxima of the CO_2 groups are plotted as a function of the absorbed fluence. With increasing fluence, the CO_2 absorption bands increase, reach a maximum and decrease again. It turns out that the evolution of the CO_2 band is rather different for U, Au and Xe. The band maximum of the CO_2 band was the highest for Au ion irradiation; it was less for Xe ions and lowest for U ions.

This trend indicates that the degradation, as manifested by the CO_2 appearance, is dependent both on the projectile atomic number and fluence. Since radiation damage scales with the transferred energy dE_e/dx, this result is unexpected, since U with its largest energy transfer is supposed to lead to the largest damage (cp. Fig. 5.8). This apparent contradiction will later be discussed when the complementary results of mass analysis will be shown.

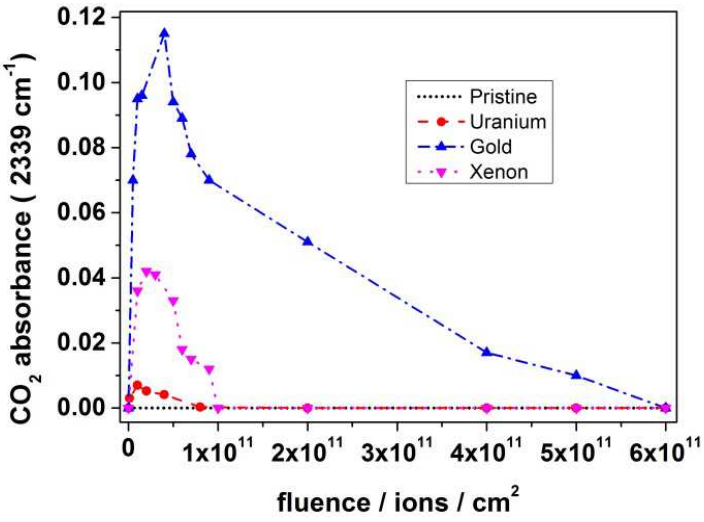

Figure 5.9: Intensity of the CO_2 band at 2339 cm^{-1} as a function of fluence for irradiations with U (8.6 MeV/u), Au (4.8 MeV/u) and Xe (11.4 MeV/u) ions.

In order to investigate the dynamic behaviour of CO_2 evolution and loss, a series of ion irradiation experiments were carried out. When a fluence of about 4.5 x 10^{10} ions / cm^2 was reached, the beam was stopped and the intensity of the CO_2 band was recorded for about 10 minutes after the irradiation (Figure 5.10). The graph shows that the area of the CO_2 band increased with ion fluence, and decreased when the polymer was no longer irradiated. This process was repeated at accumulated fluences of 8.5×10^{10}, 1.4×10^{11} and 2.2×10^{11} ions / cm^2 (Figure 5.11). In each step, the formation of CO_2 is observed under ion irradiation. The decrease is due to its mobility and volatility. It diffuses out of the polymer, desorbs and leaves the solid into vacuum, hence, its IR signal decreases. Clearly, from the very beginning of CO_2 formation under ion irradiation on, the molecules are subject to out diffusion. However, in the beginning, the growth rate is larger than the loss rate, leading to an increase. The rates of CO_2 generation and loss depend on ion atomic number and fluence.

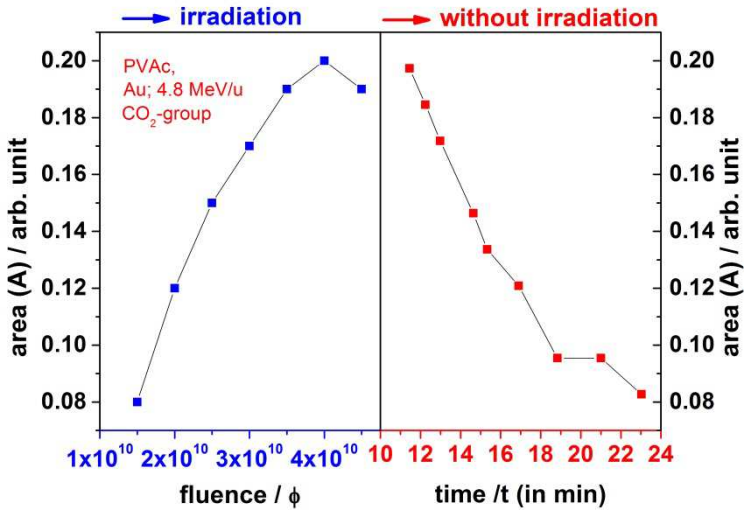

Figure 5.10: The area of the CO_2 band at 2339 cm^{-1} increases as a function of fluence (left) and decreases after irradiation (right).

A similar behaviour has been found by Severin et al. for ion irradiation of Polyimide (PI) at low temperature [13]. At cryogenic temperature the CO_2 band appeared and disappeared during heating up.

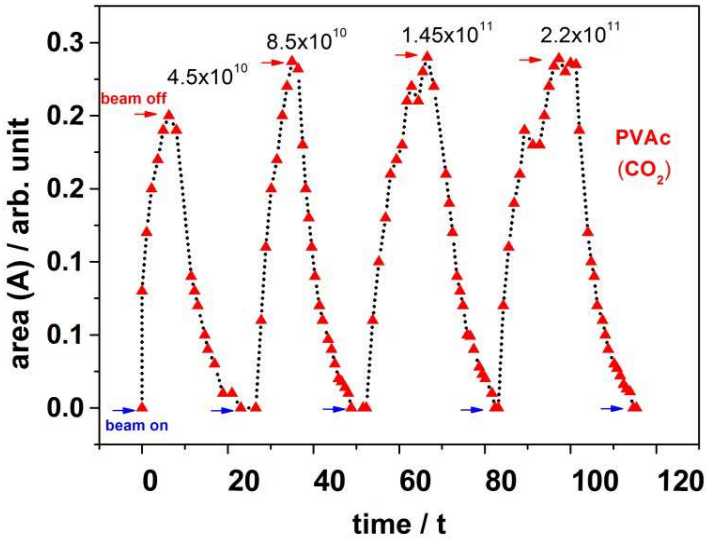

Figure 5.11: Area of CO_2 band at 2339 cm^{-1} as a function of time for irradiations with Au ions of 4.8 MeV/u.

5.1.1.4 Polyvinyl Alcohol (PVA)

Figure 5.12 shows the FT-IR spectra of irradiated polyvinyl alcohol in comparison with the non-irradiated foil.

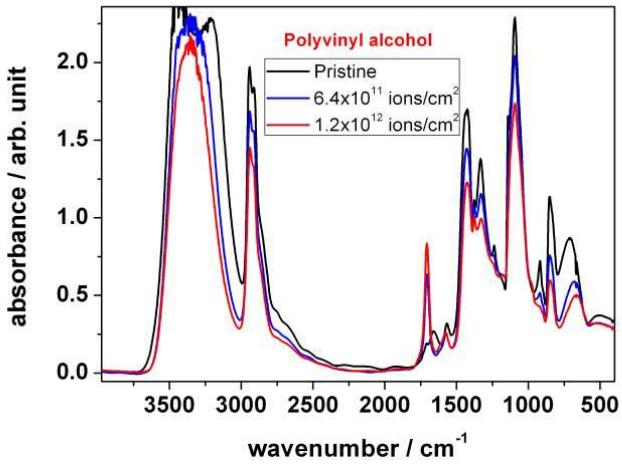

Figure 5.12: FT-IR spectra of polyvinyl alcohol, comparing the unirradiated material with the one treated with two different ion fluences.

The peak intensities of the IR spectra changed significantly with the increase of the number of ions hitting the material. Before irradiation the hydroxyl band (3600-3000 cm^{-1}) shows a noisy peak, which is due to the high absorbance saturation effect. During irradiation this band becomes smaller and sharper, which indicates the decrease of the number of hydroxyl groups with an increase in fluence due to their elimination. The peak intensity at 1702 cm^{-1}, corresponding to carbonyl formation, increases and the peak at 916 cm^{-1} of $–CH_2$ bonds disappears. A strong reduction of the number of –OH groups while -C=O increases indicates on one hand that the hydroxyl group is dehydrogenated forming an oxygen double bond, on the other hand the hydroxyl group can be eliminated by H_2O formation in combination with backbone hydrogen abstraction leading to the loss of $–CH_2$ by C=C double bond formation.
This mechanism seems to be similar to the one found for thermal decomposition. Tsuchiya and Sumi carried out an early investigation on non-oxidative thermal decomposition of PVA [103]. They state that the mechanism is based on elimination of the –OH group as water, leaving a conjugated polyene structure behind. Scission of CC bonds leads to formation of mainly terminal C=O groups with adjacent C=C groups. Thomas et al. described the thermal degradation of Polyvinyl alcohol in a non-oxidizing gas atmosphere, namely nitrogen, with elimination of water from the –OH groups as the first step, followed by pyrolysation [104]. Their IR measurements show a slow decay of the O-H stretching mode at 3370 cm^{-1}, followed

by a sharp drop at around 240° C to very low levels. The C-H stretching mode at 2940 cm^{-1} is less affected at lower temperature, however, does also drop at 240° C. In the same temperature regime, the C=O and C=C stretching modes at 1715 cm^{-1} and 1595 cm^{-1} appear. The melting temperature is in this regime. The authors conclude that chain scission and rearrangement yields the carbonyl group as a product. The C=C modes increase, but only slightly due to formation of aromatic species upon further degradation. Holland and Hay degraded PVA in argon gas between 260 and 290°C [105]. They observed a reduction of –OH bands at 3450 cm^{-1} and of –C-H at 2930 cm^{-1}. At 1705 cm^{-1}, a band assigned to unsaturated –C=O was formed. They explain their observation by elimination of water with formation of a C=C double bond which migrates towards the next hydroxyl group leading to formation of a keto group due to keto-enol tautomerization. This process eliminates the C=C bond, thus explaining the much higher loss rate of –O-H groups in comparison to –C-H groups.

The comparison shows that due to both, heat and ion energy input into PVA, the hydroxyl groups are either eliminated or dehydrogenate into a keto group. Additionally, the CH backbone loses hydrogen, forming C=C bonds.

5.1.1.5 Polymethyl-methacrylate (PMMA)

The FT-IR spectra of pristine and ion irradiated PMMA are represented in Figure 5.13. During irradiation at fluences below 1×10^{10} ions/cm^2 of 4.5 MeV/u Au there were no detectable changes of wavenumber and peak intensity found in the IR spectrum. Apparently, the volume of modified material around the ion tracks is still too low to be differentiated by the spectrometer. However, above a fluence of 1×10^{10} ions/cm^2 the intensities of all absorption bands decreased (Figure 5.13) and two new absorption bands appeared, indicating the formation of carbon double bonds (at 1641 cm^{-1}) and carbon dioxide (at 2340 cm^{-1}).

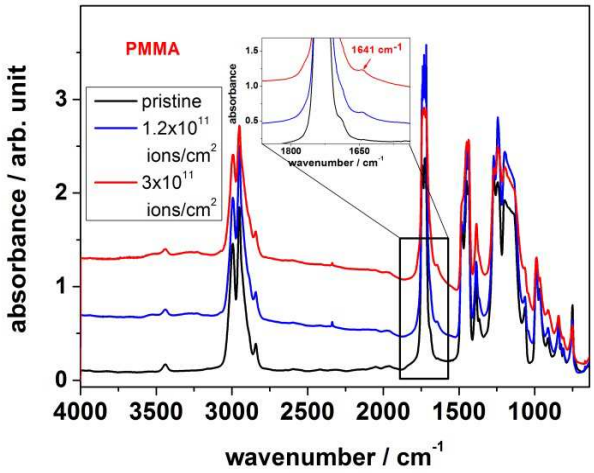

Figure 5.13: FT-IR spectra of the pristine (black) and the irradiated (blue, red) PMMA foil (4.5 MeV/u Au ions).

The investigation of FT-IR spectra of PMMA foil irradiated with He ions (500 keV) gave a new absorption band at 1600 cm^{-1} after irradiation which was explained by cross-linking of the material [106] and a slow decrease of the modes assigned to the carboxylic ester. Swift heavy ion irradiation of the present study, however, led to a considerable decrease of all band intensities, including side chains and backbone, and the two new above mentioned bands were observed. Comparison of ion induced changes by light and heavy mass ions shows that heavy ions with their electronic energy loss an order of magnitude higher than the light mass ions induce much more damage for a given fluence, as it was to be expected.

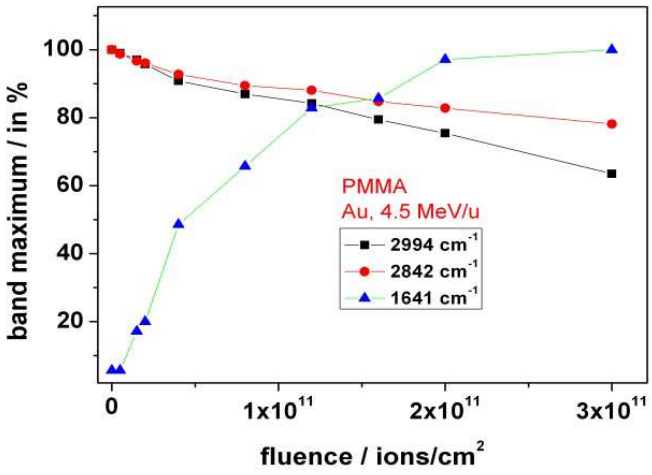

Figure 5.14: Maximum intensity of absorption bands at 2994, 2842 and 1641 cm^{-1} as a function of the fluence during irradiation with 4.5 MeV/u Au ions.

In order to show the evolution of the materials modification process, the maximum band intensities (in %) of bands at 2994, 2842 and 1641 cm^{-1} are plotted as a function of fluence in Figure 5.14. The intensities of the bands at 2994 and 2842 cm^{-1} of the hydrocarbon groups are decreasing with increasing ion fluence, with the curve following to first order a logarithmic function. The increasing absorption band at 1641 cm^{-1} indicates radiation induced creation of carbon double bonds. When they are conjugated becoming polyenes, it is to be expected that PMMA loses its characteristic material properties such as high optical transmission and electrical resistivity.

5.1.2 Residual Gas Analysis

As mentioned before, the analysis of ion induced fragmentation into small volatile molecules was performed by means of mass spectrometry (residual gas analysis (RGA)). On-line analysis of the gases outgassing from the polymer into the vacuum chamber gives detailed information about the volatile degradation products produced during irradiation of polymer samples. In the following, the individual behaviour of PVF, PVAc, PVA and PMMA are discussed.

5.1.2.1 Polyvinyl Formal (PVF)

Complementary to IR structural analyses of the irradiated material, mass spectrometry was performed giving information about the volatile degradation products. Figure 5.15 shows a typical mass spectrum of PVF together with the ones of PVAc and PVA recorded at room temperature during irradiation with a flux of 2×10^7 Au ions/cm^2 s at around 900 MeV kinetic ion energy.

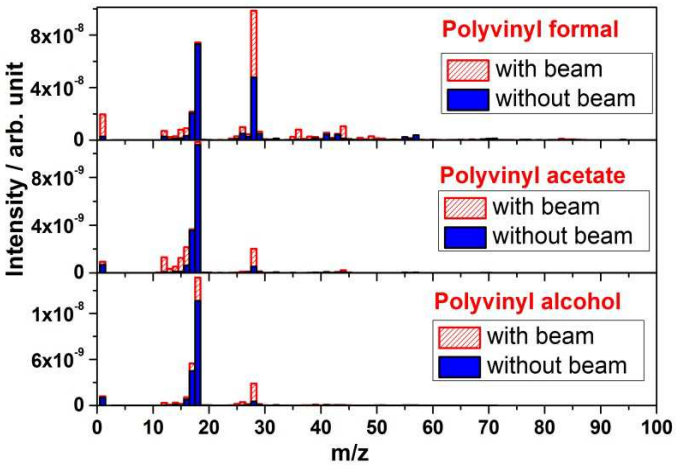

Figure 5.15: Outgassing spectra of polyvinyl formal, polyvinyl acetate and polyvinyl alcohol polymers at RT recorded on-line during irradiation with 4.5 MeV/u Au ions.

All molecular masses within the range of 0-100 m/z were checked for changes in comparison to the situation without ion irradiation. The vacuum chamber with the polymer on the sample holder shows a typical background spectrum, arising from gas desorption from the chamber walls, leakage, outgassing of the polymer, and to a small extent from the vacuum pump system such as oil from the forepumps, as mentioned before.

It is observed that outgassing of PVF under ion bombardment leads to an intensity increase of volatile species like hydrogen (H_2, m/z=2), carbon (C, m/z=12), oxygen (O, m/z=16), hydroxyl (OH, m/z=17), water (H_2O, m/z=18), carbon monoxide with some contribution of ethene (CO/C_2H_4, m/z=28), ethyne (C_2H_2 m/z=26), carbon dioxide and acetaldehyde (CO_2/C_2H_4O, m/z=44), and some larger species such as $C_4H_yO_2$ (m/z = 83–86), and to species not corresponding to regular molecules, either ionic or radical, like C_2H_3O(m/z = 43) and C_3H_5O (m/z=57). During irradiation of polyvinyl formal, a new volatile molecule appears at m/z=36. According to the mass number, the only reasonable molecule would be the doubly charged ion of $C_3H_4O_2$. This interpretation, however, requires a peak of M^+ (singly charged $C_3H_4O_2$) at m/z=72. Since there is no according mass to be found in the spectrum, additional chemical elements have to be considered. One possible interpretation of this peak at m/z=36 may be derivatives of HCl. During the preparation of polyvinyl formal foil, CH_2Cl_2 has been used as a solvent, which might be a precursor of the outgassing product hydrochloride (HCl) during irradiation. The number of fragment masses is smaller for PVAc and PVA, since they are less complex compared to PVF with its additional acetale ring subunit.

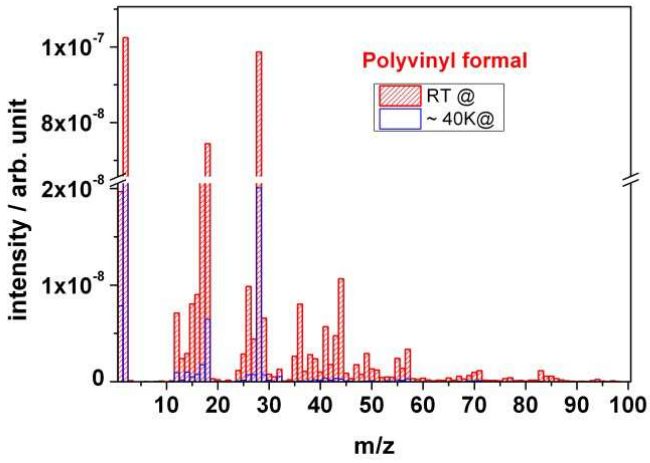

Figure 5.16: Outgassing spectra of a polyvinyl formal foil at RT and 40K recorded on-line during irradiation with 4.5 MeV/u Au ions.

Figure 5.16 compares the outgassing fragments of PVF at cryogenic and room temperature irradiations. At cryogenic temperature (CT) the spectrum is characterized by the presence of large H_2 (m/z=2) and CO (m/z=28) peaks, where H_2 is the major gas species formed compared to smaller peaks of C, O, H_2O, C_nH_x. The masses with possible fragments are presented in Table 5.1 together with their relative intensities and probable compound assignments. Under cryogenic conditions, most of the mass signals are significantly smaller

compared with those of room temperature (RT) irradiation. While the boiling point of hydrogen (H_2) is very low and thus the gas is not immobilized at 40 K, other molecules are kept in a frozen state, particularly the large ones such as acetic acid and larger ketones and aldehydes. Water from the polymer would also be frozen; however, this signal does also arise from the vacuum chamber and is therefore still significantly recorded.

In the cryogenic case, it is the combined effect of the direct gas radiolysis and the gas transport out of the matrix which determines which volatiles will most likely be present in the vacuum chamber and will be detected by the mass spectrometer.

Table 5.1 shows that polyvinyl formal is broken up into a large number of fragments upon ion irradiation. The main product in all cases is hydrogen which is the main component of the polymer with respect to atomic percentage. The acetale subunit bears 10 H atoms (+ 6 C atoms and 2 O atoms), in acetate the atomic ratio H:C:O is 6:4:2 and in alcohol 4:2:1. Since the ion beam cuts all bonds easily, the process will release large quantities of hydrogen. From the hydrocarbon backbone, C_xH_y fragments of different sizes are cut out, mainly the small ones with 1, 2 or 3 C-atoms. Since all subunits bear O atoms, oxygen itself, and its compounds with H and C are formed. Therefore, water/hydroxyl on one side, and carbon oxides and aldehydes and ketones on the other side are formed. The amount of smaller fragments, such as formaldehyde and acetaldehyde, is larger than the bigger ones, such as butenal.

The appearance of the large number of fragments can be explained by opening of the acetaledioxane ring with multiple scission, side-group elimination of acetate and alcohol, and backbone scission.

Table 5.1: Outgassing fragments of polyvinyl formal during irradiation at room temperature (RT, 297 K) and cryogenic temperature (CT, 40 K); (r/i) means radical/ion

m/z	Fragments	Possible compounds	Intensity at RT [in %]	Intensity at CT [in %]
2	H_2	Hydrogen molecule	100	64
12	C	Carbon (r/i)	7	1
13-15	CH_{1-4}	Hydrocarbon (r/i): methyl, carbene	2-8	0.2-0.9
16	O	Oxygen (r/i)	9	0.7
17	OH	Hydroxyl (r/i)	2	1.7
18	H_2O	Water	73	6
24-30	C_2H_{0-6}	Hydro(di)carbon (r/i)	0.4-10	0-0.7
28	CO / C_2H_4	Carbon monoxide/ Ethene	96	20
29	CHO	Formaldehyde (r/i)	6.4	0.7
30	CH_2O	Formaldehyde	0.8	0.2
32	CH_3OH	Methanol	1.2	0.5
37-41	C_3H_{1-5}	Hydro(tri)carbons	1-5	0-0.3
42	C_2H_2O	Ketene	1.7	0.2
43	C_2H_3O	Acetaldehyde (r/i)	5	0.3
44	CO_2 / C_2H_4O	Carbon dioxide / Acetaldehyde	10	0.2
57	C_3H_5O	Acetone (r/i)	3.3	0.3
58	C_3H_6O	Acetone	0.3	b
59	$C_2H_3O_2$	Acetic acid (anion)	0.2	b
60	$C_2H_4O_2$	Acetic acid	0.3	b
66	C_5H_6	Cyclopentadiene	0.1	b
70	C_4H_6O	Butenal	1.0	b
83-84	$C_4H_{3-4}O_2$	Diketene, Dioxin, Furanone	1.1-0.6	b
85-86	$C_4H_{5-6}O_2$	Methacrylic acid (r/i), Butenoic acid, Butanedione, γ-Lactone	0.6-0.3	b

b: below limit of detection

5.1.2.2 Outgassing During Heating Up

In Figure 5.16 it has been shown that ion beam induced degradation of polyvinyl formal at a temperature of 40 K had yielded considerably less masses and mass intensities of fragment molecules. In principal, there are two possible explanations for this observation: one is that the radiation damage is lower at cryogenic temperature, the other one, as mentioned before, is that the fragment molecules have been trapped in the polymer matrix in a frozen state. The latter explanation is more likely since, according to the FT-IR result, the polymer is also degraded at low temperature. In order to check whether or not small fragment molecules have been trapped at low temperature, the sample was slowly heated up to RT in order to set the molecules free. Figure 5.17 shows a plot of outgassing profiles of four masses as a function of the temperature. It turns out that the gas release starts immediately when the temperature rises above 40 K. Mass m/z=28 is the major outgassing product.

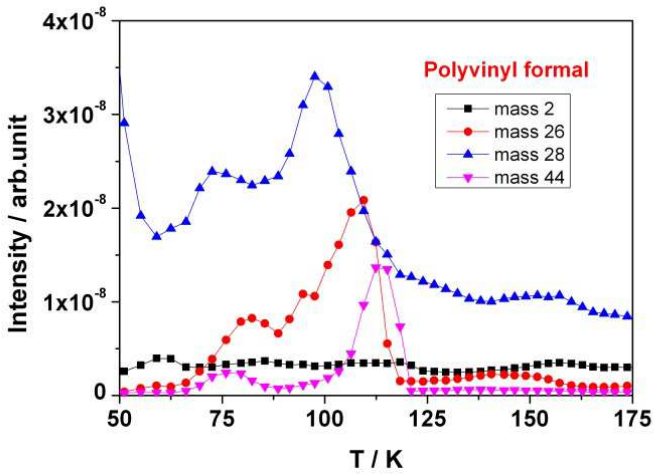

Figure 5.17: Outgassing profiles of different masses m/z during heating of polyvinyl formal after the exposure to 4.5 MeV/u Au ions.

The graph shows that two peaks appear in the low temperature region at 73 K and 98 K during heating up. This is an indication that either the species is trapped in two binding states, which is not likely, or that there are two molecules of the same mass. For m/z=28, two compounds are reasonable: CO and C_2H_4. Their boiling temperatures at normal pressure give an indication of the sequence of appearance during heat up: while carbon monoxide boils at 81.5 K, the boiling temperature of ethane is 169.5 K. As a consequence, the peak at 73K can most likely be assigned to carbon monoxide and the peak at 98K to ethene. In the temperature region (65-130) K peaks appear of m/z=26, m/z=28 and m/z=44, corresponding to ethyne (m/z=26), carbon monoxide/ethene (m/z=28), and carbon dioxide / acetaldehyde (m/z=44). In

the latter case, the compound evaporating at higher temperature shows a larger peak area, indicating that the aldehyde is the main product, in accordance with the mechanism postulated on the basis of FT-IR and MS measurements. The boiling of H_2 is not visible at 40K because it is below the presented temperature area. This is consistent with the results shown in Figure 5.16.

5.1.2.3 Polyvinyl Acetate (PVAc)

Figure 5.18 shows the mass spectra of polyvinyl acetate before and during ion irradiation at RT. Before the irradiation, characteristic signals appeared at the mass ratio of 17 and 18, corresponding to OH and H_2O, respectively. Upon irradiation, the partial pressures of these molecules were increasing and some new types of molecules and ions appeared, including those of hydrogen (H_2, m/z=2), carbon (C, m/z=12), oxygen (O, m/z=16), hydroxyl (OH, m/z=17), water (H_2O, m/z=18), hydrocarbons (C_nH_x, m/z=13-15, C_2H_2 26), carbon monoxide / ethene (CO, C_2H_4 m/z=28), and carbon dioxide / acetaldehyde (CO_2, C_2H_4O, m/z= 44). Above here latter mass the signals become very small, indicating that heavier fragments are hardly formed (not shown in this spectrum, see Figure 5.15). The mass signal m/z=17 of hydroxyl exhibits only a small intensity in comparison with other outgassing fragments, which indicates that the OH molecule either comes from the H_2O molecule or from -OH formation from an ester group during irradiation. FT-IR spectroscopy of PVAc had shown that a new stretching mode of the -OH band appeared in the region from 3500 cm^{-1} and 3200 cm^{-1} with increasing fluence.

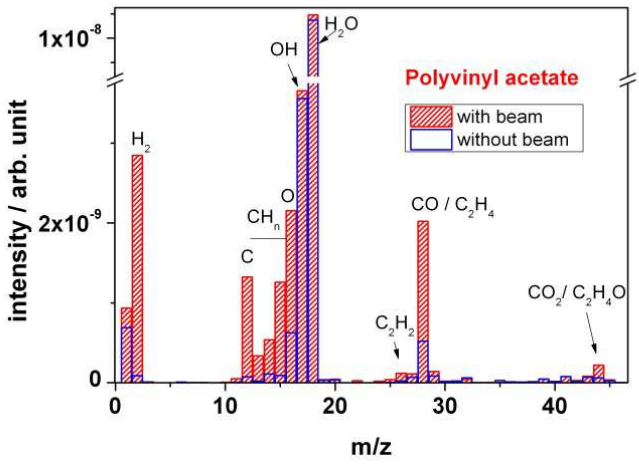

Figure 5.18: Outgassing spectra of a PVAc foil recorded on-line during irradiation with 4.5 MeV/u Au ions.

In thermal degradation, the main product found by Costa et al. [102] is acetic acid, together with minor amounts of keten, water, methane and the two carbon oxides. Blasevska-Gilev and Spaseska [107] found 87% acetic acid, several percent of acetone and benzene, and a few percent of acetaldehyde and cyclopentadiene. The main products came from side chain elimination, followed by breakdown of the unsaturated polymer backbone. The latter took place in a higher temperature regime.

In contrast to these findings, in ion induced degradation we observe a different mechanism. In thermally induced degradation, the scission of the side chain leads to formation of acetic acid, either by reaction of two acetate side chains, or by a bond break between the ester oxygen bridge and the polymer backbone [102, 107]. Under ion bombardment, almost no fragments with masses corresponding to acetic acid or acetic anhydride have been observed. The only fragments found were those with one O atom only which is acetaldehyde. This means that in case of ion bombardment, the side chain is preferentially cleaved within the carboxylate group between the oxygen next to the backbone and the keto carbon atom, leading to an aldehyde as fragment.

The remaining oxygen either creates an alcohol group or becomes a keto group by double bond migration and keto-enol tautomerism. The formation of –OH has been observed with FT-IR, as mentioned above, supporting this mechanism.

The formation of carbon monoxide which appears in large amounts is most likely due to ion induced scission of the formed aldehyde from the side chain and the formed ketone of the backbone. Hence it turns out that ion induced scission leads to smaller fragments, more governed by the high-energy electron excitation process and less by the regular chemical reaction rules.

5.1.2.4 Presence of CO_2

In Figure 5.19 typical mass distributions of PVAc foils recorded before and during irradiation with U, Au and Xe ions are depicted. The results show that only outgassing fragments with small masses appear during irradiation. Before irradiation there were contributions of some molecules or their fragments formed under electron impact ionisation in the mass spectrometer such as carbon (C, m/z=12), oxygen (O, m/z=16), hydrocarbon (CH_n, m/z=12-16; C_2H_n, m/z=25-27), water (H_2O, m/z=18), and carbon monoxide / ethene (CO/C_2H_4, m/z=28). They stem from gas desorption and pump oil residues and leakage, following corresponding measurements of the vacuum system. During irradiation the intensities of H_2,

CH_3, C_2H_4/CO and CO_2 increase. Since leakage and pump residues are independent of the ion beam, the changes must be due to outgassing of the polymer. This directly shows the degradation process by covalent bond breaking of the polymeric chain.

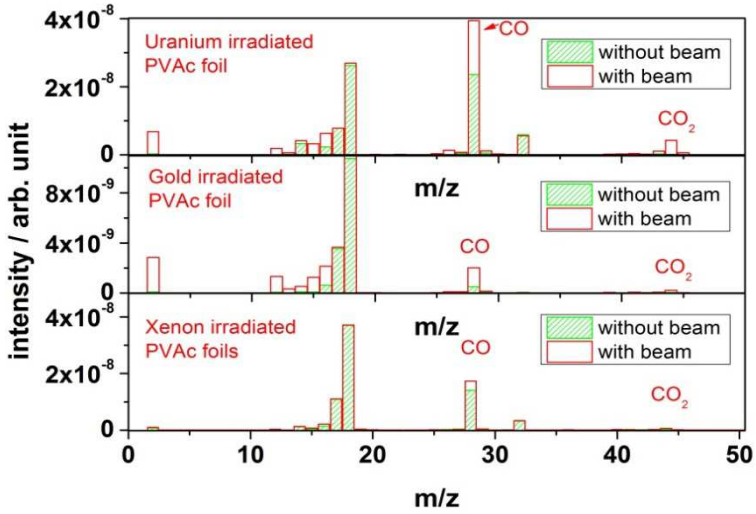

Figure 5.19: Outgassing of PVAc foils recorded before and during irradiation with U, Au and Xe ions.

The mass signal m/z = 44 arising from CO_2 increases with increasing ion fluence. This corresponds to FT-IR spectroscopy with the appearance of a new CO_2 absorption band at 2339 cm^{-1}. Also, the mass signal of CO at m/z=28 increases under ion irradiation. Since pump residues and leakage with nitrogen (m/z=28) are constant, it can be subtracted and the difference must stem from the polymer. The appearance of carbon oxides indicates the covalent bond scission of the oxygen-bearing side chains. The degradation process of the side chain is initiated by homolytic bond scission between the CH_3COO- group and the polymer backbone. The free CH_3COO radical, constituting the dehydrogenated formic acid methyl ester, is unstable and decays into small fragments e.g. to CH_3 which may be hydrogenated to CH_4, and to CO_2. These molecular species have also been found in an earlier investigation on Au ion irradiation of PMMA foils [96]. Another possible reaction step is the bond scission of the ester bond, leading to the observed mass m/z=32, with methanol (CH_3OH) as fragment. This reaction leaves back an aldehyde group which in turn can form CO (m/z = 28) when the C-C bond to the backbone is broken. Hence, the large amounts of CO observed in the mass spectra are most likely due to multiple fraction of the acetate side-chain.

The evolutions of the CO and CO_2 mass signals are considerably differing from each other for U, Au and Xe ion irradiation. The signals are much larger for U ion irradiation in comparison to Au and Xe irradiation. Table 5.2 shows the masses with possible fragments together with

their relative intensities and probable compound assignments. Although normalisation does not strictly give quantitative information, it can be used to see the trend. The maximum intensities of the outgassing mass signals of CO and CO_2 (m/z=28 and 44) show the following sequence: U irradiation >>Xe irradiation > Au irradiation. In contrast, FT-IR spectroscopy showed the evolution of the CO_2 band at 2339 cm^{-1} for different ions following the sequence Au irradiation >Xe irradiation > U irradiation, as discussed in the previous FT-IR section.

Table 5.2: Outgassing fragments of polyvinyl acetate during irradiation at room temperature (RT); the intensities are normalized to the maximum intensity found for mass m/z=28; (r/i) means radical/ion

m/z	Fragments	Possible compounds	Intensity for U-ion irradiation	Intensity for Au-ion irradiation	Intensity for Xe-ion irradiation
2	H_2	Hydrogen molecule	41	18	1
12	C	Carbon (r/i)	12	8	2
13-15	CH_{1-4}	Hydrocarbon (r/i): methyl, carbene	3-19	2-7	0.3-3
16	O	Oxygen (r/i)	25	10	5
17	OH	Hydroxyl (r/i)	0	0.06	1
18	H_2O	Water	4	1	11
24-30	C_2H_{0-6}	Hydro(di)carbon (r/i)	0.5-2	0.1-0	0.1-0
26	C_2H_2	Ethyne	8	0.6	0
28	CO / C_2H_4	Carbon monoxide/ Ethene	100	10	21
29	CHO	Formaldehyde (r/i)	4	0.4	0.3
30	CH_2O	Formaldehyde	1	0	0
43	C_2H_3O	Acetaldehyde (r/i)	5	0	0
44	CO_2	Carbon dioxide	26	1	3

The inverse order in the results of IR spectroscopy and mass spectrometry on CO_2 evolution can be explained as follows: Uranium, being the heaviest projectile, deposits the largest

amount of energy and creates most radiation damage. This gives the largest amount of volatile fragments. It is known that small volatile species are able to diffuse inside the material at enlarged rates by radiation enhanced diffusion where the molecules are able to move along damage tracks [108]. U ions create the largest amount of CO_2, according to mass analysis. On the other hand, IR spectroscopy probes the residual CO_2 in the solid. Therefore, the order is inversed; U gives the smallest CO_2 bands.

5.1.2.5 Polyvinyl Alcohol (PVA)

Figure 5.20 shows the mass spectrum of PVA. The outgassing molecules and atoms of PVA are hydrogen (H_2, m/z=2), carbon (C, m/z=12), oxygen (O, m/z=16), hydroxyl (OH, m/z=17), water (H_2O, m/z=18), hydrocarbons (C_nH_x, m/z=13-15, 26) and carbon monoxide / ethene (CO, C_2H_4 m/z=28), which were found also in PVAc and in PVF. In contrast to PVAc and PVF, hardly any heavier masses are observed. This is due to the fact that PVA has non aliphatic side chain or ring structures.

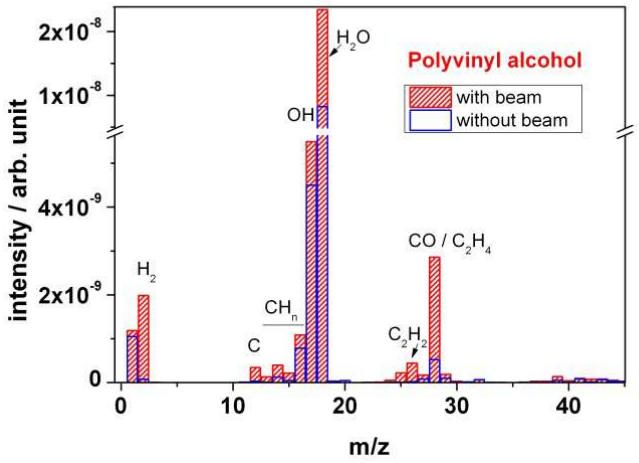

Figure 5.20: Outgassing spectra of a PVA foil at RT recorded on-line during irradiation with 4.5 MeV/u Au ions.

Figure 5.21 depicts the mass spectra of PVA and PVAc polymers in comparison. Concerning the observed species, they appear similar. During irradiation, both polymers show an overall increase in peak intensity of the characteristic fragment molecules. However, in PVA the O-based outgassing fragments (H_2O, OH and CO molecules) at mass signals m/z=18, m/z=17 and m/z=28 exhibit a significantly larger intensity in comparison to that of PVAc polymer, which can be explained by the elimination of the –OH group. The large quantities of CO are due to scission of the keto-bearing backbone, in accordance with the FT-IR observations. In

contrast, peak intensities of other outgassing fragments such as hydrogen (H_2) and hydrocarbon (C_xH_y) of PVA are smaller than the ones of PVAc.

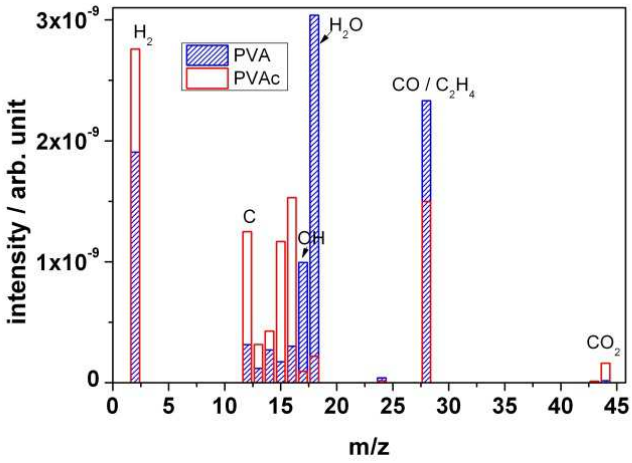

Figure 5.21: Outgassing spectra of PVA and PVAc foil recorded on-line during irradiation with 4.5 MeV/u Au ions.

In thermal degradation studies on PVA, Tsuchiya and Sumi [103] had also found water as the main product, but also aldehydes and ketones, such as acetaldehyde, crotonaldehyde (butenal) and hexadienal, and acetone by means of gas chromatography. Hay and Holland [13] identified gas phase products by IR and found bands of water and saturated and unsaturated ketones and, in particular, aldehydes at 1715 to 1760 cm^{-1}.

These findings are similar to the present results. Apparently, elimination of H_2 with formation of keto groups and elimination of water with formation of C=C double bonds are the main mechanisms both for thermal and ion induced degradation. The difference between the two degradation processes seems to be that in the thermal process reactions to larger fragment units are possible, while in ion induced degradation the fragments remain smaller, in analogy to the observations on PVAc.

5.1.2.6 Polymethyl-methacrylate (PMMA)

Typical mass spectra of PMMA foils are presented in Figure 5.22, recorded before and during irradiation with an ion flux of 2×10^7 ions/cm^2s with 4.5 MeV/u ions of Au. Outgassing fragments of the polymer were mainly found in the lower mass region, up to a mass-to-charge ratio m/z=45. The number of fragments heavier than m/z=45 was small and their intensities were very low, however, masses up to m/z=60 were significantly present. The vacuum chamber itself has the already mentioned gas inventory composed of hydrogen, water,

oxygen, carbon dioxide, and hydrocarbons, coming from wall desorption, leakage, and pump residues. Additionally, outgassing of the pristine polymer takes place due to incorporated gas and solvent residues. During irradiation, the residual gas in the vacuum chamber shows an intensity increase of species like hydrogen (H_2, m/z=2), carbon (C, m/z=12), oxygen (O, m/z=16), hydroxyl and water (OH, H_2O, m/z=17/18) hydrocarbons (CH_n, m/z=12-16; C_2H_n, m/z=25-27, with dehydrogenated methane and ethane, including ethane and ethyne), carbon monoxide / ethene (CO/C_2H_4, m/z=28), methanol (CH_3OH, m/z=32, and dehydrogenated methanol, m/z=31) and carbon dioxide (CO_2, m/z=44), with H_2, CH_3, C_2H_4/CO and CO_2 causing the main part of partial gas pressure detected during irradiation. They directly show the covalent bond scission of the hydrocarbon polymeric backbone and the oxygen-bearing side chains, with a general dehydrogenation being one of the main steps.

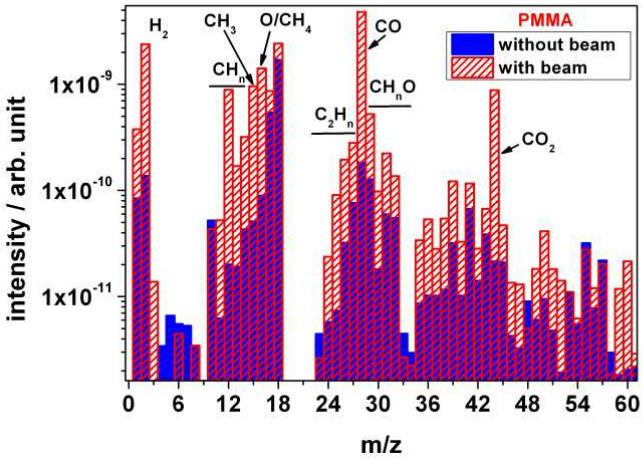

Figure 5.22: Outgassing spectra of PMMA polymer irradiated with 4.5 MeV/u Au ions.

The degradation process of the side chain, as later schematically shown in Figure 5.23, is initiated by homolytic bond scission between the CH_3OCO- side chain and the polymer backbone. The free CH_3OCO radical (m/z=59), constituting the dehydrogenated formic acid methyl ester, is unstable and decays into small fragments e.g. to CH_3 which is hydrogenated to CH_4. These molecular species have been found in an earlier investigation on ion irradiation with 10 MeV H, He and C [109], too. CH_4 as a volatile product can also be produced by homolytic bond breaking between -CH_3 and O-C=O bond of the methyl ester side chain, followed by hydrogenation of CH_3. Another possible reaction step is the bond scission of the ester bond, leading to the observed masses m/z=31 and 32, with CH_3O and CH_3OH, i.e. both dehydrogenated and complete methanol, as fragments. This reaction leaves back an aldehyde

group which in turn can form CO (m/z = 28) when the C-C bond to the backbone is broken. Also backbone scission will take place, leading to all kinds of small hydrocarbons, as observed in the mass spectrum.

5.1.2.7 Discussion of Degradation Mechanism of Polyvinyl Polymers

When analyzing the non-oxidative chemical degradation reactions taking place by high-energy heavy ion irradiation of polymers in vacuum, one has to take into account that regular reaction steps of organic chemistry and their rules can only partially be applied since around the track of the heavy ions in the polymer the energy level is extremely high. In this non-equilibrium regime, thermodynamics of chemical reactions at regular reaction temperatures do not apply. When the ion crosses the polymer, it releases huge amounts of its kinetic energy into the material by exciting electrons and by setting them free from their covalent bonds. These electrons themselves ionize atoms and create further energetic electrons in collision cascades. These electrons are easily able to cut bonds. Table 5.3 shows the bond dissociation energies of the atoms involved in increasing order [110]. The dissociation energies of the covalent bonds of the involved atoms in the polyvinyl polymers are between 300 and 500 kJ/mole, corresponding to about 3 to 5 eV of the individual interatomic bonds.

Table 5.3: Bond dissociation energies, from ref. [110]

Bond	**kJ/mole**	**eV per bond**
C–C	346	3.59
C–O	358	3.71
H–C	411	4.25
H–O	459	4.75
C=C	602	6.23

The energy transferred from the energetic ion into the polymer can be derived from theory. The software SRIM (Stopping and Range of Ions in Solids) calculates ion-atom-interactions including electronic and atom bond structure which is long-range affected in terms of electron excitations and plasmons [34]. By using the bond strengths of Table 5.3, SRIM gave for each single Au ion for a PVF foil of a thickness of 20 µm more than 2000 displaced atoms, i.e.

atoms cut out of their positions within the polymeric chain, and an average transferred energy of around 1600 eV per 100 pm length of the ion track in the polymer, see Table 5.4. The C-C bond length is 154 pm [111]. This means that all types of bonds suffer from scissions; even single atoms can be cut out of the polymer backbone. Often, the bond scission is homolytic, leading to radicals. Radicals and ions created under these non-equilibrium conditions are metastable and highly reactive such as O, OH and C. When they meet a chemical reaction partner and when they are able to get rid of their excess energy, they will react. Those species set free from the bonds in the near-surface region can leave the polymer. In the present case of high vacuum, the mean free path λ of the species is considerably larger than the vacuum chamber dimensions and the distance x between polymer sample and the mass spectrometer, $\lambda > 1\ m > x$ [112]. Whatever species leaves the sample into the direction of the spectrometer does not meet any other molecule for reaction. Others are reflected from the chamber walls until they most probably disappear in the vacuum pump or, by chance, hit the mass spectrometer orifice. This is the reason why highly reactive and unstable species are to be found in the mass spectrum. Another reason, of course, is the electron impact ionization process in the mass spectrometer which does also create such species. When fragments are formed in depth of the polymer, they have to diffuse to the surface. On their way, they may react and form new bonds. The smaller the molecules are, the easier they can escape. This is the reason why large numbers of hydrogen molecules and also water and carbon monoxide are found.

Table 5.4: Transferred energy dE/dx (per 100 pm ion track length x) and integral radiation damage per ion (accumulated number of C, O, and H atoms, displaced from their position in the polymer chain, up to the given depth), for 4.5 MeV/u Au ions in PVF, calculated by SRIM [34] for different depths/thickness of the material. The average ion range is 66.3 ± 0.4 µm, i.e. in a depth of e.g. 100 µm there is no more damage (dE/dx=0)

Position (depth)	**dE/dx**	**displacement per ion**
10 µm	1667 eV	979
20 µm	1712 eV	2158
60 µm	297 eV	18857
100 µm	0 eV	39264

Hence, one part of the degradation reaction products are non-equilibrium species, one part of the products obeys the rules of organic chemical reactions. When the ion has passed and its created energetic electrons have cooled down to room temperature, regular organic chemistry applies and the reaction products can be compared to those found in thermal degradation.

It has been found for mass spectrometry of PVA that the ion induced process yielded less heavy fragments than the thermally induced one. In the thermodynamically controlled equilibrium process, the chance for chemical reactions to larger molecules is higher than in the non-equilibrium process by energetic ions in vacuum where small molecular fragments have a better chance to be ejected from the solid before reaction.

Based on the results and on these considerations, in the following a few reaction paths are proposed which may explain the main findings. Apart from them, however, several other degradation reactions occur, especially ion induced backbone scission which can take place at any position due to the very high energy input with a locally highly non-equilibrium character. Also, a large number of free radical reactions will happen, since the ion beam process produces lots of them. In addition more complex reactions such as inter-molecular cyclisation reactions which lead to aromatic compounds or to the heterocyclic structures, where both FT-IR and RGA give evidence, are not shown since they are of minor importance, in contrast to thermal degradation.

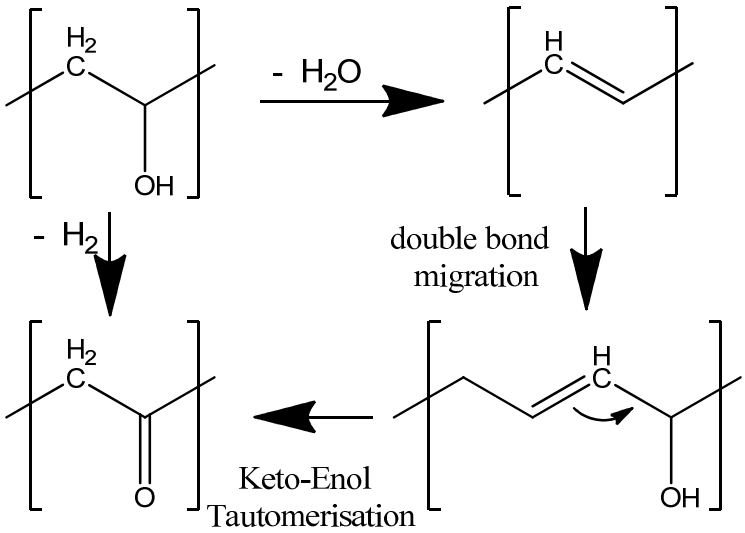

Figure 5.23: Proposed ion induced main degradation reactions of polyvinyl alcohol.

Figure 5.23 shows the proposed main ion induced degradation reaction in PVA. In FT-IR it had been observed that the –OH and –CH bands had decreased under ion irradiation, at the same time a slight growth of a –C=O keto band was observed. The main fragments were H_2 and H_2O. The latter is created by scission of the alcohol function and a neighbouring hydrogen, leading to both the observed reduction of the above mentioned bands and an increase in the C=C bands. Another reaction path is elimination of hydrogen, leaving back oxygen at the polymer backbone as a –C=O keto group. An indirect reaction path is double bond migration to the next carbon atom, with a neighbouring –OH group, leading to an enol. As described in Erlenmeyer's rule [113] the keto form is, in general, more stable than its enol tautomer. This is also the reason why PVA is not produced via polymerisation of its monomer vinyl alcohol, which is unstable and exists mainly as its tautomer acetaldehyde, but indirectly by polymerization of vinyl acetate and hydrolysis of the ester bonds. As a consequence, a ketone-type -C=O bond is formed resulting from keto-enol tautomerism. Hence, the reaction leads to two products: a keto group and/or a C=C double bond, potentially a polyene.

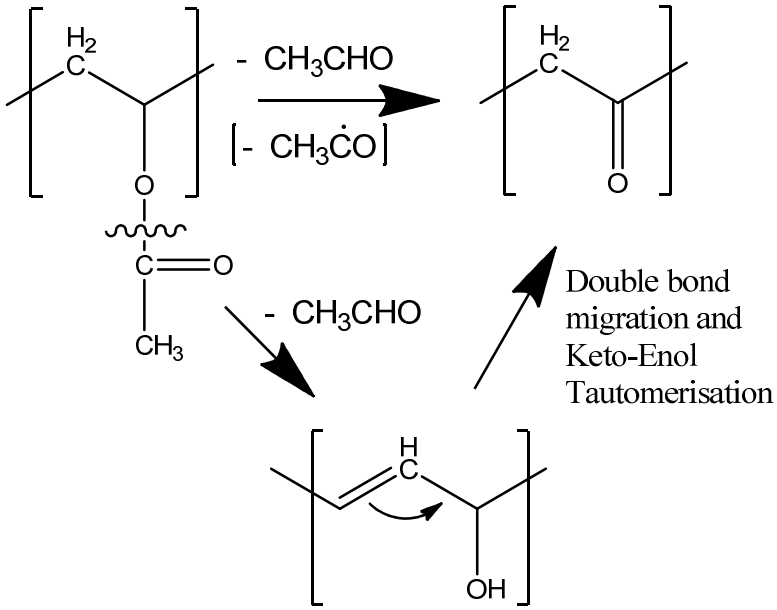

Figure 5.24: Proposed ion induced main degradation reactions of polyvinyl acetate.

In Figure 5.24, the degradation of the acetate subunit is depicted. The mechanism is mainly based on the elimination of the acetate side chain, thus forming either a C=O keto group with hydrogen elimination at the backbone C atom or to an –OH group when hydrogen is abstracted from a neighbouring carbon atom, thus forming a C=C double bond. If double bond migration takes place, again a keto-enol tautomerisation might happen.

As a consequence of the reactions, the acetate bands decrease in intensity, and, to a certain extent, also the aliphatic bands. This has been observed by FT-IR. This mechanism is also consistent with the mass spectrometric observation of acetic aldehyde and its dehydrogenated radical or ion CH_3CO as specific molecular fragment product, next to hydrocarbons and carbon oxides. In contrast to this reaction, thermal degradation favours the formation of acetic acid as main reaction product.

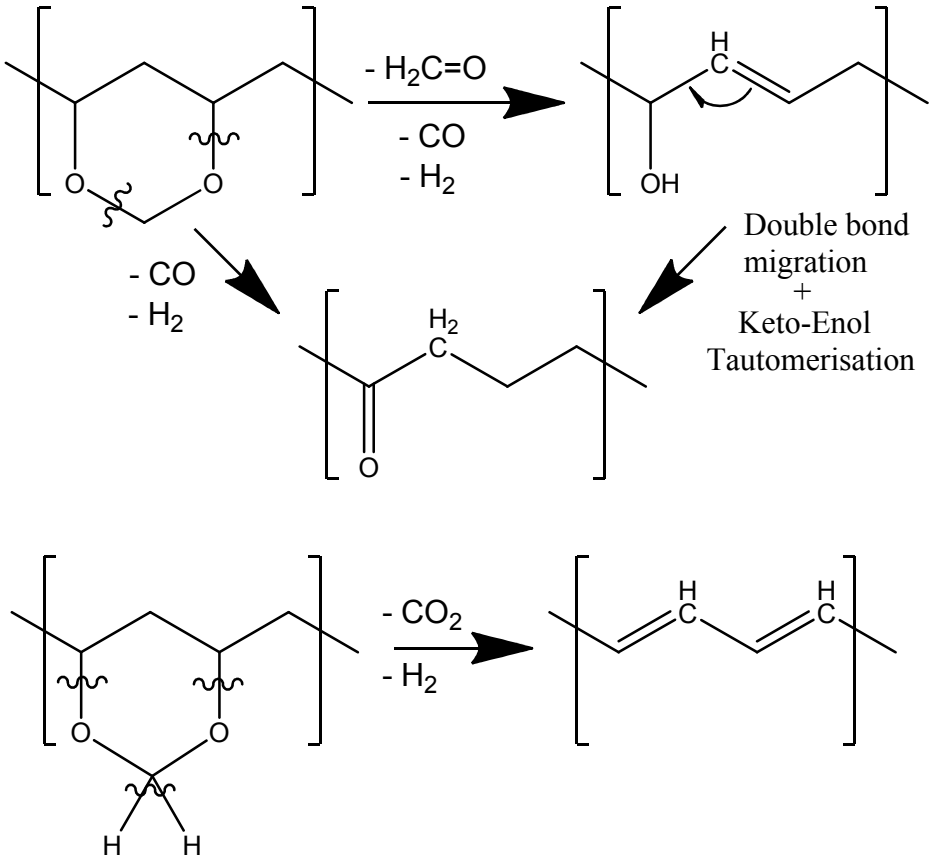

Figure 5.25: Proposed ion induced main degradation reactions of polyvinyl acetale.

These reactions also take place in PVF. Both the reduction in ester carbonyl vibration, and formation of keto groups, and an increase in unsaturated C=C bonds with a decrease of the aliphatic –C-H ones are observed, together with the above mentioned fragments. In contrast to PVA and PVAc, however, the mass 28, corresponding to CO, is the largest part of the fragments after hydrogen. Its intensity is double as that of PVAc and PVA. Also, H_2O and CO_2 are formed in large quantities. From this observation, it is concluded that in addition to the side chain eliminations of PVA and PVAc, it is the scission of the acetale subunit which creates both the additional fragments. Figure 5.25 shows the formation of CO and ethene combined with formation of –OH or –C=O keto groups, the formation of formaldehyde, as well as the creation of polyenes with adjacent C=C bonds with emission of CO_2 and H_2. These reactions are in accordance with both the results of FT-IR and mass spectrometry.

The role of –OH is complex. On one hand its elimination has been shown with PVA, on the other hand, there are production reactions from acetate and acetale subunits in PVF. PVF polymer shows no significant net changes of the band intensity, because PVAc and PVA

show reverse tendency of –OH band development with increasing ion fluence. This explains the unexpected seeming stability of the –OH groups of PVF.

The degradation process of the side chain of PMMA, schematically shown in Figure 5.26, is initiated by homolytic bond scission between the CH_3OCO- side chain and the polymer backbone. The free CH_3OCO radical (m/z=59), constituting the dehydrogenated formic acid methyl ester, is unstable and decays into small fragments e.g. to CH_3 which is hydrogenated to CH_4, and to CO_2. These molecular species have also been found in an earlier investigation on ion irradiation with 10 MeV H, He and C [109]. CH_4 as a volatile product can also be produced by homolytic bond breaking between -CH_3 and O-C=O bond of the methyl ester side chain, followed by hydrogenation of CH_3. Another possible reaction step is the bond scission of the ester bond, leading to the observed masses m/z=31 and 32, with CH_3O and CH_3OH, i.e. both dehydrogenated and complete methanol, as fragments. This reaction leaves back an aldehyde group which in turn can form CO (m/z = 28) when the C-C bond to the backbone is broken. Also backbone scission will take place, leading to all kinds of small hydrocarbons, as observed in the mass spectrum.

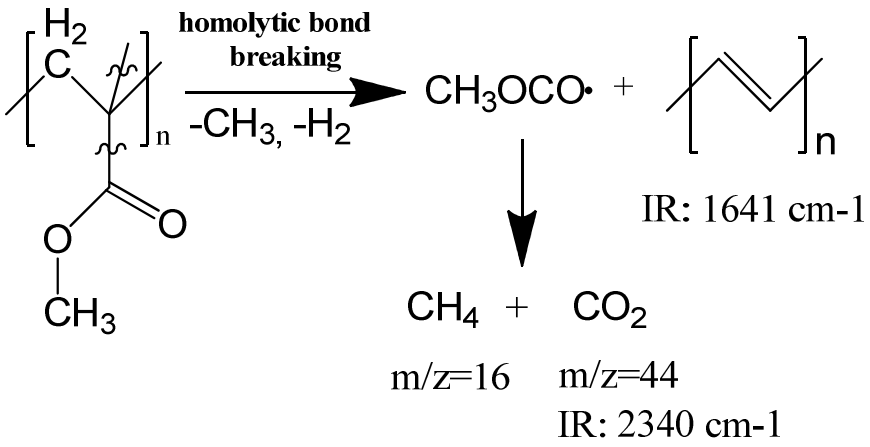

Figure 5.26: A possible mechanism of volatile products formation of PMMA foil.

The FT-IR spectrum of polyvinyl formal at 40 K shows very similar results in comparison to the RT experiments. In contrast, in the outgassing experiments under cryogenic irradiation conditions, most of the mass signals are significantly smaller compared to room temperature irradiation. This result indicates that at low irradiation temperatures small fragments are frozen in and accumulated in the sample, which is correlated to the results of heating experiments. This observation is not only relevant for the degradation mechanism, but is also

of technical importance. Whenever a component which has been working under cryogenic conditions, either in space or in a superconducting coil of an accelerator, is heated up, by irradiation from sun in space or due to maintenance in an accelerator, it will release large amounts of gases, leading to gas pressure increase. This may cause damage, particularly, when the material is already weakened by ion induced degradation. It should also be emphasized that low temperature does well protect a polymer from degradation, trivially by prohibiting temperature-induced reactions, but it does not help when highly energetic ions are involved leading to non-equilibrium conditions with an extreme local electronic energy input.

5.1.3 UV-Vis Spectroscopy

As mentioned before, ion beam induced radiation damage leads to formation of new bonds [63, 88, 114] and the resulting electronic states of polymers, such as the pi-bonds in either isolated or conjugated double bonds. If the latter are formed, electronic absorption of light will strongly be affected. The optical absorption method can provide information about the bond structure and energy gap in materials. The excitation of Π electrons requires small energy and hence transition of this type occurs at longer wavelengths. For this reason, the colouration of ion irradiated polymer samples has been investigated by UV-visible absorption spectroscopy.

5.1.3.1 PVF, PVAc and PMMA

Figures 5.27, 5.28 and 5.29 show the UV-Vis spectra of the pristine and irradiated PVF, PVAc and PMMA foils indicating significant reduction of the transmission at the ultraviolet wavelength region with increasing ion fluence.

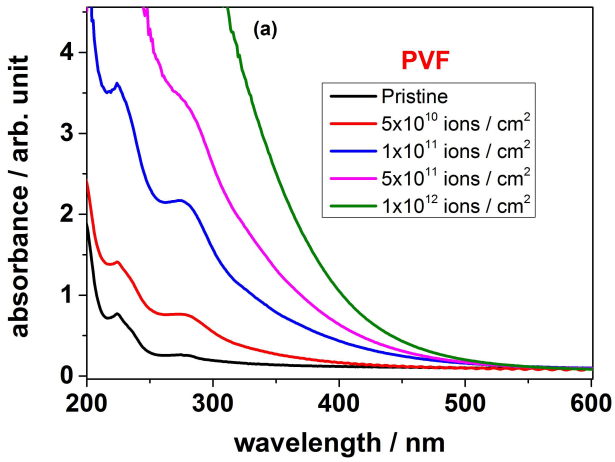

Figure 5.27: UV/Vis spectroscopy of pristine and irradiated (Au, 11.1 MeV/u, up to 1 ×10^{12} ions/cm^2) cured polyvinyl formal (PVF).

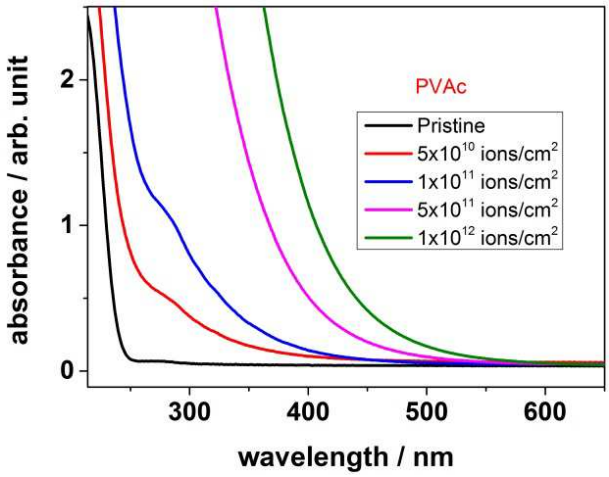

Figure 5.28: UV-Vis absorption spectra of Au ion irradiated PVAc at 11.1 MeV/u to various fluences.

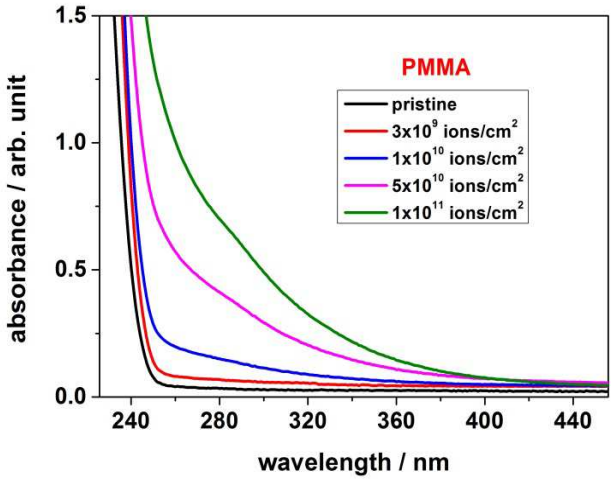

Figure 5.29: UV-Vis absorption spectra of U ion irradiated PMMA at 8.3 MeV/u to various fluences.

The spectra of the pristine vinyl-polymers are based on the presence of optically inactive carbon single bonds. The thin foils are transparent to Vis light and parts of UV light (both UVA and UVB) and filter UV only below 280 nm (UVC). During irradiation at fluences below 1×10^{10} ions/cm^2 no detectable changes of the absorption edge were observed in the UV-Vis spectrum compared to the pristine samples. At higher fluences, however, the absorption increases and the absorption edges shift from the ultraviolet wavelength region towards the visible blue region indicating the formation of double bonds along the polymeric

backbone. Non-conjugated carbon double bonds or those conjugated with only one or two other carbon double bonds absorb in the UV region. Here, the maximum absorptions λ_{max} of diene or triene molecules such as benzene (203 nm), butadiene (220 nm), cyclohexadiene with (256 nm), and hexadiene with (258 nm) are to be found [74]**.** More double bonds lead to a shift to higher wavelengths. As an example, decatetraene, with ten C atoms and four conjugated carbon double bonds, absorbs at 295 nm [115]. For this reason, the modified polymers increasingly absorb UV light. With increasing number of conjugated double bonds, the spectrum extends into the Vis region. The polymers change their colour and become yellowish.

The differential ($A-A_0$) absorbances of different wavelengths of the wavelength region 220-350 nm of PMMA are plotted as a function of ion fluence in Figure 5.30. In the observed fluence range, they show a logarithmic increase with increasing ion fluence providing information about the optical band gap.

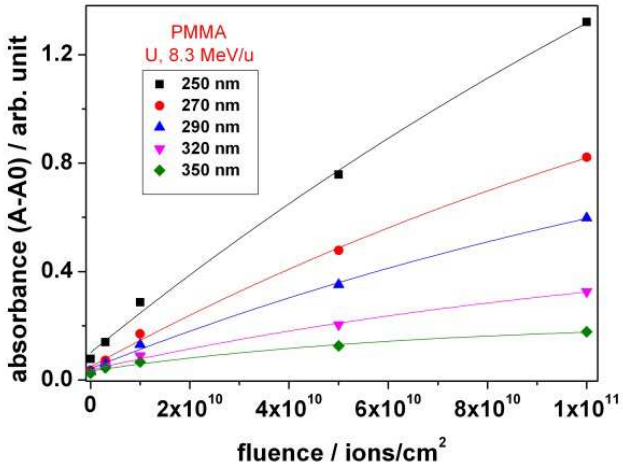

Figure 5.30: Radiation induced changes in wavelength region between 260-350 nm for PMMA as a function of fluence.

The electronic transitions resulting from the absorption of UV-Vis occur between the energy levels of the molecules in the valence band (VB) and the conduction band (CB). Only incident photons of energy values equal or larger than the gap between the two bands lead to electronic excitation. This optical gap Eg can be determined from the absorption spectra by means of the Tauc plot [88] (see chapter Analysis techniques).

Table 5.5 presents the different values of the optical band gap of polymers (PVF, PVAc and PMMA) for different fluences.

Table 5.5: Estimated band gap energy of vinylpolymers (PVF, PVAc and PMMA). PVF and PVAc are irradiated at 11.1 MeV/u Au ions and PMMA at 8.3 MeV/u U ions

Polymer	Fluence (ions/cm^2)	Band gap (ev)	Reduction (%)
PVF	Pristine	4.0	0
	5×10^{10}	3.2	20
	1×10^{11}	2.7	32
	5×10^{11}	2.6	35
	1×10^{12}	2.5	37
PVAc	Pristine	5.1	0
	5×10^{10}	3.5	31
	1×10^{11}	3.2	37
	5×10^{11}	2.8	45
	1×10^{12}	2.5	51
PMMA	Pristine	5.0	0
	3×10^{9}	4.9	2
	1×10^{10}	4.1	18
	5×10^{10}	3.7	26
	1×10^{11}	3.5	30

The energy gap is decreasing with increasing ion fluence for all three polymers. But the percentage is different for different polymers. Compared to the energy gap of all three polymers, PMMA is seen to decrease less with increasing ion fluence. The decrease follows PVAc> PVF> PMMA. The maximum decrease in energy gap corresponds to about 37% in PVAc polymers samples at fluence of 1×10^{11} ions/cm^2. The minimum decrease is about 30% in PMMA polymers. The different band gaps for different polymers support different degradation mechanism resulting from their different structure. While PVF has a ring which is more easily subject to be broken creating double bond, as explained, PMMA is apparently somewhat less prone to form optically active bonds. The optical absorption method can be used for the investigation of the optically induced transitions and can provide information about the bond structure and energy gap in crystalline and non-crystalline materials.

5.1.4 Thermo Gravimetric Analysis

5.1.4.1 Polyvinyl Formal (PVF)

Structural modifications, such as C-C double bond formation, lead to changes in macroscopic properties, such as the thermal stability and decomposition behaviour, resp. This was studied by Thermo gravimetric analysis where the polymer was heated up and the residual mass and mass los rate were recorded as function of temperature in a controlled non-oxidizing atmosphere. Figure 5.31 compares the decomposition behaviour of pristine and Au ion-irradiated PVF foils from RT to 650 °C indicating a strong reduction of the thermal stability with increasing ion fluence. A broad degradation phase was observed for 6.2×10^{11} ions/cm^2 irradiated sample occurring between 110 and 420 °C with a residual char of 10%. The decomposition values of the samples for different fluences are listed in Table 5.6 showing that the initial decomposition temperature ($T_{(d,\ 10\%)}$) and maximum decomposition temperature $T_{(d,\ max)}$ of irradiated samples are decreasing. On the other hand above 6.2×10^{11} ions/cm^2 an increase of $T_{(d,\ max)}$ is observed which may be relate to the increasing char residue forming at higher fluences.

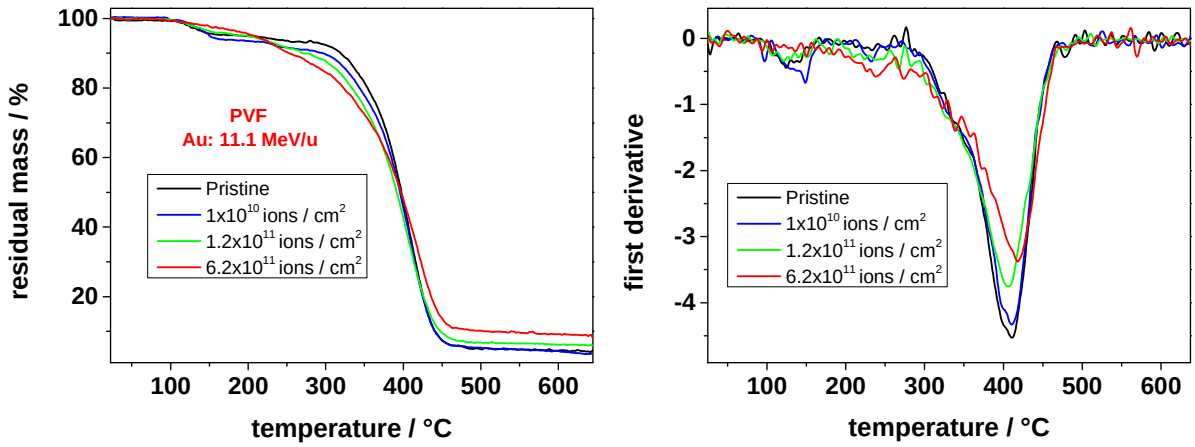

Figure 5.31: TGA curves of pristine (black) and irradiated PVF foils with different fluences (left) and their derivatives (right).

Table 5.6: Results of TGA measurements of 11.1 MeV/u Au-ion irradiated polyvinyl formal (PVF)

Fluence / ions / cm^2	$T_{d,\ 10\%}$	$T_{d\ ,\ max}$	Char residue / %
Pristine	319	411	5
1×10^{10} ions / cm^2	291	409	5
1.2×10^{11} ions / cm^2	268	405	7
6.2×10^{11} ions / cm^2	250	419	10

5.1.4.2 Polyvinyl Acetate (PVAc)

Figure 5.32 shows the decomposition behaviour of pristine and Au ion-irradiated PVAc foils (left in the figure). The temperatures at maximum decomposition rate ($T_{d,\ max}$) are indicated as peaks in the derivative curves (right in the figure). Thermo-degradation of PVAc was observed from RT to 650 °C. The pristine PVAc foil shows two steps, first a significant weight loss of about 65 % occurring between 280 and 350 ºC which is theoretically corresponding to the release of the ester group which later degrades to CO_2. In the second stage, structural degradation of the polymer proceeds leading to the evolution of polyene and aromatic structures as a consequence of backbone scission and double bond formation. Ion irradiated PVAc shows a slightly different behaviour. With increasing ion fluence the decomposition temperatures $T_{d,\ max}$ with the largest rate slightly increase, see Table 5.7, the derivative peak heights decrease, and, eventually, at the highest fluence, the curve becomes very noisy. At the same time, the onset temperature of thermal degradation, here given as $T_{d,\ 5\%}$, where 5% mass has been lost, decreases. Here, we find a similarity to thermal degradation.

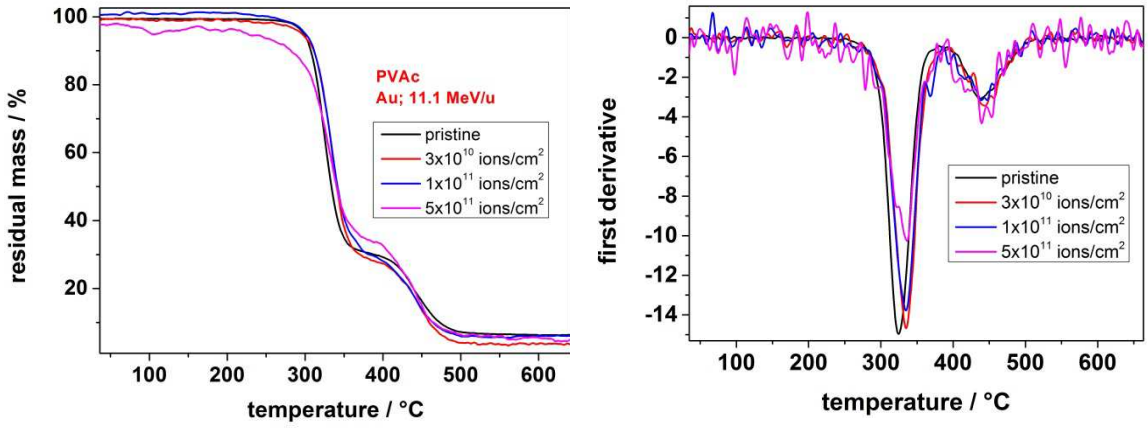

Figure 5.32: TGA curves of pristine and ion irradiated PVAc foils (left) and their derivatives (right). The irradiation was performed with Au ions at 11.1 MeV/u at room temperature.

Table 5.7: Results of TGA measurements of 11.1 MeV/u Au-ion irradiated polyvinyl acetate (PVAc)

Fluence / ions / cm^2	$T_{d, 5\%}$	$T_{d, max}$	Char residue (%)
Pristine	300	325	7
3×10^{10} ions / cm^2	300	335	4
1×10^{11} ions / cm^2	296	335	6
5×10^{11} ions / cm^2	261	336	6

Sivalingam et al. investigated the thermal degradation of PVAc foils by TG analysis and found a loss in thermal stability after pre-degradation with different temperatures [116]. Ion irradiation with the energy input via ion momentum and energy transfer into the polymer rather than via an input of heat modifies the course of the radiolysis process resulting in reduced temperatures of onset of degradation, but an increase of the temperature of maximum degradation rate. It is assumed that this behaviour is due to the weakening of the polymer with dangling bonds and zones of reduced density on one hand, and the formation of carbonized zones with carbon clusters on the other hand with the former being responsible for the earlier onset of degradation and the latter for the higher step between the two decomposition zones and the char residues since they are not decomposed at the used temperatures. The inhomogeneous structural character of the polymer after ion irradiation which is due to the localized radiation damage along the ion trajectories is also reflected by the shape of the TGA curve and its derivative with its noisy character.

Both polymers indicate specific material modifications induced by the irradiation. The change in char residue follows almost a uniform trend for both polymer samples while the chemical structure of a given polymer plays an important role for forming a char residue [56]. In a previous study above 50% of char residue are observed for polyimide (PI) with its aromatic structure [19] whereas about (4-10) % of char residue are found for PVF and PVAc. Both effects are explained by ion induced synthesis of carbon clusters which are not decomposed at the used temperatures. The results are in accordance with other analytical methods like mass loss analysis.

5.1.5 Mass Loss Analysis

5.1.5.1 PVF, PVAc and PVA

When energetic ions impinge onto polymers in a vacuum system, usually an increase in gas pressure is recorded. The polymer loses mass by ion induced fragmentation. This mass loss can directly quantitatively be measured. For this purpose, foils of PFV, PVAc and PVA were weighed before and after ion irradiation. The results of this mass loss analysis are depicted in Figure 5.33. Under ion irradiation, first a strong decrease of residual mass is observed for the samples, with the rate becoming smaller at higher fluence. Upon ion irradiations with higher fluences the PVAc foils break. This is assumed to be due to creation of stress and embrittlement. Therefore, no mass loss results of PVAc are shown above 1×10^{12} ions / cm^2. Compared to PVF a greater decrease is found at higher fluence (5×10^{12} ions/cm^2) for PVA. The results show that roughly around 20% of mass has been lost at a fluence of 1×10^{12} and around 60% at 5×10^{12} Au ions per cm^2.

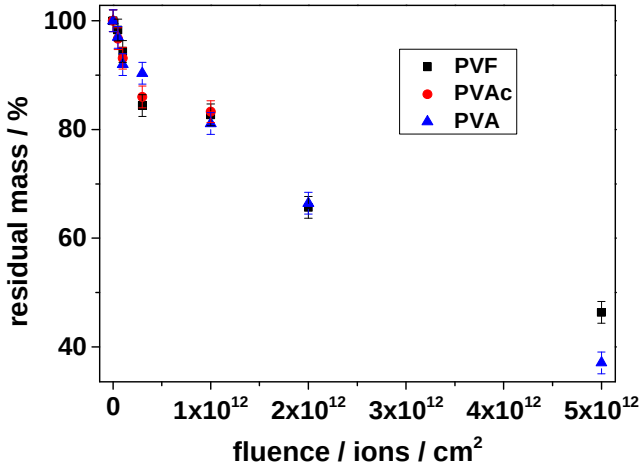

Figure 5.33: Residual mass as a function of ion fluence for PVF, PVAc and PVF irradiated with 11.1-MeV/u Au ions.

The same analysis was performed with PVF foils irradiated with 11.1 MeV/u U and Au ions. Figure 5.34 shows the trend of the residual mass of PVF samples. A larger decrease in residual mass was found for U irradiated samples compared to the Au irradiated samples. This trend may be explained by the different projectile masses and the resulting energy transfer dE/dx.

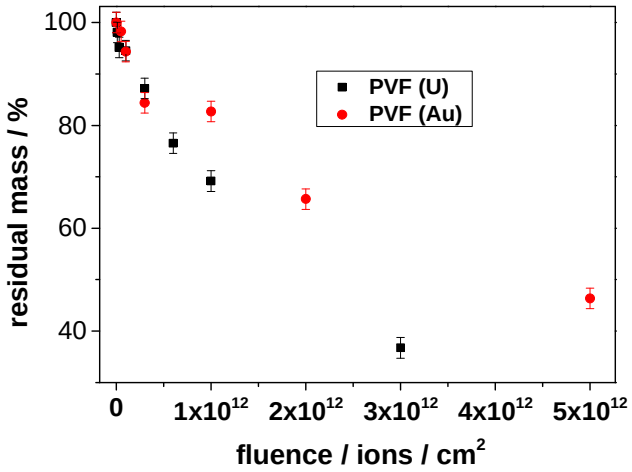

Figure 5.34: Residual mass as a function of ion fluence for PVF after irradiation with 11.1 MeV / u U and Au ions (with U irradiation: black and with Au ion irradiation: red).

The uniform trend of residual mass of PVF, PVAc and PVA shows the dependence of molecular structure of materials and points to the almost same degradation behaviour. If the ion beam induced process were only cutting out small volatile species and leaving the rest of the polymer unaffected the process were linear. However, the loss rate decreases with fluence. This means that the polymer changes its structure, becoming less prone to further mass loss. These results are consistent with the other analytical methods used in this study. This simple method gives in addition precise information about the absolute mass loss.

It is remarkable that the energy imposed to the polymers, despite the fact that the temperature remains low, leads to a considerable mass loss. More than half of the polymer is gone due to the ion beam induced damage.

Mass spectrometry had shown that a large number of different small molecules had been emitted upon irradiation. Mass loss analysis gives precise information how the sum of the species add up to a macroscopic loss of material.

5.2 Ion Induced Modification of Fluoropolymers

5.2.1 FT-IR Spectroscopy and Residual Gas Analysis [117]

As mentioned above, the ionizing radiation affects the molecular structure of the polymers. In this chapter fluorine-containing polymers are studied. It should be noted that for beam availability reasons the experiments with FT-IR and outgassing were performed with different ion masses (Au and Sm). However it can be assumed that the general degradation mechanism discussed here is the same for both ion types. In the following, the individual behaviour of PVDF, ETFE, FEP and PFA as analysed by FT-IR and mass spectrometry is discussed in detail. Eventually, upon comparing, a general conclusion is drawn. The study focuses on chain scission and fragmentation, since they can be most easily detected with the employed techniques. Especially at high radical concentrations, cross linking of different polymer strands displays alternative reaction pathways. They are not considered here. Further studies should use alternative techniques such as solid state NMR (to detect tertiary carbon atoms formed by cross linking) to evaluate the degree of cross linking [118].

5.2.1.1 Polyvinylidene Fluoride (PVDF)

Figure 5.35 presents the FT-IR absorption spectra of pristine and irradiated PVDF foil with Au ions at different fluences up to 2×10^{12} ions/cm^2. At first glance, there are three general observations. The spectra show a decrease of the main bands, an increase in the background, and the appearance of new bands. Well visible on the background are the two absorption bands at 3024 and 2981 cm^{-1} which are identified as symmetric and asymmetric vibration modes of the aliphatic -CH_2-groups which constitute half of the molecular structure of PVDF. Ion irradiation within the explored fluence regime leads to a decrease in intensity of these bands and to the development of two small shoulders at 2921 and 2851 cm^{-1} assigned to the asymmetric and symmetric stretching vibrations of other CH-groups, i.e. ones with a different molecular environment. The decrease of band intensity and appearance of two new shoulders reflect the molecular modification of the polymer. The observed –CH_2 band degradation of PVDF by ion irradiation is known from the literature [10, 63, 68] In addition, in the spectrum of PVDF, irradiated with 3×10^{11} ions/cm^2, three new peaks appear at 1752, 1711 and 1622 cm^{-1}. These signals are explained by the stretching vibrations of developing unsaturated C-bonds: -CF=CH-, and terminal -$CH=CF_2$, - and -$CF=CH_2$. This finding is corroborated by the mass spectrometric observation of high amounts of outgassing H and F atoms, mostly

found as their reaction products H_2 and HF (Figure 5.36). The carbon chain compensates the loss of H and F bonding partners by the formation of unsaturated C-bonds. While the C-H bonds (around 3000 cm^{-1}) and the C-F bonds (1140-1280 cm^{-1}) [119] are reduced in number, the number of C=C bonds (1600-1800 cm^{-1}) is rapidly increasing with ion fluence, as can be seen in Figure 5.35. The low wavenumber region between 1500 and 500 cm^{-1}, the fingerprint region, contains a complex series of absorption bands. These may be ascribed to wagging, twisting and rocking vibration of the C-H and C-F groups. During irradiation all band intensities in this region are decreasing with increasing ion fluence. Besides, a broad band is observed in the high wavenumber region of 3100-3700 cm^{-1} (red curve in Figure 5.35) which can be assigned to the CH vibration of –CH=CH- and –CH=CH_2- groups.

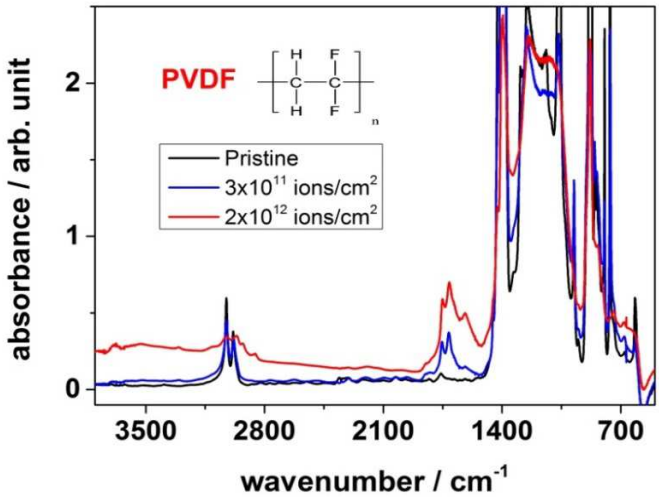

Figure 5.35: FT-IR spectra of PVDF: Pristine (black), irradiated with Au ions of 4.5 MeV/u with fluences of 3×10^{11} cm^{-2}(blue) and 2×10^{12} ions/cm^2 (red).

In accordance with the FT-IR results, mass spectra show that not only the side elements bonded to the carbon backbone are cut off but also the PVDF backbone structure itself is broken up upon ion irradiation, yielding several C-containing fragments such as C, CH_2F or CHF_2. Prior to irradiation, as usual a gas inventory composed of hydrogen, water, oxygen, carbon dioxide, and hydrocarbons has been found in the vacuum chamber. The volatile fragments of the polymer add to these components. The main outgassing fragments are the above-mentioned small volatile species hydrogen (H, m/z=2) and hydrogen fluoride (HF, m/z=20).

From the viewpoint of risk evaluation, it therefore must be considered that the irradiation of PVDF with heavy ions releases substantial quantities of these gases, particularly of the

aggressive HF. Interestingly, no F_2 molecule ions were detected with mass spectrometry. This is probably related to the extreme reactivity of the F radical and the high bond strength within the HF molecule, leading to the nearly complete reaction of the outgassing F to HF, rather than to F_2. This observation is in accord with literature describing the selective and fast abstraction of H atoms by fluorine radicals in the case of CHF_3 molecules which contain both H and F substituents [120] and with the well-established mechanism of radicalic substitution of hydrocarbons by halogens, resulting in a consecutive replacement of hydrogen atoms [121]**.** The results suggest the reactions shown in Figure 5.37 as the main degradation mechanism. The degradation process can be initiated by the i) homolytic C-C bond breaking, ii) release of an H atom, or iii) an F atom, creating either a terminal difluoro-ethylene radical or a dihydro-ethylene radical which later form carbon-carbon double bonds by elimination of hydrogen-fluoride (HF). The intensity decrease of hydrocarbon groups found by FT-IR spectroscopy is correlated with mass spectrometric results which show a main mass signal at m/z=20 (HF). Hence, the proposed mechanism is supported by both analysis methods.

In this schematic the backbone scission, forming C_1- and C_2-based species, is not shown, as well as the cross linking reaction between C-atoms of different chains. Of course, these reactions take place, however, to a lesser extent, as the mass spectrum shows for the scissions.

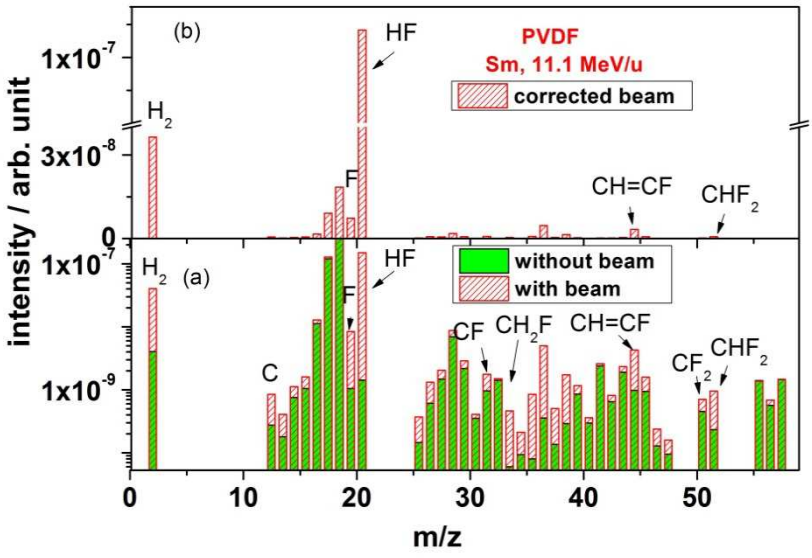

Figure 5.36: (a) Outgassing spectra of PVDF on-line recorded without irradiation and during irradiation with 11.1 MeV/u Sm ions, (b) difference spectrum, indicating the outgassing species caused by the heavy ion irradiation alone.

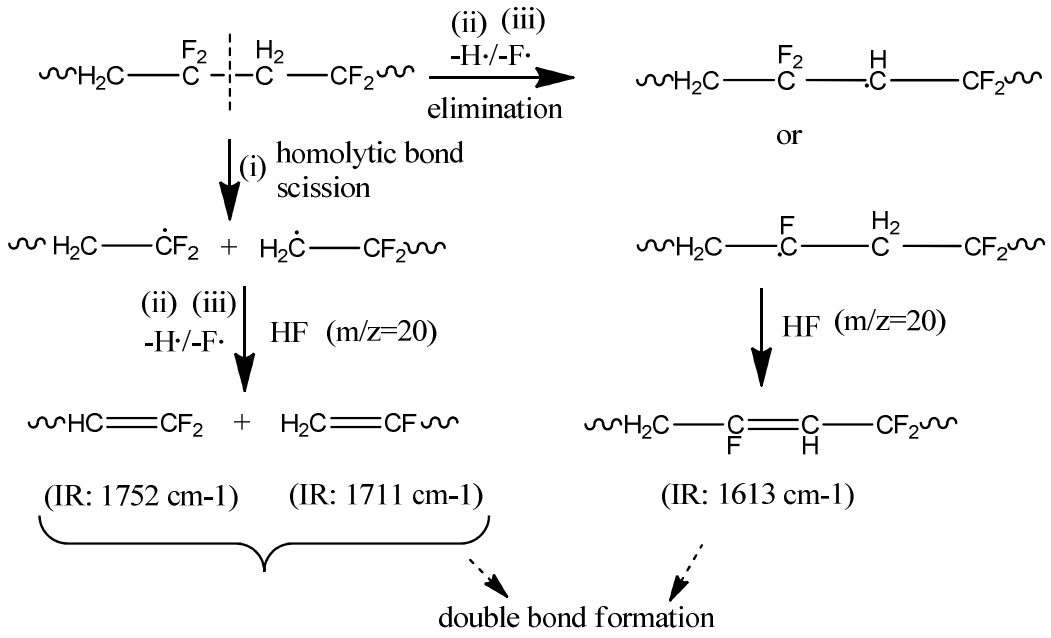

Figure 5.37: Schematic presentation of the main heavy ion induced degradation reactions of PVDF

5.2.1.2 Ethylene Tetrafluoroethylene (ETFE)

The vibrational-spectroscopic features observed for pristine and Sm-irradiated ETFE are presented in Figure 5.38. Pristine ETFE exhibits two absorbance bands at 2975 and 2881 cm^{-1} in the wavenumber range 3000-2800 cm^{-1}. They correspond to the symmetric and asymmetric stretching vibration of -CH_2 groups. At the low wavenumber region (1500-500 cm^{-1}), several absorbance bands can be assigned to the presence of hydrocarbon and C-F bonds.

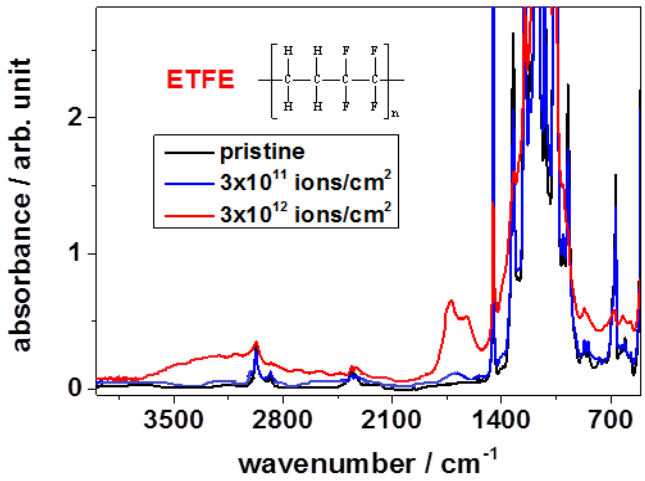

Figure 5.38: FT-IR spectra of ETFE: Pristine (black), irradiated with Sm ions with a fluence of 3×10^{11} cm^{-2}(blue) and 3×10^{12} $ions/cm^2$ (red).

A significant change of all characteristic vibration bands of irradiated ETFE foils has been observed with increasing ion fluence. During irradiation at fluences above 3×10^{12} ions/cm^2, the hydrocarbon bands at 2975 and 2881 cm^{-1} decrease and a broad shoulder appears which is an indication for a mixture of alkene-containing degradation products. This is the same situation as with PVDF. No characteristic absorption bands were found in the wavenumber range 1800-1600 cm^{-1} for pristine ETFE foil, but the sample irradiated with 3×10^{11} ions/cm^2 exhibits two new absorption bands at 1722 and 1624 cm^{-1} corresponding to the carbon-carbon double bond of –CF=CH- and –CH=CH- groups. The overall decreasing tendency of absorption bands at low wavenumber region between 1500 and 500 cm^{-1} is basically the same as in the case of PVDF.

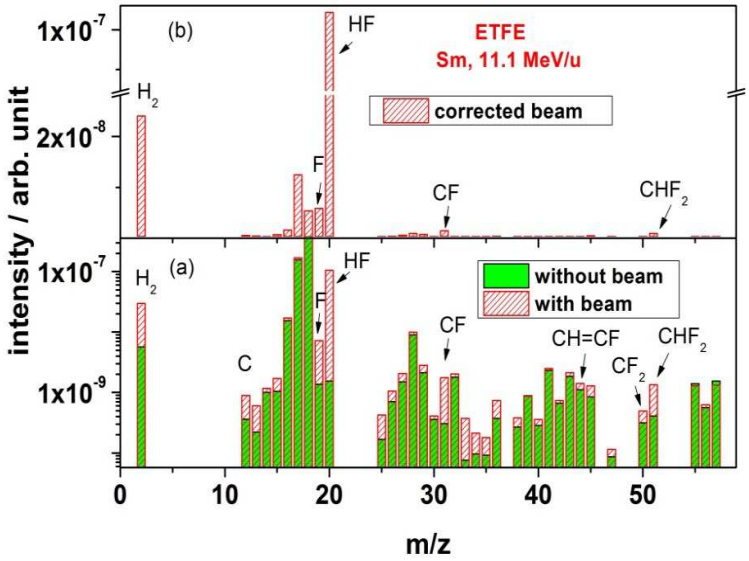

Figure 5.39: (a) Outgassing spectra of ETFE on-line recorded during irradiation with 11.1 MeV/u Sm ions, (b) difference spectrum, indicating the outgassing species caused by the heavy ion irradiation.

Hence, ion induced degradation shows a reduction in the number of aliphatic C-H groups at 2975 and 2881 cm^{-1}, and an increase in carbon-carbon double bonds at 1722 and 1624 cm^{-1} due to the scission of H and F, under release of HF.

Figure 5.39 shows the typical mass spectra of pristine and irradiated ETFE foils indicating outgassing fragments of hydrogen (H_2, m/z=2), fluorine (m/z=19), hydrogen fluoride (HF, m/z=20), CF (m/z=31) and CHF_2 (m/z=51). A possible degradation mechanism of ETFE is depicted in Figure 5.40 indicating the unsaturation of carbon bonds found by FT-IR spectroscopy and the presence of outgassing fragments by mass spectrometry. Hence, the degradation process for both polymers (PVDF and ETFE) is very similar and mainly based on

the homolytic bond breaking within the backbone and the elimination of hydrogen and fluorine as free radicals, forming either hydrogen molecules or HF. This causes the formation of C=C double bonds. As a consequence of the reaction, the hydrocarbon bands are decreased at 2975 and 2881 $cm^{-1}$and the C=C double bond signal is increased in intensity as observed by FT-IR spectroscopy. This mechanism is consistent with the mass spectrometric observation of ETFE.

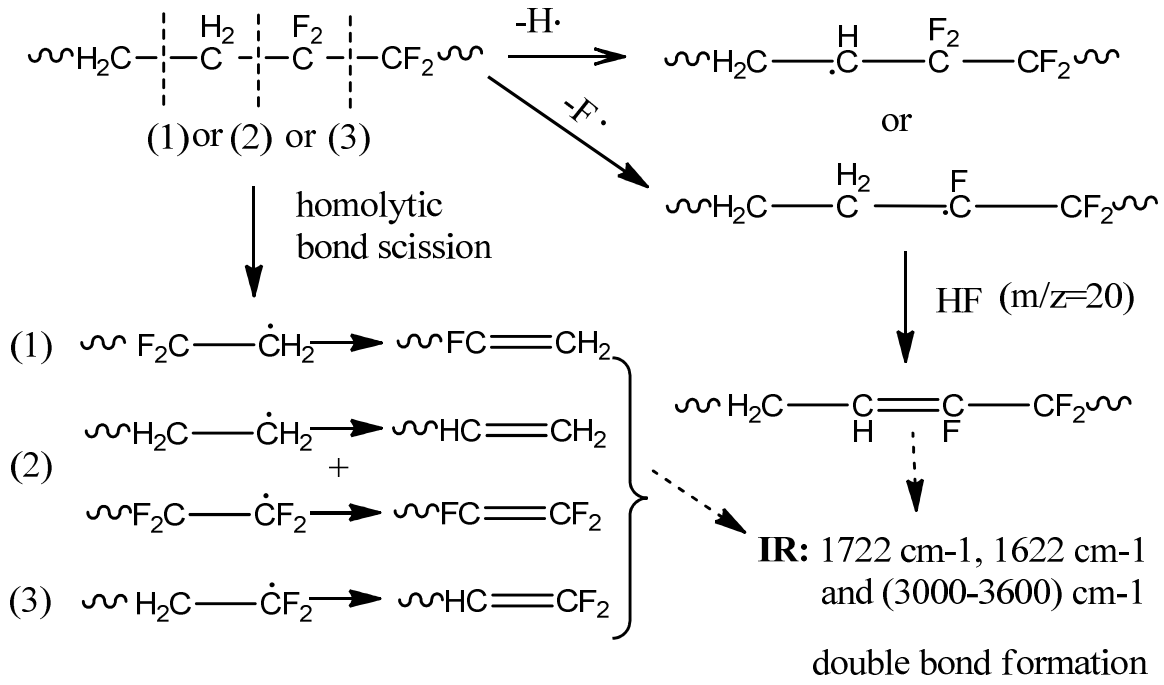

Figure 5.40: Scheme representing the degradation mechanism of ETFE polymer.

5.2.1.3 Tetrafluoroethylene-per-fluoromethoxyethelene (PFA)

The FT-IR spectra of PFA foil irradiated with Sm ions of two fluences in comparison with the non-irradiated foil are presented in Figure 5.41. The major absorption bands of pristine PFA are found in the low wavenumber region. The bands at 994 and 775 cm^{-1} as well as at 741 and 720 cm^{-1} are assigned to the $–CF_3$ vibration bands of the side chain. Other absorption bands above the fingerprint region (550-500 cm^{-1}) indicate the presence of C-H and C-F bending vibrations.

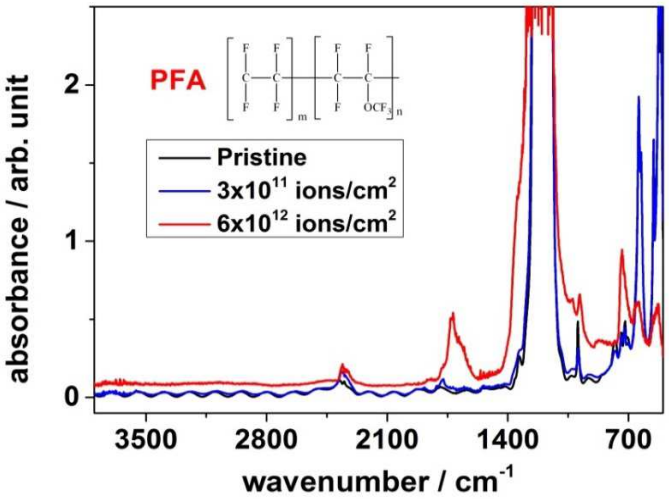

Figure 5.41: FT-IR spectra of PFA: Pristine (black), irradiated with Sm ions with 3×10^{11} cm^{-2}(blue) and 6×10^{12} ions/cm^2 (red).

As shown in Figure 5.41, a new broad IR absorption band at 1717 cm^{-1} appears with the increase of ion fluence. According to the literature [74], the new broad band at about 1717 cm^{-1} can be assigned to the stretching vibration of the –CF=CF- group. Once the foil was irradiated with a fluence beyond 3×10^{11} ions/cm^2, the intensities of characteristic absorption bands of at 738, 724 and 704 cm^{-1}, as well as the bands at 550-500 cm^{-1} decreased, which is consistent with the results of the before mentioned other fluoropolymers (PVDF and ETFE).

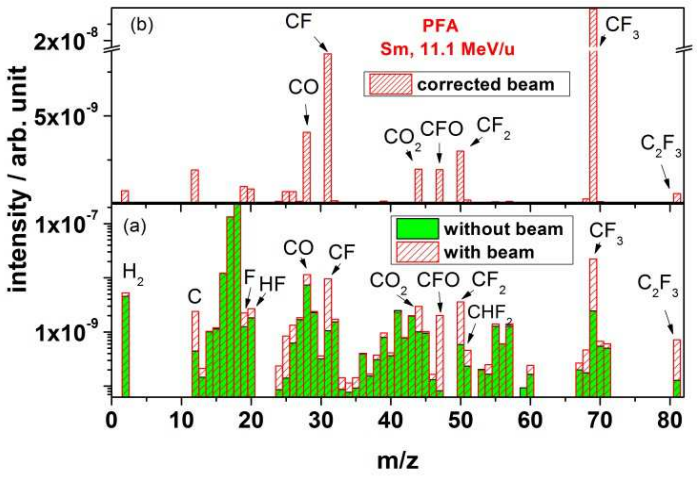

Figure 5.42: (a) Outgassing spectra of PFA polymer on-line recorded during irradiation with 11.1 MeV/u Sm ions, (b) difference spectrum, indicating the outgassing species caused by the heavy ion irradiation.

Figure 5.42 shows the mass spectrum of pristine and irradiated PFA. The main characteristic outgassing fragments are carbon (C, m/z=12), fluorine (F, m/z=19), hydrogen fluoride (HF, m/z=20), carbon monoxide (CO; m/z=28), CF (m/z=31), CO_2 (m/z = 44), CFO (m/z= 47), CF_3 (m/z=69) and C_2F_3 (m/z=81). It is important to note that PFA has a fully fluorinated carbon chain structure with a small amount of oxygen atoms in the side chain so that the amount of oxygen-bearing fragments is rather small, while there are several carbon-based fragment molecules with different numbers of F atoms. It turns out that the mass signal m/z=69 of $CF_3$is particularly large, considerably larger than CF and more than an order of magnitude above the value of CF_2. A possible mechanism may be the scission of CF_2 radicals from the polymeric backbone followed by recombination with adjacent fluorine atoms to form CF_3 molecules [122]. Since the C-F bonds are stronger than the C-C bonds, it can be assumed that the latter are more easily broken. With 490 kJ/mole, the polar C-F bond is, indeed, the strongest single bond in organic chemistry, while the C-C bond has a dissociation energy of only 350 kJ/mole [123, 124]. Consequently, the scission of the backbone occurs easier than the disintegration of the trifluoromethyl-group.

In PFA, double bond formation becomes visible at fluences of 1×10^{12} ions / cm^2. These are either isolated double bonds or dienes, but also a certain fraction of longer polyene sequences are found. This has also been observed for aliphatic polymers [97].

Backbone scission and elimination of the side chain $–OCF_3$ are believed to be free radical reactions, see Figure 5.43. It starts at a low fluence irradiation and gives double bond formation within the macromolecular backbone. With increasing fluence, chain scission occurs to some extent, as a result of which more $-OCF_3$ groups are eliminated and end-chain unsaturation appears. This mechanism explains both the appearance of CF_3, CF and CFO in the mass spectrum, as well as the observed double bond formation in the IR spectrum.

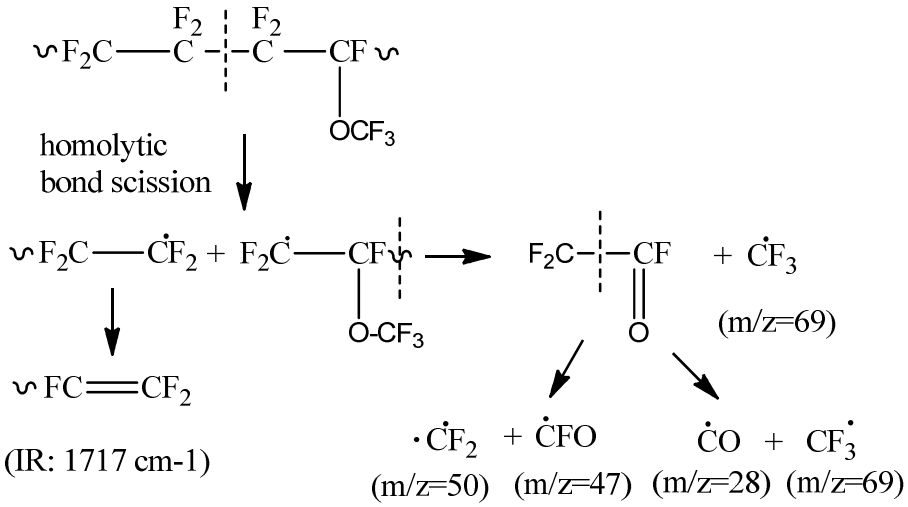

Figure 5.43: Schematic presentation the degradation mechanism of PFA.

5.2.1.4 Tetrafluoroethylene-hexa-fluoropropylene (FEP)

The FT-IR spectra of FEP observed after Sm irradiations at 11.1 MeV/u are presented in Figure 5.44. The characteristic absorption bands of pristine FEP in the low wavenumber region are mainly 982, 779, 749 and 704 cm^{-1}, which are assigned to the $–CF_3$ side chain and –CF backbone vibration bands. This is similar to the case of PFA, since the structures of PFA and FEP are mostly identical, with PFA bearing only an additional ether bridge to the side chain.

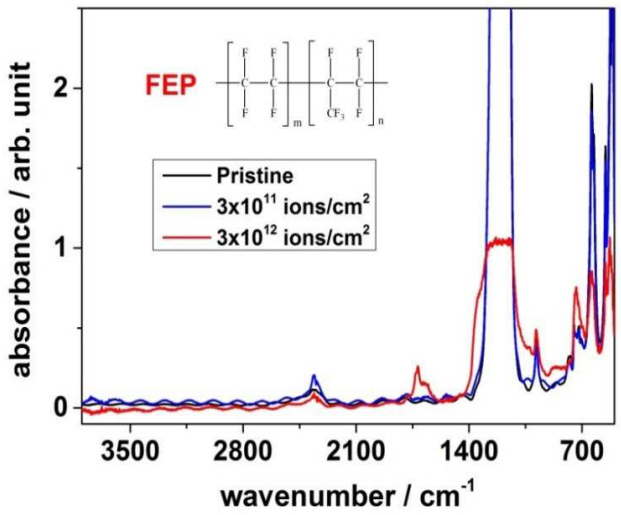

Figure 5.44: FT-IR spectra of FEP: Pristine (black), irradiated with Sm ions with $3×10^{11}$ cm^2 (blue) and $3×10^{12}$ ions/cm^2 (red).

During irradiation, all absorption bands of FEP polymer are affected in their shapes and intensities. Two new absorption bands appear at 1707 and 1672 cm^{-1} with increasing beam

fluence. These are assigned to stretching vibrations of -CF=CF_2 and -CF=C- groups, in accordance with the other three polymers.

A typical mass spectrum of pristine and irradiated FEP is presented in Figure 5.45. Again, before irradiation, the usual gas inventory of the vacuum chamber has been found. During irradiation, the gas in the vacuum chamber shows an intensity increase of species like carbon(C, m/z=12), fluorine (F, m/z=19), hydrogen fluoride (HF, m/z=20), carbon monoxide (CO; m/z=28), CF (m/z=31), CF_2 (m/z=50), CF_3 (m/z=69) and C_2F_3 (m/z=81), with CF_x (x=1,2,3) causing the main part of partial gas pressure detected during irradiation. These fragments arise from the covalent bond scission of the fluorine-bearing polymeric backbone (-CF_2-). Reaction with an adjacent fluorine atom creates CF_3 (m/z=69), in analogy to the case of PFA. The difference to the latter is that the oxygen-containing fragments (such as CFO) are not present, since the side chain has no ether bridge.

The main degradation mechanism of FEP is presented in Figure 5.46. It is governed by homolytic C-C bond scission of the polymer backbone and between the backbone and the side chain.

Elimination of fluorine radical from the backbone was detected above a fluence of 1×10^{11} ions/cm^2. The F radical reacts both with hydrogen from residual gas (H from H_2O, H_2) and with the highly reactive CF_2 radical (m/z=50), creating HF and CF_3. These molecular species have also been found in an earlier investigation on ion irradiation with 1 MeV protons [125]. CF_3 as a volatile product can also directly be produced by homolytic bond breaking between -CF_3 side chain and R-CF_2 backbone.

In all cases, backbone scissions takes place, leading to all kinds of small fluorocarbons (CF_x, C_2F_x), as observed in the mass spectrum.

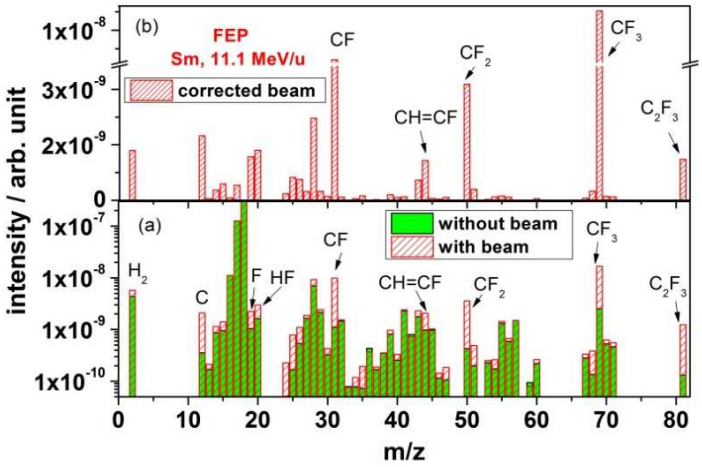

Figure 5.45: Outgassing spectra of FEP on-line recorded during irradiation with 11.1 MeV/u Sm ions, (b) difference spectrum, indicating the outgassing species caused by the heavy ion irradiation.

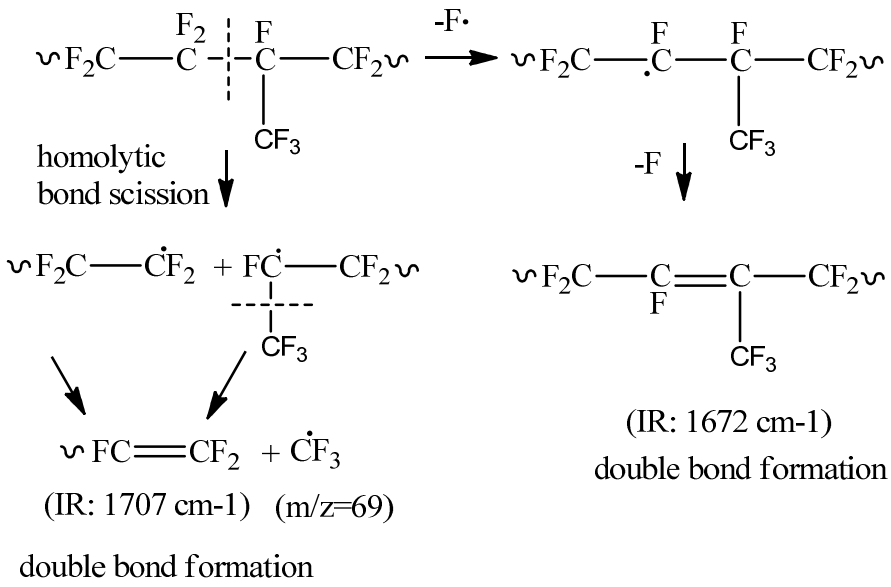

Figure 5.46: Schematic presentation of the degradation mechanism of FEP.

5.2.1.5 Comparison of the Four Fluoropolymers

In general, the absorption bands of all four polymers show an overall tendency to decrease with increasing ion fluence. This is an indication that the polymers are decomposed by the energetic ions. Carbon-carbon bond scission takes place at any position of the polymer backbone, also fluorine and hydrogen (for PVDF and ETFE) as well as the side chains are cut off. Upon bond scission and fragmentation, radicals and dangling bonds are formed which form new bonds. Since the volatile side elements fluorine, hydrogen and the side chains are

depleted, the newly formed bonds will essentially be between carbon atoms of the backbone, leading to double bonds.

For comparison, the new bands appearing in the FT-IR spectra of the four investigated polymers are listed in Table 5.8. All show new bands in the 1600-1750 cm^{-1} region assigned to carbon double bonds (PVDF: 1752, 1711 and 1622 cm^{-1}, ETFE: 1722 and 1624 cm^{-1}, PFA: 1717 cm^{-1} and FEP: 1707 and 1672 cm^{-1}). PVDF shows the development of two small shoulders at 2921 and 2851 cm^{-1} assigned to the asymmetric and symmetric stretching vibrations of the CH-groups. In case of hydrogen containing polymers PVDF and ETFE, additionally CH- vibrations next to carbon double bonds are found in the wavenumber region of 3100-3700 cm^{-1}.

Table 5.8: Interpretation of the appearing new absorption bands in polymers (PVDF, ETFE, PFA and FEP)

Polymers	Wavenumber / cm^{-1}	Assignment
PVDF	2921, 2851	symmetric and asymmetric vibration of -CH groups
	1752, 1711 and 1622	carbon double bonds
	3100-3700	stretching vibration of CH- at carbon double bonds
ETFE	1722, 1624	carbon double bonds
	3100-3700	stretching vibration of CH at carbon double bonds
PFA	1717	carbon double bonds
FEP	1707, 1672	carbon double bonds

In Table 5.9, the RGA results for all polymers are listed. Each observed m/z value was attributed to an outgassing fragment and normalized to the value of the polymer with the highest intensity in %. All four polymers show more or less the same outgassing fragments. But the percentages of intensities of these fragments are strongly differing. Even polymers without hydrogen (PFA) and oxygen (PVDF, ETFE, FEP) in their molecular structure show hydrogen- and oxygen-containing fragments due to the omnipresence of hydrogen and oxygen in the vacuum chamber.

Table 5.9: Outgassing fragments of fluoropolymers (PVDF, ETFE, PFA and FEP) for Sm (11.1 MeV/u) ion irradiation. Signal intensities from mass spectrometric measurements are calculated in percent (%) for each m/z value, normalized to the highest value which was set to 100%

PVDF Intensity in %	ETFE Intensity in %	PFA Intensity in %	FEP Intensity in %	Possible compounds	Fragments / m/z
100	66.1	2.1	3.7	H_2	2
100	79.8	13.6	16.2	F	19
100	70.4	0.6	0.9	HF	20
43.9	22.4	100	54.5	CO	28
9.0	16.4	96.8	100	CF	31
100	8.9	59.8	32.5	$CH=CF$ /CO_2	44
3.3	1.5	100	4.1	CFO	47
8.0	5.7	96.0	100	CF_2	50
76.7	100	23.6	31.3	CHF_2	51
2.3	0	100	71.0	CF_3	69
0	0	53.1	100	C_2F_3	81

H_2, HF and F have been observed as dominant outgassing fragments (66.1 to 100% relative intensity) of PVDF and ETFE due to their large hydrogen content. The results showed that the ion induced process of these polymers yielded less heavy fragments than that of PFA and FEP. This is due to the scission of the CF_3 side chain with its comparatively high mass. It is also interesting to note that the mass signal m/z=19 of the F atom was detected only with a small intensity in the mass spectra of PFA and FEP despite the fact that they are fully fluorinated. A significantly reduced amount of F fragments is observed in contrast to the other two polymers (PVDF and ETFE), which possess only 50% F in the backbone (13.6 and 16.2% relative intensity for PFA and FEP, compared to 100 and 79.8% for PVDF and ETFE). This may be related to the F radical who reacts with the carbon backbone in the absence of H as an efficient F scavenger. This reaction consumes the large amount of F, leading to the observed small F mass signal, and at the same time to the large CF_3 signal. For the same reason, also the CF_2 and the C_2F_3 signal are much larger in case of PFA and FEP (53.1 to 100% relative intensity versus 0 to 8.0% relative intensity in the case of PVDF and ETFE).

That the mass signal m/z=51 of CHF_2 is highest for ETFE is unexpected and is apparently due to the adjacent CH_2-CH_2 and CF_2-CF_2 building blocks in the polymer backbone.

The mass signals m/z= 28 and 47 of CO and CFO exhibit the highest intensity for PFA in comparison with other polymers (PVDF; ETFE and FEP). This is quite conceivable because of its O containing molecular structure. Furthermore, the mass signal m/z=44 showed the highest intensity for PVDF, less for PFA (59.8%), and lowest for FEP (32.5%) and ETFE (8.9%). According to the molecular structure of the four polymers, this may be an indication that the mass consists of two different molecular species, molecules CH=CF and CO_2. Therefore, the mass signal m/z=44 can most likely be assigned to CH=CF for PVDF and to CO_2 for PFA. In the case of PVDF, the especially high intensity of the CH=CF fragment is also probably related to the specific backbone structure with alternating C-F and C-H bonds. Because each unit of neighbouring carbon atoms is terminated by both H and F atoms, upon heavy ion irradiation, the formation of mixed, F- and H-containing C_2 fragments is favoured.

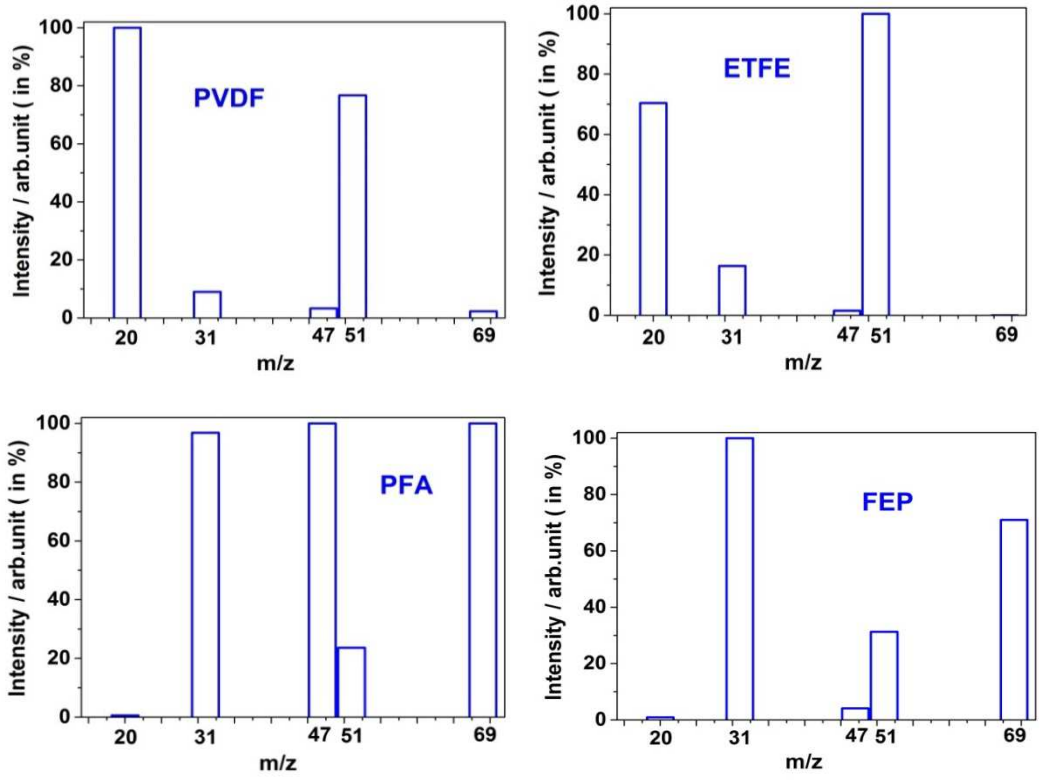

Figure 5.47: Outgassing fragments (m/z = 20, 31, 47, 51 and 69) of fluoropolymers (PVDF, ETFE, PFA and FEP). The intensities are calculated in percent (%) for each m/z value.

In general, concerning the two independent analysis methods FT-IR and mass spectrometry, complementary results were obtained.

In Figure 5.47, five characteristic fragments of the four polymers are compared in bar plots. They significantly differ from each other. Each polymer gives a characteristic degradation product fingerprint. It is directly related to its molecular structure, particularly the side chains. In turn, one would be able to identify a polymer by this fingerprint under ion irradiation. Taking the very similar structural units of the polymers into account, these large differences are intriguing.

5.2.2 UV-Vis Spectroscopy

5.2.2.1 ETFE, PFA and FEP

The optical absorption method can provide information about the bond structure and energy gap in materials. The samples change their colour to the visible light from transparent to yellowish with the influence of the ion beam (increase of the fluence) [125]. This is generally believed to be caused by the formation of new bonds and the resulting electronic states of polymers, such as the Π- Π* electron transition [112, 114, 126]. This type of transition occurs in the unsaturated centres of the molecules in either isolated or conjugated double bonds. The excitation of Π electrons requires small energy and hence transition of this type occurs at longer wavelengths. For this purpose the colouration of ion irradiated fluoropolymer foils has been investigated by UV-visible absorption spectroscopy. The UV-Vis spectra of PVDF are not analysed and shown in this section. Figure 5.48 shows the changes in UV-Vis absorption spectra of the fluoropolymers (ETFE, FEP and PFA) with variation of fluence. The UV-Vis spectra show a shift of the absorption edge from UV toward the visible with increasing ion fluence. The three polymers behave differently. While ETFE shows a fast and strong shift, FEP is somewhat less prone to the shift, and PFA is remarkably more stable in its behaviour. While PFA essentially remains in the UV wavelength region, at high fluence ETFE even shifts into the red region. These differences are quantitatively visible in the optical band gap, which can be determined by a linear fit of the Tauc plot [88] (see experiment section)Table 5.10 presents the different values of the optical band gap of polymers (ETFE, FEP and PFA) for different fluences.

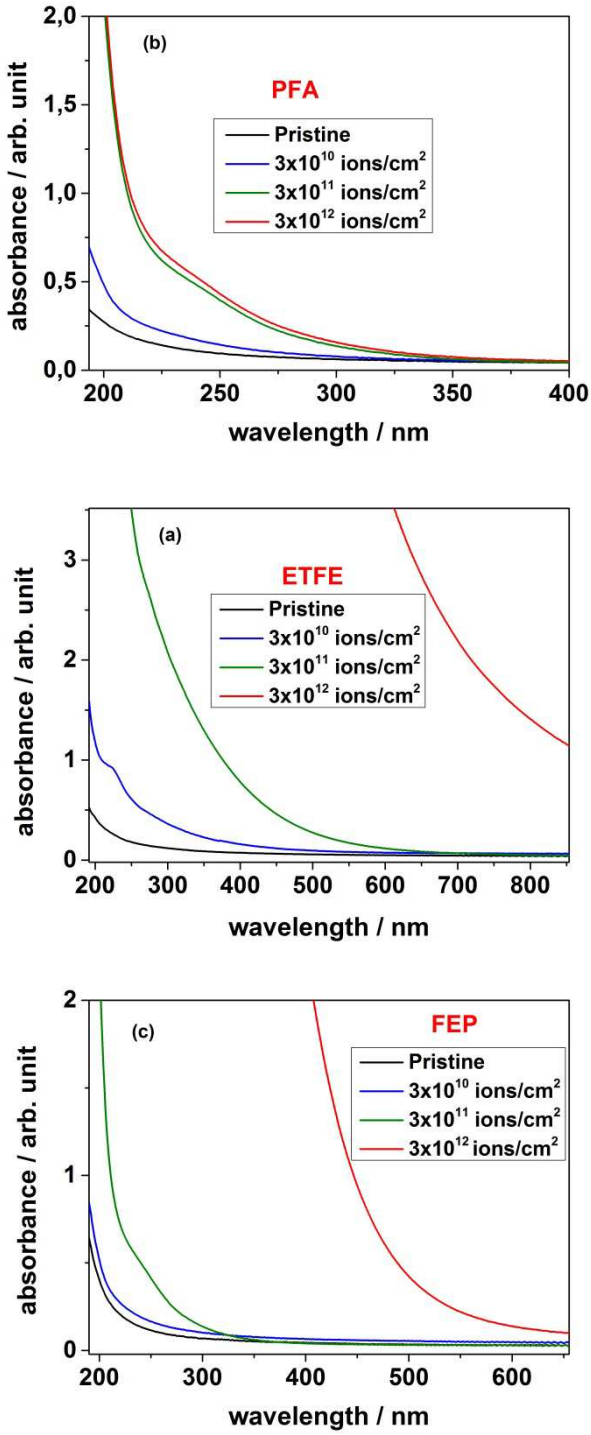

Figure 5.48: UV-Vis spectra of (a) ETFE, (b) PFA and (c) FEP polymers irradiated with 11.1 MeV/u Sm ions. The applied fluences were from 3×10^{10}-3×10^{12} ions/cm^2.

Table 5.10: Estimated band gap energy of fluoropolymers (ETFE, PFA and FEP) for Sm ion irradiated at 11.1 MeV/u

Polymer samples	Fluence (ions/cm^2)	Band gap (eV)	Reduction (%)
ETFE	Pristine	4.1	0
	3×10^{10}	3.5	15
	3×10^{11}	3.1	24
	3×10^{12}	1.9	54
PFA	Pristine	6.1	0
	3×10^{10}	5.7	7
	3×10^{11}	4.6	25
	3×10^{12}	4.5	26
FEP	Pristine	5.9	0
	3×10^{10}	5.6	5
	3×10^{11}	4.6	22
	3×10^{12}	2.6	56

The polymers start with different band gaps, with ETFE with 4.3 eV showing the lowest, and ETFE and FEP being equally high with 6.1 eV. While ETFE rapidly decreases, the reduction in FEP initially is lower but eventually reaches a similar low value above 50%, like ETFE. In contrast, PFA decays much slower and stays with a low value of reduction around 26% at the highest ion fluence. The decrease follows the following sequence: ETFE > FEP > PFA. In analogy to the vinyl polymers, the hydrogen-containing polymer ETFE changes its structure more rapidly. According to the mass spectra, it loses large amounts of H, F, and HF. In contrast, FEP and PFA emit CO and CF, potentially leaving back less CC double bonds than ETFE. More difficult is to understand the difference between FEP and PFA. Structurally, they differ only by an O-atom, creating an ether bridge to the side chain. This shows that even small structural differences lead to significant changes in ion irradiation induced band gap shifts. The different band gap values for different polymers are also correlated with the appearing new bands at 1700-1800 cm^{-1} region observed by the FT-IR spectroscopy. Carbon enriched domains created in polymers during irradiation may be responsible for the decrease in band gap as indicated by some studies [127-132]. The optical absorption method can be

used for the investigation of the optically induced transitions and can provide information about the bond structure and energy gap in crystalline and non-crystalline materials.

6. Conclusion

This thesis reports on modification of aliphatic polymers by highly energetic heavy ions. The work especially considers ion induced degradation of polyvinyl formal (PVF) used as insulating material of superconducting accelerator magnets in the future accelerator at the Facility for Antiproton and Ion Research (FAIR). For the interpretation of the results on the complex polymer PVF three other polyvinyl polymers (PVAc, PVA, and PMMA) were analysed, with PVA and PVAc being subunits of PVF. Thus, information was gained about the influence of different side chains of these vinyl-polymers. As the second technically relevant polymer group, Fluoropolymers (PVDF, ETFE, PFA and FEP) were analysed and the results were compared.

The irradiation experiments were performed at the GSI Helmholtz-Centre for Heavy Ion Research. Two different beamlines (X0 beamline for post irradiation analysis and M3 beamline for on-line analysis) were used. Two complementary orthogonal methods, FT-IR spectrometry and mass spectrometry, were applied for studying the ion induced damage, namely the structural change, as function of the number of ions (fluence) and the ionic species. Since the used polymers were all transparent / translucent, in addition, an optical technique could be used. Furthermore, direct analysis of the mass loss due to ion induced fragmentation was carried out, and the thermal behaviour was evaluated by thermo gravimetric analysis.

FT-IR spectroscopy of all polymer samples revealed that ion irradiation led to the decrease of all characteristic band intensities showing the general degradation of the polymer. This is caused by an extreme electronic excitation and ionisation due to energetic electrons released by the ions. These break all types of covalent bonds. As a consequence of the structural modification, new bands appeared, such as those of C=C double bonds or of carbon dioxide. Mass spectrometry showed that the polymers were degraded in all parts of side-chains and backbones leading to a number of small volatile fragment molecules which leave the polymer into vacuum and reduce its mass. In the ion induced process, the polymers essentially are dehydrogenated, since the relative loss of hydrogen is larger than the one of carbon. Also, oxygen is lost. As a consequence, double bonds are formed; the polymer is “carbonized”. The considerable structural changes will lead to a modification/deterioration of specific macroscopic properties, such as electrical resistance and mechanical strength, and is therefore of importance for applications in environments with energetic particles, such as space and

accelerators. As an example of a macroscopic property, UV-Vis transmission was analysed. The absorption edge shifted upon ion irradiation from the ultraviolet region towards the visible region indicating the formation of double bonds and conjugated double bonds. The optical gap decreased strongly with increasing ion fluence. The decrease percentage of gap is different for different polymers and follows PVAc > PVF > PMMA. As an example, the degradation of PVAc can be described as essentially scission of the backbone chain accompanied by the split of ester groups. The appearance of a new absorption band of a CO_2 group at 2339 cm^{-1} with increasing fluence was observed for three different heavy ions (U, Au and Xe) with different intensities. On-line mass spectrometry identified the outgassing fragment CO_2 as a prominent degradation product during irradiation. TGA analysis of PVF and PVAc showed trends in thermal degradation and char residue under irradiation. Compared to aromatic polymers less char residues was observed for aliphatic (PVF and PVAc) polymers as compared to aromatic ones; in general, all radiation damage for aliphatic polymers was larger than the ones of aromatic polymers. In resume, the results of the experiments on all used aliphatic polymers with the proposed individual molecular degradation reaction steps give a consistent picture of the degradation mechanism.

Ion induced modification of PVDF, ETFE, FEP and PFA show similar results corresponding to the chemical transformations in the polymers. All four polymers show the appearance of new absorption bands by FT-IR spectroscopy indicating a modification of the polymer structure towards unsaturation by destroying the carbon single bonds to C, F and H, respectively. Mass spectrometric results indicate that several chemical species are ejected out of the polymer surface; such as CF_3. Each polymer gives its own mass pattern, depending on its composition and molecular structure. Ion induced degradation causes double bond and conjugated double bond formation, as shown by UV-Vis transmission analysis, giving an absorption edge shift of the ultraviolet region towards the visible region. The energy gap is seen to decrease with increasing ion fluence and follows ETFE > FEP >PFA. Here, too, the complementary picture of the different analysis methods gives a consistent view of the ion induced degradation mechanisms.

The results are not only of basic interest about polymer degradation by extremely strong electronic excitation by a densely ionizing type of radiation, but also as an experimental simulation of damage of polymers in large scale accelerators and in space applications.

7. Outlook

While already a number of different powerful characterisation methods have been used for studying heavy ion induced degradation of aliphatic polymers, there are still other ways to investigate the modifications, such as Nuclear Magnetic Resonance. Also, the product of radiation damage will become Raman-active, so that this method can be used in addition to IR. With radicals involved, Electron Spin Resonance might be useful. To a certain extent, also Photoelectron emission and X-ray absorption could be used. Their use will give further insight into the ongoing processes.

Furthermore, characterization of macroscopic properties such as electrical conductivity and mechanical stability with elastic modulus and hardness, just to name of few, should be carried out.

Apart from the investigated properties and the used methods, it would also be interesting to change the ion irradiation conditions, spanning a wider range of ion masses, ion energies, fluences and fluxes.

Finally, for a further insight into chemical effects, more polymer types with further functional groups and elements (N, S, and Cl) should be investigated. Even in the group of aliphatic polymers, it would be interesting to compare the results with further related polymers, such as PMMA with PMA or PEMA, or PTFE with PTCFE. Eventually, also the influence of the molecular weight on radiation damage so far is unknown and would be worth to be studied.

Bibliography

[1] Van de Voorde M. Effects of radiation on materials and components. 1970. p. CERN 70-5.

[2] Clough RL. High-energy radiation and polymers: A review of commercial processes and emerging applications. Nuclear Instruments and Methods in Physics Research Section B: Beam Interactions with Materials and Atoms. 2001;185:8-33.

[3] Reed R, Marshall P, Johnston A, Barth J, Marshall C, LaBel K, et al. Emerging optocoupler issues with energetic particle-induced transients and permanent radiation degradation. Nuclear Science, IEEE Transactions on. 1998;45:2833-41.

[4] Gopakumar S. RP in medicine: a case study in cranial reconstructive surgery. Rapid Prototyping Journal. 2004;10:207-11.

[5] Chang TC, Liao CL, Wu KH, Chen HB, Yang JC. Degradation of some poly(methyl-phenylsiloxane)-poly(methyl methacrylate) interpenetrating polymer networks. Polymer Degradation and Stability. 1999;66:127-32.

[6] Rajkumar T, Vijayakumar CT, Sivasamy P, Sreedhar B, Wilkie CA. Thermal degradation studies on PMMA–HET acid based oligoesters blends. Journal of Thermal Analysis and Calorimetry. 2010;100:651-60.

[7] Troitskii BB, Troitskaya LS, Yakhnov AS, Lopatin MA, Novikova MA. Retardation of thermal degradation of PMMA and PVC by C60. European Polymer Journal. 1997;33: 1587-90.

[8] Chapiro A. General consideration of the radiation chemistry of polymers. Nuclear Instruments and Methods in Physics Research Section B: Beam Interactions with Materials and Atoms. 1995;105:5-7.

[9] Davenas J, Stevenson I, Celette N, Cambon S, Gardette JL, Rivaton A, et al. Stability of polymers under ionising radiation: The many faces of radiation interactions with polymers. Nuclear Instruments and Methods in Physics Research Section B: Beam Interactions with Materials and Atoms. 2002;191:653-61.

[10] Balanzat E, Betz N, Bouffard S. Swift heavy ion modification of polymers. Nuclear Instruments and Methods in Physics Research Section B: Beam Interactions with Materials and Atoms. 1995;105:46-54.

[11] Steckenreiter T, Balanzat E, Fuess H, Trautmann C. Chemical modifications of PET induced by swift heavy ions. Nuclear Instruments and Methods in Physics Research Section B: Beam Interactions with Materials and Atoms. 1997;131:159-66.

[12] Severin D, Ensinger W, Neumann R, Trautmann C, Walter G, Alig I, et al. Degradation of polyimide under irradiation with swift heavy ions. Nuclear Instruments and Methods in Physics Research Section B: Beam Interactions with Materials and Atoms. 2005;236:456-60.

[13] Severin D, Balanzat E, Ensinger W, Trautmann C. Outgassing and degradation of polyimide induced by swift heavy ion irradiation at cryogenic temperature. Journal of Applied Physics. 2010;108:024901.

[14] Seidl T, Plotnikov A, Mustafin E, Lopez R, Severin D, Floch E, et al. Influence of swift heavy ion beams and protons on the dielectric strength of polyimide. Polymer Degradation and Stability. 2012;97:2396-402.

[15] Seidl T, Baake O, Hossain UH, Bender M, Severin D, Trautmann C, et al. In-situ investigation of polyvinyl formal irradiated with GeV Au ions. Nuclear Instruments and Methods in Physics Research Section B: Beam Interactions with Materials and Atoms. 2012;272:400-4.

[16] Augustin I. Status of the FAIR project. Nuclear Instruments and Methods in Physics Research Section B: Beam Interactions with Materials and Atoms. 2007;261:1014-7.

[17] Spiller P, Franchetti G. The FAIR accelerator project at GSI. Nuclear Instruments and Methods in Physics Research Section A: Accelerators, Spectrometers, Detectors and Associated Equipment. 2006;561:305-9.

[18] http://www.gsi.de/portrait/fair.html. Facility for Anti Proton and Ion Research (FAIR).

[19] Seidl T. Radiation hardness of superconducting magnet insulation materials for FAIR, PhD thesis, Technical University of Darmstadt. 2013.

[20] Koch L, Engelmann J, Goret P, Juliusson E, Petrou N, Rio Y, et al. The relative abundances of the elements scandium to manganese in relativistic cosmic rays and the possible radioactive decay of manganese 54. Astronomy and Astrophysics. 1981;102:L9-L11.

[21] Peters E. Polymer Data Handbook, JE Mark ed. Oxford University Press: New York; 2009.

[22] Dhara MG, Banerjee S. Fluorinated high-performance polymers: poly (arylene ether) s and aromatic polyimides containing trifluoromethyl groups. Progress in Polymer Science. 2010;35:1022-77.

[23] Hansen NM, Jankova K, Hvilsted S. Fluoropolymer materials and architectures prepared by controlled radical polymerizations. European Polymer Journal. 2007;43:255-93.
[24] Humer K, Weber H, Tschegg E. Radiation effects on insulators for superconducting fusion magnets. Cryogenics. 1995;35:871-82.
[25] Egusa S, Kirk M, Birtcher R. Effects of neutron irradiation on polymer matrix composites at 5 K and at room temperature: II. Degradation of mechanical properties. Journal of nuclear materials. 1987;148:53-60.
[26] Melot M, Ngono-Ravache Y, Balanzat E. Role of the irradiation temperature on the modifications of swift-heavy-ion irradiated polyethylene. Nuclear Instruments and Methods in Physics Research Section B: Beam Interactions with Materials and Atoms. 2003;209:205-11.
[27] Leo WR. Techniques for nuclear and particle physics experiments: a how-to approach: Springer; 1994.
[28] Jackson JD. Klassische Elektrodynamik: Walter de Gruyter; 2006.
[29] Spohr R. Ion tracks and microtechnology: principles and applications: Springer, Wiesbaden; 1990.
[30] Bloch F. Zur bremsung rasch bewegter teilchen beim durchgang durch materie. Annalen der Physik. 1933;408:285-320.
[31] Bethe H. Zur Theorie des Durchgangs schneller Korpuskularstrahlen durch Materie. Annalen der Physik. 1930;397:325-400.
[32] Schiwietz G, Luderer E, Xiao G, Grande PL. Energy dissipation of fast heavy ions in matter. Nuclear Instruments and Methods in Physics Research Section B: Beam Interactions with Materials and Atoms. 2001;175–177:1-11.
[33] Sigmund P, Selskab DV. Ion beam science: solved and unsolved problems: invited lectures presented at a symposium arranged by the Royal Danish Academy of Sciences and Letters, Copenhagen, 1-5 May 2006: E. Munksgaard; 2006.
[34] Ziegler JF, Ziegler M, Biersack J. SRIM–The stopping and range of ions in matter (2010). Nuclear Instruments and Methods in Physics Research Section B: Beam Interactions with Materials and Atoms. 2010;268:1818-23.
[35] Fink D. Fundamentals of ion-irradiated polymers: Springer, Heidelberg; 2004.
[36] Fleischer R, Price P, Walker R. Ion Explosion Spike Mechanism for Formation of Charged-Particle Tracks in Solids. Journal of applied Physics. 2004;36:3645-52.
[37] Dessauer F. Über einige Wirkungen von Strahlen. I. Z Physik. 1923;12:38-47.

[38] Gervais B, Bouffard S. Simulation of the primary stage of the interaction of swift heavy ions with condensed matter. Nuclear Instruments and Methods in Physics Research Section B: Beam Interactions with Materials and Atoms. 1994;88:355-64.
[39] Chadderton LT, Cruz SA, Fink DW. Theory for latent particle tracks in polymers. Nuclear Tracks and Radiation Measurements. 1993;22:29-38.
[40] Lee EH. Ion-beam modification of polymeric materials–fundamental principles and applications. Nuclear Instruments and Methods in Physics Research Section B: Beam Interactions with Materials and Atoms. 1999;151:29-41.
[41] Fleischer RL, Price PB, Walker RM. Nuclear tracks in solids: principles and applications: Univ of California Press; 1975.
[42] Klaumünzer S, Hou M, Schumacher G. Coulomb explosions in a metallic glass due to the passage of fast heavy ions? Physical review letters. 1986;57:850.
[43] Vineyard G. Thermal spikes and activated processes. Radiation effects. 1976;29:245-8.
[44] Toulemonde M, Dufour C, Paumier E. Transient thermal process after a high-energy heavy-ion irradiation of amorphous metals and semiconductors. Physical review B. 1992;46:14362.
[45] Toulemonde M, Paumier E, Dufour C. Thermal spike model in the electronic stopping power regime. Radiation Effects and Defects in Solids. 1993;126:201-6.
[46] Toulemonde M, Dufour C, Meftah A, Paumier E. Transient thermal processes in heavy ion irradiation of crystalline inorganic insulators. Nuclear Instruments and Methods in Physics Research Section B: Beam Interactions with Materials and Atoms. 2000;166:903-12.
[47] Trautmann C. Spuren energiereicher Ionen in Polymeren und metallischen Gläsern, PhD thesis, University of Frankfurt.: Universität Frankfurt; 1994.
[48] Toulemonde M, Assmann W, Dufour C, Meftah A, Studer F, Trautmann C. Experimental phenomena and thermal spike model description of ion tracks in amorphisable inorganic insulators. Ion Beam Science, Solved and Unsolved Problems The Royal Danish Academy of Sciences and Letters, Copenhagen, Mat Fys Med. 2006:52-2.
[49] Szenes G. Thermal spike model of amorphous track formation in insulators irradiated by swift heavy ions. Nuclear Instruments and Methods in Physics Research Section B: Beam Interactions with Materials and Atoms. 1996;116:141-4.
[50] Szenes G. Comparison of two thermal spike models for ion–solid interaction. Nuclear Instruments and Methods in Physics Research Section B: Beam Interactions with Materials and Atoms. 2011;269:174-9.

[51] Toulemonde M, Trautmann C, Balanzat E, Hjort K, Weidinger A. Track formation and fabrication of nanostructures with MeV-ion beams. Nuclear Instruments and Methods in Physics Research Section B: Beam Interactions with Materials and Atoms. 2004;216:1-8.
[52] Sun Y, Zhu Z, Wang Z, Liu J, Jin Y, Hou M, et al. The damage process induced by swift heavy ion in polycarbonate. Nuclear Instruments and Methods in Physics Research Section B: Beam Interactions with Materials and Atoms. 2003;212:211-5.
[53] Sun Y, Zhang C, Zhu Z, Wang Z, Jin Y, Liu J, et al. The thermal-spike model description of the ion-irradiated polyimide. Nuclear Instruments and Methods in Physics Research Section B: Beam Interactions with Materials and Atoms. 2004;218:318-22.
[54] Szenes G, Havancsák K, Skuratov V, Hanák P, Zsoldos L, Ungár T. Application of the thermal spike model to latent tracks induced in polymers. Nuclear Instruments and Methods in Physics Research Section B: Beam Interactions with Materials and Atoms. 2000; 166:933-7.
[55] Mélot M, Ngono-Ravache Y, Balanzat E. Very low temperature irradiation of aliphatic polymers: Role of radical migration on the creation of stable groups (O-127). Nuclear Instruments and Methods in Physics Research Section B: Beam Interactions with Materials and Atoms. 2003;208:345-52.
[56] Krevelen DW, Te Nijenhuis K. Properties of polymers: their correlation with chemical structure; their numerical estimation and prediction from additive group contributions: Elsevier Amsterdam; 2009.
[57] Wilkes CE, Summers JW, Daniels CA, Berard MT. PVC handbook: Hanser Munich; 2005.
[58] Zhudi Z, Wenxue Y, Xinfang C. Study on increase in crystallinity in γ-irradiated poly (vinylidene fluoride). Radiation Physics and Chemistry. 2002;65:173-6.
[59] Nasef MM, Saidi H, Dahlan KZM. Investigation of electron irradiation induced-changes in poly (vinylidene fluoride) films. Polymer degradation and stability. 2002;75:85-92.
[60] Lim YM, Kang PH, Lee SM, Kim SS, Jeun JP, Jung CH, et al. Effect of Electron Beam Irradiation on Poly (vinylidene fluoride) Films at the Melting Temperature. Journal of Industrial and Engineering Chemistry. 2006;12:589-93.
[61] Muñoz E, Rickards J, Adem E, Borja MA, Burillo G, Cota L. Changes in the physical and chemical properties of pvdf irradiated by 4 me v protons. Revista mexicana de física. 2003;49:537-41.

[62] Fajgar R, Vitek J, Pola J, Bastl Z, Tlaskal J, Gregora I, et al. IR laser degradation of some fluoro-polymers. Journal of fluorine chemistry. 1995;72:111-6.

[63] Betz N, Le Moël A, Balanzat E, Ramillon JM, Lamotte J, Gallas JP, et al. A FTIR study of PVDF irradiated by means of swift heavy ions. Journal of Polymer Science Part B: Polymer Physics. 1994;32:1493-502.

[64] Drobny J. Fluoroplastics: iSmithers Rapra Publishing; 2006.

[65] Sessler G, Shahi K. Electrets, Topics in Applied Physics. Journal of The Electrochemical Society. 1980;127:530C-C.

[66] Parada MA, de Almeida A. Teflon electret radiation dosimeter. Nuclear Instruments and Methods in Physics Research Section B: Beam Interactions with Materials and Atoms. 2002;191:820-4.

[67] Baake O, Seidl T, Hossain UH, Delgado AO, Bender M, Severin D, et al. An apparatus for in situ spectroscopy of radiation damage of polymers by bombardment with high-energy heavy ions. Review of Scientific Instruments. 2011;82:045103.

[68] https://www.gsi.de/forschung-bescheuniger/bescleunigeranlage.htm. GSI Helmholtz Center for heavy ion research.

[69] https://www.gsi.de/work/fairgsi/linac-operations/linac/unilac.htm. Universal Linear Accelerator (UNILAC).

[70] https://www.gsi.de/forschung-beschleuniger/beschleunigeranlage/ringbeschleuniger.htm. Heavy Ion Synchrotron (SIS).

[71] https://www.gsi.de/forschung_beschleuniger/beschleunigeranlage/speicherring.htm. Experimental Ion Source (ESR).

[72] Forck P. Lecture notes on beam instrumentation and diagnostics. Joint Universities Accelerator School (JUAS 2010), http://www-bd gsi de. 2007.

[73] Severin D, Trautmann C, Neumann R. The M-Branch, a new UNILAC irradiation facility with in-situ analytical techniques for materials research. GSI Scientific Report2008. p. 362.

[74] Hesse M, Meier H, Zeeh B. Spektroskopische Methoden in der organischen Chemie. Zürich: Georg Thieme Verlag; 2013.

[75] Hollas JM. Moderne Methoden in der Spektroskopie: Springer Heidelberg; 2000.

[76] Haken JK, Werner RL. Infra-red spectra of polyvinyl acetate and poly-α, α', β-trideuterovinyl acetate. British Polymer Journal. 1971;3:157-62.

[77] Haken JK, Werner RL. The low temperature infrared spectrum of polyvinyl acetate. British Polymer Journal. 1973;5:451-5.
[78] Haken JK, Werner RL. The infrared spectrum of polyvinyl formate. Spectrochimica Acta Part A: Molecular Spectroscopy. 1971;27:343-51.
[79] Wilmshurst J. A vibrational assignment for methyl formate and methyl acetate. Journal of Molecular Spectroscopy. 1957;1:201-15.
[80] Katritzky AR, Lagowski JM, Beard JAT. The infra-red spectra of esters—I Methyl, ethyl, n- and i-propyl, and n-, i- and s-butyl esters. Spectrochimica Acta. 1960;16:954-63.
[81] Lucier JJ, Bentley FF. The characterization of saturated aliphatic esters in the 15–40 μ region. Spectrochimica Acta. 1964;20:1-13.
[82] Lin S-Y, Cheng W-T, Wei Y-S, Lin H-L. DSC-FTIR microspectroscopy used to investigate the heat-induced intramolecular cyclic anhydride formation between Eudragit E and PVA copolymer. Polymer journal. 2011;43:577-80.
[83] Rogojanu A, Rusu E, Olaru N, Dobromir M, Dorohoi D. Development and characterization of poly (vinyl alcohol) matrix for drug release. Digest Journal of Nanomaterials & Biostructures (DJNB). 2011;6.
[84] Nguyen TT. Thermal degradation of a poly(vinyl formal)-containing adhesive film on a polyethylene rubber surface. A photoacoustic fourier transform infrared spectroscopic investigation. Journal of Applied Polymer Science. 1989;38:765-78.
[85] Brewis D, Dahm R. Adhesion to fluoropolymers: iSmithers Rapra Publishing; 2006.
[86] Kobayashi M, Tashiro K, Tadokoro H. Molecular vibrations of three crystal forms of poly vinylidene fluoride. Macromolecules. 1975;8:158-71.
[87] Boerio FJ, Koenig JL. Vibrational analysis of polyvinylidene fluoride. Journal of Polymer Science Part A-2: Polymer Physics. 1971;9:1517-23.
[88] Tauc J, Grigorovici R, Vancu A. Optical Properties and Electronic Structure of Amorphous Germanium. physica status solidi (b). 1966;15:627-37.
[89] Englman R, Jortner J. The energy gap law for radiationless transitions in large molecules. Molecular Physics. 1970;18:145-64.
[90] Lewis M, Lee E. Residual gas and ion-beam analysis of ion-irradiated polymers. Nuclear Instruments and Methods in Physics Research Section B: Beam Interactions with Materials and Atoms. 1991;61:457-65.
[91] Idesaki A, Koizumi N, Sugimoto M, Morishita N, Ohshima T, Okuno K. Gas evolution from insulating materials for superconducting coil of ITER by gamma ray irradiation at liquid

nitrogen temperature. Advances in cryogenic engineering materials: Transactions of the International Cryogenic Materials Conference-ICMC, Vol 54: AIP Publishing; 2008. p. 169-73.

[92] Chang Z, Laverne JA. Dynamic evolution of gases in the γ-and helium-ion radiolyses of solid polymers. Journal of Polymer Science Part B: Polymer Physics. 2001;39:1449-59.

[93] http://www.lesker.com/NewWeb/Technical_Info/jpg/FAQFIG4.jpg. Residual Gas Analyser.

[94] B. Wunderlich e. Thermal Analysis. Boston: Academic Press; 1990.

[95] Severin D. Study of the degradation process of polyimide induced by high energetic ion irradiation.: PhD thesis, Philipps University of Marburg; 2008.

[96] Hossain UH, Lima V, Baake O, Severin D, Bender M, Ensinger W. On-line and post irradiation analysis of swift heavy ion induced modification of PMMA (polymethyl-methacrylate). Nuclear Instruments and Methods in Physics Research Section B: Beam Interactions with Materials and Atoms. 2014;326:135-9.

[97] Hossain UH, Seidl T, Ensinger W. Combined in situ infrared and mass spectrometric analysis of high-energy heavy ion induced degradation of polyvinyl polymers. Polymer Chemistry. 2014;5:1001-12.

[98] Grassie N. The thermal degradation of polyvinyl acetate. I. Products and reaction mechanism at low temperatures. Transactions of the Faraday Society. 1952;48:379-87.

[99] Troitskii BB, Razuvaev GA, Khokhlova LV, Bortnikov GN. On the mechanism of the thermal degradation of polyvinyl acetate. Journal of Polymer Science: Polymer Symposia. 1973;42:1363-75.

[100] Ballistreri A, Foti S, Montaudo G, Scamporrino E. Evolution of aromatic compounds in the thermal decomposition of vinyl polymers. Journal of Polymer Science: Polymer Chemistry Edition. 1980;18:1147-53.

[101] Holland BJ, Hay JN. The thermal degradation of poly (vinyl acetate) measured by thermal analysis–Fourier transform infrared spectroscopy. Polymer. 2002;43:2207-11.

[102] Costa L, Avataneo M, Bracco P, Brunella V. Char formation in polyvinyl polymers I. Polyvinyl acetate. Polymer Degradation and Stability. 2002;77:503-10.

[103] Tsuchiya Y, Sumi K. Thermal decomposition products of poly(vinyl alcohol). Journal of Polymer Science Part A-1: Polymer Chemistry. 1969;7:3151-8.

[104] Thomas PS, Guerbois JP, Russell GF, Briscoe BJ. FTIR Study of the Thermal Degradation of Poly(vinyl Alcohol). Journal of Thermal Analysis and Calorimetry. 2001;64:501-8.

[105] Holland BJ, Hay JN. The thermal degradation of poly(vinyl alcohol). Polymer. 2001;42:6775-83.

[106] Davenas J, Xu X, Boiteux G, Sage D. Relation between structure and electronic properties of ion irradiated polymers. Nuclear Instruments and Methods in Physics Research Section B: Beam Interactions with Materials and Atoms. 1989;39:754-63.

[107] Blazevska-Gilev J, Spaseska D. Thermal degradation of PVAc. Journal of the University of Chemical Technology and Metallurgy. 2005;40:287-90.

[108] Fink D. Transport processes in ion-irradiated polymers: Springer, Heidelberg; 2004.

[109] Chang Z, LaVerne JA. The gases produced in gamma and heavy-ion radiolysis of poly (methyl methacrylate). Radiation Physics and Chemistry. 2001;62:19-24.

[110] Huheey J, Keiter E, Keiter R. Inorganic Chemistry: Principles of Structure and Reactivity, 1993, 292. Harper Collins College Publishers, New York.

[111] Lide Jr DR. A survey of carbon-carbon bond lengths. Tetrahedron. 1962;17:125-34.

[112] Chambers A, Chambers A. Modern vacuum physics: Chapman & Hall/CRC Boca Raton; 2005.

[113] Jakubke H-D, Jeschkeit H. Concise Encyclopedia Chemistry. trans. rev. Eagleson, Mary. Berlin: Walter de Gruyter. ISBN 0-89925-457-8; 1994.

[114] Guzman AM, Carlson JD, Bares JE, Pronko PP. Chemical and physical changes induced in polyvinylidene fluoride by irradiation with high energy ions. Nuclear Instruments and Methods in Physics Research Section B: Beam Interactions with Materials and Atoms. 1985;7–8, Part 2:468-72.

[115] Blout ER, Fields M. Absorption Spectra. V. The Ultraviolet and Visible Spectra of Certain Polyene Aldehydes and Polyene Azines1. Journal of the American Chemical Society. 1948;70:189-93.

[116] Sivalingam G, Karthik R, Madras G. Effect of metal oxides on thermal degradation of poly (vinyl acetate) and poly (vinyl chloride) and their blends. Industrial & engineering chemistry research. 2003;42:3647-53.

[117] Hossain UH, Muench F, Ensinger W. A comparative study on degradation characteristics of fluoropolymers irradiated by high energy heavy ions. RSC Advances. 2014;4:50171-9.

[118] Oshima A, Murata K, Oka T, Miyoshi N, Matsuura A, Kudo H, et al. Heavy ion beam induced phenomena in polytetrafluoroethylene. Nuclear Instruments and Methods in Physics Research Section B: Beam Interactions with Materials and Atoms. 2007;265:314-9.

[119] Madaeni SS, Zinadini S, Vatanpour V. A new approach to improve antifouling property of PVDF membrane using in situ polymerization of PAA functionalized TiO2 nanoparticles. Journal of Membrane Science. 2011;380:155-62.

[120] Clyne MA, McKenney DJ, Walker RF. Reaction Kinetics of Ground State Fluorine, F (2P), Atoms. I. Measurement of Fluorine Atom Concentrations and the Rates of Reactions F+ CHF3 and F+ Cl2 using Mass Spectrometry. Canadian Journal of Chemistry. 1973;51:3596-604.

[121] Jensen SR, Brown WA, Heath E, Cooper DG. Characterization of polychlorinated alkane mixtures—a Monte Carlo modeling approach. Biodegradation. 2007;18:703-17.

[122] Parada M, Minamisawa R, Moreira M, de Almeida A, Muntele I, Ila D. Damage effects of gamma and X-rays in polymer film electrets. Surface and Coatings Technology. 2007;201:8246-9.

[123] O'Hagan D. Understanding organofluorine chemistry. An introduction to the C-F bond. Chemical Society Reviews. 2008;37:308-19.

[124] Lemal DM. Perspective on fluorocarbon chemistry. The Journal of organic chemistry. 2004;69:1-11.

[125] Parada M, de Almeida A, Muntele C, Muntele I, Ila D. Effects of MeV proton bombardment in thin film PFA and FEP polymers. Surface and Coatings Technology. 2005;196:378-82.

[126] Calcagno L, Compagnini G, Foti G. Structural modification of polymer films by ion irradiation. Nuclear Instruments and Methods in Physics Research Section B: Beam Interactions with Materials and Atoms. 1992;65:413-22.

[127] Fink D, Klett R, Chadderton LT, Cardoso J, Montiel R, Vazquez H, et al. Carbonaceous clusters in irradiated polymers as revealed by small angle X-ray scattering and ESR. Nuclear Instruments and Methods in Physics Research Section B: Beam Interactions with Materials and Atoms. 1996;111:303-14.

[128] Saha A, Chakraborty V, Chintalapudi SN. Chemical modification of polypropylene induced by high energy carbon ions. Nuclear Instruments and Methods in Physics Research Section B: Beam Interactions with Materials and Atoms. 2000;168:245-51.

[129] Virk HS, Chandi PS, Srivastava AK. Physical and chemical changes induced by 70 MeV carbon ions in polyvinylidene difluoride (PVDF) polymer. Nuclear Instruments and Methods in Physics Research Section B: Beam Interactions with Materials and Atoms. 2001;183:329-36.

[130] Phukan T, Kanjilal D, Goswami T, Das H. Study of optical properties of swift heavy ion irradiated PADC polymer. Radiation measurements. 2003;36:611-4.

[131] Kumar R, De U, Prasad R. Physical and chemical response of 70 MeV carbon ion irradiated polyether sulphone polymer. Nuclear Instruments and Methods in Physics Research Section B: Beam Interactions with Materials and Atoms. 2006;248:279-83.

[132] Fink D, Chung W, Klett R, Schmoldt A, Cardoso J, Montiel R, et al. Carbonaceous clusters in irradiated polymers as revealed by UV-Vis spectrometry. Radiation effects and defects in solids. 1995;133:193-208.

List of Figures

Figure 1.1: Pictures of the existing GSI Helmholtz-Centre of Heavy Ion Research (left) and the planed FAIR facility (right) [17]

Figure 2.1: SRIM (Stopping and Range of Ions in Matter) calculations for Au ion in polyvinyl formal. Displayed is the stopping power per µm versus specific energy of the projectile.

Figure 2.2: SRIM 2011 calculation for electronic energy loss (dE_e / dx) of two different ions in PVF versus the projected range (R).

Figure 2.3: SRIM 2011 calculation for electronic energy loss (dE_e / dx) of Au ions in different aliphatic and fluoropolymers versus the projected range (R).

Figure 3.1: Sample preparation by solution grown technique. Left: preparation process, right: example of a transparent 20 µm PVF film.

Figure 3.2: Scheme representing the structure of (i) polyvinyl formal (PVF), (ii) polyvinyl alcohol (PVA) and (iii) polyvinyl acetate (PVAc).

Figure 3.3: Molecular structure of polymethyl-methacrylate (PMMA).

Figure 3.4: Structure of (i) polyvinylidene fluoride (PVDF), (ii) ethylene-tetrafluoroethylene (ETFE), (iii) tetrafluoroethylene-per-fluoromethoxyethylene (PFA) and (iv) tetrafluoroethylene-hexa-fluoropropylene (FEP).

Figure 4.1: Schematic represents the GSI accelerator facilities for swift heavy ion irradiation research [1]. The used irradiation sites (M-Branch and X0-Branch) are marked in red colour.

Figure 4.2: Schematic showing X0-beamline of GSI accelerators facilities.

Figure 4.3: Photographs of the target station at X0-beamline showing the sample exchange system for remote control irradiation (left side) with the magazine (right side).

Figure 4.4: Schematics view of the ionization chamber.

Figure 4.5: Schematics of beamline M3. Ions have to pass the aperture for ion beam shaping, a beam diagnostic unit providing a SEETRA, a Faraday cup, a luminescence screen, and a heater chamber to reach the multipurpose diagnostic chamber. Reprinted with permission from [67].

Figure 4.6: Schematics of the multipurpose chamber at target station M3. IR source and detection unit are placed outside of the chamber. The angle between IR radiation and ion beam normal is -45°. The RGA is mounted near the IR detection unit and tilted down 30°.

The sample holder can be moved up and down and is rotatable. Reprinted with permission from [67].
Figure 4.7: Photograph of the sample holder for on-line analysis. Sample holder for RGA analysis is shown in the left side and sample holder for the FT-IR measurement on the right side.
Figure 4.8: Photograph of the experimental setup at M3 beamline. Left side of the picture is the multipurpose chamber; right sight: Residual Gas Analyser by means of quadrupole mass spectrometry (QMS); bottom of the picture: FT-IR spectroscopy placed outside of the diagnostic chamber.
Figure 4.9: Schematics and principle of infrared spectroscopy (IR)
Figure 4.10: Infrared spectra of pristine PVF, PVAc, PVA and PMMA.
Figure 4.11: Infrared spectra of pristine PVDF, ETFE, PFA and FEP foils.
Figure 4.12: An example Tauc plot of a pristine ETFE.
Figure 4.13: UV-Vis spectrum of 25 µm thickness of pristine ETFE foil.
Figure 4.14: Schematics of the Residual Gas Analyser (RGA) containing an ionizer, a separator device and a detector.
Figure 4.15: Typical mass spectrum of the polyvinyl formal (PVF) on the sample holder as background spectrum.
Figure 4.16: Schematics of a Thermo gravimetric analysis (TGA).
Figure 4.17: TGA analysis of a 20 µm thickness of pristine polyvinyl formal (PVF) foil.
Figure 5.1: FT-IR spectra of polyvinyl formal before (black) and after (blue, red) irradiation with 4.5 MeV/u Au ions performed at RT
Figure 5.2: Maximum intensity of absorption bands at 1735 and 1722 cm^{-1} as a function of the fluence during irradiation with 4.5 MeV/u Au ions.
Figure 5.3: Band deconvolution of the irradiated data set using Lorentzian functions as a fit.
Figure 5.4: FT-IR spectra of polyvinyl formal during irradiation at 40 K and RT.
Figure 5.5: FT-IR spectra of polyvinyl acetate irradiated with different fluences.
Figure 5.6: Expanded FT-IR spectra of polyvinyl acetate irradiated with different fluences; left: the region of 1850-1600 cm^{-1}, right: the region of 3700-3100 cm^{-1}.
Figure 5.7: FT-IR spectra of 20 µm thick pristine and Au ion irradiated PVAc foils with 4.8 MeV/u at RT. The magnified inset indicates the appearance of the new CO_2 group at 2339 cm^{-1}.

Figure 5.8: FT-IR spectra of the CO_2 – region of PVAc foils, before and after irradiation with U (8.6 MeV/u), Au (4.8 MeV/u) and Xe (11.4 MeV/u) ions (links); Band deconvolution of the irradiated data set using Gaussian functions as a fit (right).
Figure 5.9: Intensity of the CO_2 band at 2339 cm^{-1} as a function of fluence for irradiations with U, Au and Xe ions.
Figure 5.10: The area of the CO_2 band at 2339 cm^{-1} increases as a function of fluence (left) and decreases during time (right).
Figure 5.11: Area of CO_2 band at 2339 cm^{-1} as a function of time for irradiations with Au ions 4.8 Mev/u.
Figure 5.12: FT-IR spectra of polyvinyl alcohol, comparing the unirradiated material with the one treated with two different ion fluences.
Figure 5.13: FT-IR spectra of the pristine (black) and the irradiated (blue, red) PMMA foil (4.5 MeV/u Au ions).
Figure 5.14: Maximum intensity of absorption bands at 2994, 2842 and 1641 cm^{-1} as a function of the fluence during irradiation with 4.5 MeV/u Au ions.
Figure 5.15: Outgassing spectra of polyvinyl formal, polyvinyl acetate and polyvinyl alcohol polymers at RT recorded on-line during irradiation with 4.5 MeV/u Au ions.
Figure 5.16: Outgassing spectra of a polyvinyl formal foil at RT and 40K recorded on-line during irradiation with 4.5 MeV/u Au ions.
Figure 5.17: Outgassing profiles of different masses m/z during heating of polyvinyl formal after the exposure to 4.5 MeV/u Au ions.
Figure 5.18: Outgassing spectra of a PVAc foil recorded on-line during irradiation with 4.5 MeV/u Au ions.
Figure 5.19: Outgassing of PVAc foils recorded before and during irradiation with U, Au and Xe ions.
Figure 5.20: Outgassing spectra of a PVA foil at RT recorded on-line during irradiation with 4.5 MeV/u Au ions.
Figure 5.21: Outgassing spectra of PVA and PVAc foil recorded on-line during irradiation with 4.5 MeV/u Au ions.
Figure 5.22: Outgassing spectra of PMMA polymer irradiated with 4.5 MeV/u Au ions.
Figure 5.23: Proposed ion induced main degradation reactions of polyvinyl alcohol.
Figure 5.24: Proposed ion induced main degradation reactions of polyvinyl acetate.
Figure 5.25: Proposed ion induced main degradation reactions of polyvinyl acetale.

Figure 5.26: A possible mechanism of volatile products formation of PMMA foil.
Figure 5.27: UV/Vis spectroscopy of pristine and irradiated (Au, 11.1 MeV/u, up to 1 $\times 10^{12}$ ions/cm^2) polyvinyl formal (PVF).
Figure 5.28: UV-Vis absorption spectra of Au ion irradiated PVAc at 11.1 MeV/u to various fluences.
Figure 5.29: UV-Vis absorption spectra of U ion irradiated PMMA at 8.3 MeV/u to various fluences.
Figure 5.30: Radiation induced changes in wavelength region between 260-350 nm for PMMA as a function of fluence.
Figure 5.31: TGA curve of pristine (black) and irradiated PVF foils with different fluences (left) and their derivatives (right).
Figure 5.32: The TGA curve of pristine and ion irradiated PVAc foils. The irradiation was performed with Au ions at 11.1 MeV/u at room temperature.
Figure 5.33: Residual mass as a function of ion fluence for PVF, PVAc and PVF irradiated with 11.1-MeV/u Au ions.
Figure 5.34: Residual mass as a function of ion fluence for PVF after irradiation with 11.1 MeV / u U and Au ions (with U irradiation: black and with Au ion irradiation: red).
Figure 5.35: FT-IR spectra of PVDF: Pristine (black), irradiated with Au ions of 4.5 MeV/u with fluences of 3×10^{11} cm^{-2}(blue) and (c) 2×10^{12} ions/cm^2 (red)
Figure 5.36: (a) Outgassing spectra of PVDF on-line recorded without irradiation and during irradiation with 11.1 MeV/u Sm ions, (b) difference spectrum, indicating the outgassing species caused by the heavy ion irradiation alone.
Figure 5.37: Scheme representing the degradation mechanism of PVDF polymer. Schematic presentation of the main heavy ion induced degradation reactions of PVDF.
Figure 5.38: FT-IR spectra of ETFE: Pristine (black), irradiated with Sm ions by 3×10^{11} ions/cm^2 (blue) and irradiated by 3×10^{12} ions/cm^2 (red).
Figure 5.39: (a) Outgassing spectra of ETFE on-line recorded during irradiation with 11.1 MeV/u Sm ions, (b) difference spectrum, indicating the outgassing species caused by the heavy ion irradiation.
Figure 5.40: Scheme representing the degradation mechanism of ETFE polymer.
Figure 5.41: FT-IR spectra of PFA: Pristine (black), irradiated with Sm ions by 3×10^{11} ions/cm^2 (blue) and irradiated by 6×10^{12} ions/cm^2 (red).

Figure 5.42: (a) Outgassing spectra of PFA polymer on-line recorded during irradiation with 11.1 MeV/u Sm ions, (b) difference spectrum, indicating the outgassing species caused by the heavy ion irradiation.
Figure 5.43: Scheme representing the degradation mechanism of PFA.
Figure 5.44: FT-IR spectra of FEP: Pristine (black), irradiated with Sm ions by 3×10^{11} ions/cm^2 (blue) and irradiated by 3×10^{12} ions/cm^2 (red).
Figure 5.45: (a) Outgassing spectra of FEP polymer on-line recorded during irradiation with 11.1 MeV/u Sm ions, (b) difference spectrum, indicating the outgassing species caused by the heavy ion irradiation.
Figure 5.46: Scheme representing the degradation mechanism of FEP.
Figure 5.47: Outgassing fragments (m/z = 20, 31, 47, 51 and 69) of fluoropolymers (PVDF, ETFE, PFA and FEP). The intensities are calculated in percent (%) for each m/z value.
Figure 5.48: UV-Vis spectra of ETFE, PFA and FEP polymers irradiated with 11.1 MeV/u Sm ions. The applied fluences were from 3×10^{10} - 3×10^{12} ions/cm^2.

List of Tables

Table 3.1: Material properties of used polyvinyl polymers (PVF, PVAc, PVA and PMMA).
Table 3.2: Material properties of used fluoropolymers (PVEF, ETFE, PFA and FEP).
Table 3.3: Used ion beam at X0 beamline for post irradiation analysis.
Table 3.4: Used ion beam at M3 beamline for on-line analysis.
Table 4.1: Characteristic absorption bands of some functional groups.
Table 4.2: IR bands of the used polyvinyl polymers (PVF, PVAc, PVA and PMMA).
Table 4.3: IR spectra of the used fluoropolymer materials (PVDF, ETFE, PFA and FEP).
Table 4.4: characteristic absorption of organic chromophores.
Table 4.5: Mass loss values induced by ion irradiation for used polymer sample.
Table 5.1: Outgassing fragments of polyvinyl formal during irradiation at room temperature (RT, 297 K) and cryogenic temperature (CT, 40 K); (r/i) means radical/ion.
Table 5.2: Outgassing fragments of polyvinyl acetate during irradiation at room temperature (RT); the intensities are normalized to the maximum intensity found for mass m/z=28; (r/i) means radical/ion.
Table 5.3: Bond dissociation energies, from ref. [110].
Table 5.4: Transferred energy dE/dx (per 100 pm ion track length x) and integral radiation damage per ion (accumulated number of C, O, and H atoms, displaced from their position in the polymer chain, up to the given depth), for 4.5 MeV/u Au ions in PVF, calculated by SRIM for different depths/thickness of the material. The average ion range is 66.3 ± 0.4 µm, i.e. in a depth of e.g. 100 µm there is no more damage (dE/dx=0).
Table 5.5: Estimated band gap energy of polyvinyl polymers (PVF, PVAc and PMMA). PVF and PVAc are irradiated at 11.1 MeV/u Au ion and PMMA at 8.6 MeV/u U ion.
Table 5.6: Results of TGA measurements of 11.1 MeV/u Au-ion irradiated polyvinyl formal (PVF)
Table 5.7: Results of TGA measurements of 11.1 MeV/u Au-ion irradiated polyvinyl acetate (PVAc)
Table 5.8: Interpretation of the appearing new absorption bands in polymers (PVDF, ETFE, PFA and FEP)
Table 5.9: Outgassing fragments of fluoropolymers (PVDF, ETFE; PFA and FEP) for Sm (11.1 MeV/u) ion irradiation. Signal intensities from mass spectrometric measurements are

calculated in percent (%) for each m/z values, normalized to the highest value which was set to 100%.

Table 5.10: Estimated band gap energy of fluoropolymers (ETFE, PFA and FEP) for Sm ion irradiated at 11.1 MeV/u.

Abbreviations

ASTM	Analytical Thermal Spike Model
ECR	Electron Cyclotron Resonance
EGA	Evolved Gas Analysis
ETFE	Ethylene tetrafluoroethylene
FAIR	Facility for Antiproton and Ion Research
Formvar^{TM} / PVF	Trade mark of polyvinyl formal / Polyvinyl formal
FEP	Tetrafluoroethylene-hexa-fluoropropylene
FT-IR	Fourier-Transform-Infrared
GSI	GSI Helmholtz-Centre of Heavy Ion Research (Darmstadt, Germany)
ITSM	Inelastic Thermal Spike Model
MS	Mass Spectrometry
PE	Polyethylene
PET	Polyethylene terephthalate
PI	Polyimide
PTFE	Polytetrafluoroethylene
PVA	Polyvinyl alcohol
PVAc	Polyvinyl acetate
PVDF	Polyvinylidene fluoride
PFA	Tetrafluoroethylene-per-fluoromethoxyethylene
PMMA	Polymethylmethacrylate
QMS	(Quadrupole) Mass Spectrometer
RGA	Residual Gas Analysis
SC	Superconducting
SDBS	Structural Database of Organic Compounds
T_g	Glass transition temperature
TGA	Thermal Gravimetric Analysis
TU	Technical University

Curriculum vitae

Personal Details

Name:	Umme Habiba Hossain
Date of Birth:	09.11.1980
Birthplace:	Munshiganj

Education

08/2009-	**PhD-student** in the Department of Geological and Materials Science at the Technical University of Darmstadt Focus in Swift heavy ion induced modification of aliphatic polymers **External PhD-student** of the GSI Helmholtz-Centre for Heavy Ion Research GmbH, Department of Material Science
10/2004-03/2009	**Diploma** student in chemistry at the Philipps-University of Marburg **Degree: Diploma in Chemistry** Focus in Physical Chemistry
01/2003 – 09/2004	**Language** Schools in Kassel and Kassel University Language courses and preparation for DSH examination **DSH degree** (German language examination for university admission of foreign applicants)
1998 – 2002	**National University** (under: Govt Haraganga College.), Munshiganj, Bangladesh; Degree: Bachelor of Science with Honours in Chemistry
1995 – 1997	**Govt. Haraganga College**, Munshiganj, Bangladesh
1990 – 1995	Mirkadim Hazi Amzad Ali High School, Mirkadim, Munshiganj, Bangladesh; **Secondary School Certificate Examination**

Scientific Publications

U.H. Hossain, F. Muench and W. Ensinger, A Comparative study on degradation characteristics of fluoropolymers irradiated by high energy heavy ions, RSC Adv., 4 (2014) 50171-50179

U.H. Hossain, T. Seidl and W. Ensinger, Combined in-situ infrared and mass spectrometric analysis of high-energy heavy ion induced degradation of polyvinyl polymers. Polym. Chem., 5 (2014) 2001-2012

U.H. Hossain, V. Lima, O. Baake, D. Severin, M. Bender, and W. Ensinger, On-line and post irradiation analysis of swift heavy ion induced modification of PMMA (polymethyl methacrylate), Nucl. Instr. Meth. B., 326 (2014) 135-139

F. Muench, A. Eils, M.E. Toimil-Molares, **U.H. Hossain**, A. Radetinac, C. Stegmann, U. Kunz, S. Lauterbach, H.-J. Kleebe, W. Ensinger, Polymer activation by reducing agent absorption as a flexible tool for the creation of metal films and nanostructures by electroless plating, Surface and Coatings Technology, 241 (2014) 100-108

T. Seidl, O. Baake, **U.H. Hossain**, M. Bender, D. Severin, C. Trautmann, W. Ensinger. In-situ investigation of polyvinyl formal irradiated with GeV Au ions. Nucl. Instr. Meth. B, 272 (2012) 400-404

O. Baake, T. Seidl, **U. H. Hossain**, A. O. Delgado, M. Bender, D. Severin and W. Ensinger. An apparatus for in-situ spectroscopy of radiation damage of polymers by bombardment with high-energy heavy ions. Rev. Sci. Instr. 82 (2011) 045103

GSI Scientific Reports

U. H. Hossain, T. Seidl, C. Fasel, D. Severin and W. Ensinger**;** Ion induced weight loss and thermal gravimetric analysis of ion-irradiated polyvinyl formal. GSI scientific report, PNI-INHOUSE-EXP-36, 2012

T. Seidl, E. Floch, V. Lima, **U.H. Hossain**, T. Wietoska, C. Trautmann, W. Ensinger; Dielectric strength of two fiber reinforced plastics irradiated with heavy ions. GSI scientific report, PNI-INHOUSE-EXP-37, 2012

U. H. Hossain, T. Seidl, O. Baake, A. O. Delgado, V. Lima, D. Severin, M. Bender and W. Ensinger. In-situ FT-IR spectroscopy of polyvinyl formal irradiated with gold ions. GSI scientific report, PNI-MR-20, 2011

V. Lima, T. Seidl, **U.H. Hossain**, O. Baake, D. Severin, M. Bender, C. Trautmann, and W. Ensinger. Degradation of polyethylene oxides during irradiation with uranium ions. GSI scientific report, PNI-MR-21, 2010

T. Seidl, O. Baake, **U.H. Hossain**, A.O. Delgado, D. Severin, C. Trautmann, W. Ensinger. In-situ infrared analysis of ion degraded polyimide. GSI scientific report, PNI-MR-19, 2009

Conferences

U.H. Hossain, "Swift Heavy Ion Induced Modifications of Polyvinyl Formal" GSI-CIMAP (Centre de Recherche sur les Ions, les Matériaux et la Photonique) meeting, Caen (France), oral presentation (2011)

U.H. Hossain, T. Seidl, V. Lima, M. Bender, D. Severin, E. Floch, A. Stabiniak and W. Ensinger, „Degradation studies on irradiated polyvinyl polymers – a wire insulation material" Seminar, Accelerator physics for intense ion beams, Bad Honnef (Germany), poster presentation (2012)

U.H. Hossain, Workshop „Ionenstrahlen – Forschung und Anwendung" Leibniz-Institut für Oberflächenmodifizierung, Leipzig (Germany), (2013)

U.H. Hossain, T. Seidl, D. Severin and W. Ensinger, „ Swift heavy ion induced modification of aliphatic polymers", Radiation Effects in Insulators (REI), Helsinki (Finland), poster presentation (2013)

U.H. Hossain and W. Ensinger, "Swift heavy ion induced modifications of aliphatic polymers", Deutsche Tagung für Forschung mit Synchrotronstrahlung, Neutronen und Ionenstrahlen an Großgeräten (SNI), Bonn (Germany), poster presentation (2014)

Acknowledgement

It has been a long journey to create a dissertation with the depth and scope of science-based work. This is an undertaking that would not have been possible without the help of many people. At this point I would like to thank all those who contributed to this work. In particular, I express my sincere gratitude to the following persons:

- **Prof. Dr. Wolfgang Ensinger** for giving me the opportunity to perform this doctoral work under his kind supervision. I am grateful for allocating me research independence. He was always available to discuss obstacles and progress associated with my research. I do also appreciate the detailed scientific discussion. I especially thank him for his efforts to support me.
- **Prof. Dr. M. Rehahn** for accepting to be the second referee of this dissertation.
- **Prof. Dr. C. Trautmann** for the opportunity to perform PhD research work as a permanent guest in the material research department of GSI and the many helpful scientific discussions.
- Dr. T. Seidl for support and initially introducing me into the field during the beginning of my PhD.
- Drs. D. Severin and M. Bender for their versatile help and support during the beam time.
- Drs. M. Tomut and I. Alber for all the shared experiences, being best colleagues and back up during the whole PhD.
- Elko Schubert for all his technical support helps to make the sample holder for in-situ experimental measurements at M3-beamline.
- All members of the Materials Research Department at GSI for the friendly atmosphere during this work.
- My parents, brothers and sisters for their prayers and good wishes for my success.
- Finally, I would like to make especial mention of my husband for his encouragements and my dear son “Lamin Hossain” brings to me all love and happiness of this world.

The **BMBF** is acknowledged for financing the majority of this work through the projects **05KK7RD1** and **06DA90251.**